

UNIVERSITÉ DU QUÉBEC À MONTRÉAL

PROPRIÉTÉS GÉOCHIMIQUES ET ISOTOPIQUES DES SÉDIMENTS DU DÉTROIT
DE FRAM, OCÉAN ARCTIQUE. IMPLICATIONS PALEOCÉANOGRAPHIQUES ET
PALEOCLIMATIQUES

THÈSE
PRÉSENTÉE
COMME EXIGENCE PARTIELLE
DU DOCTORAT EN SCIENCE DE LA TERRE ET DE L'ATMOSPHÈRE

PAR
JENNY MACCALI

SEPTEMBRE 2012

UNIVERSITÉ DU QUÉBEC À MONTRÉAL
Service des bibliothèques

Avertissement

La diffusion de cette thèse se fait dans le respect des droits de son auteur, qui a signé le formulaire *Autorisation de reproduire et de diffuser un travail de recherche de cycles supérieurs* (SDU-522 – Rév.01-2006). Cette autorisation stipule que «conformément à l'article 11 du Règlement no 8 des études de cycles supérieurs, [l'auteur] concède à l'Université du Québec à Montréal une licence non exclusive d'utilisation et de publication de la totalité ou d'une partie importante de [son] travail de recherche pour des fins pédagogiques et non commerciales. Plus précisément, [l'auteur] autorise l'Université du Québec à Montréal à reproduire, diffuser, prêter, distribuer ou vendre des copies de [son] travail de recherche à des fins non commerciales sur quelque support que ce soit, y compris l'Internet. Cette licence et cette autorisation n'entraînent pas une renonciation de [la] part [de l'auteur] à [ses] droits moraux ni à [ses] droits de propriété intellectuelle. Sauf entente contraire, [l'auteur] conserve la liberté de diffuser et de commercialiser ou non ce travail dont [il] possède un exemplaire.»

AVANT-PROPOS

Cette thèse a été rédigée sous forme de trois articles en anglais formant chacun un chapitre. Le premier a été soumis et accepté à *Paleoceanography* (doi : 10.1029/2011PA002152), revue à comité de lecture. Le deuxième est soumis à *Quaternary Science Reviews (JQSR-D-11-00441)*, revue spécialisée à comité de lecture. Le troisième article sera soumis prochainement dans une revue spécialisée à comité de lecture. La mise en page de ces trois chapitres suit donc les directives propres à chaque revue. Pour cette raison, les titres et figures de chaque chapitre ne sont pas nécessairement numérotés selon le *Guide de présentation des mémoires et thèse*; à la place, les numéros tels qu'apparaissant dans les articles ont été conservés. De plus, les formats des références sont légèrement différents d'un chapitre à l'autre, afin de rester conformes aux revues dans lesquelles ils ont été ou seront publiés.

Ma contribution aux publications qui constituent le corps de cette thèse couvre la quasi-totalité du domaine analytique. Dans les chapitres I, II et III j'ai réalisé l'ensemble les traitements chimiques préalables aux analyses (lessivage). J'ai également réalisé l'intégralité des analyses des isotopes du Nd, Sr et Pb sur les carottes MC04 et MC16. J'ai effectué les analyses de ^{210}Pb de la carotte MC16. Les autres analyses géochimiques et/ou isotopiques, ont été réalisées en collaboration avec les équipes de géochimie et micropaléontologie du Geotop et du CRPG. J'ai collecté l'ensemble des données obtenues et réalisé le travail interprétatif. J'ai également rédigé les manuscrits, aux fins de publication sous la supervision et les conseils de mes directeurs de thèse, Jean Carignan, Claude Hillaire-Marcel et Laurie Reisberg. Les co-auteurs de l'article qui constitue le chapitre 3 ont participé à mes recherches en effectuant des analyses des isotopes de Nd et Sr sur la carotte MC-18 et en discutant l'interprétation des résultats. J'ai pour ma part réalisé les analyses complémentaires des isotopes de Nd et Sr sur la carotte MC16 ainsi que l'interprétation et la rédaction de ce chapitre.

Le premier chapitre est un article accepté à la revue *Paleoceanography* (doi : 10.1029/2011PA002152) et ayant pour titre « *Pb isotopes and geochemical monitoring of Arctic sedimentary supplies and water-mass exports through Fram Strait since the Last*

Glacial Maximum », avec pour co-auteurs Claude Hillaire-Marcel, Jean Carignan et Laurie Reisberg. Ce chapitre porte sur la validation d'outils géochimiques et isotopiques afin de déterminer la provenance des sédiments du détroit de Fram. Ce chapitre présente notamment deux tendances temporelles avec un changement de source pendant un intervalle de temps correspondant au Dryas Récent.

Le deuxième chapitre, « *Geochemical signatures of sediment to document sea-ice and water mass exports through Fram Strait since the Last Glacial Maximum* », est un article soumis à *Quaternary Science Reviews (JQSR-D-11-00441)* et écrit avec Jean Carignan, Claude Hillaire-Marcel et Laurie Reisberg. Il présente la distribution des éléments dans les sédiments du détroit de Fram en mettant en évidence une fraction terrigène, une fraction biogénique et une fraction authigène. Enfin, les données présentées dans ce chapitre permettent d'affiner la détermination des sources et donc améliorent les reconstructions de l'origine et de la circulation de la glace de mer dans l'Océan Arctique depuis le dernier maximum glaciaire.

Le troisième chapitre, « *Canadian radiogenic isotope signature of Younger Dryas age ice rafted sediments in cores from Lomonosov Ridge and Fram Strait* », est un article qui sera soumis prochainement et écrit avec Christelle Not, Claude Hillaire-Marcel et André Poirier. L'intervalle correspondant au Dryas Récent présente une forte excursion isotopique vers des sources canadiennes, dans deux carottes arctiques, et confirmerait donc un drainage de la calotte Laurentienne par le Nord, vers l'océan Arctique.

REMERCIEMENTS

« Ever tried. Ever failed. No matter. Try again. Fail again. Fail better. »

Samuel Beckett - *Worstward Ho*

On investit beaucoup de sa personne dans une thèse et ceci ne paraît pas nécessairement dans un manuscrit, si ce n'est ici. Je me permets donc une petite touche personnelle qui sera sans doute illustrée par le désordre avec lequel cela sera écrit.

Je tiens à remercier mes directeurs de thèse Claude Hillaire-Marcel, Jean Carignan et Laurie Reisberg. Tout d'abord pour votre confiance dans ce projet, de ma deuxième année de *master* en chimie analytique à un doctorat en géochimie isotopique appliquée à la paleocéanographie, ça fait un bond. Je tiens à vous remercier de votre soutien, de votre présence et du temps que vous m'avez consacré tout au long de ces années. Je vous remercie de m'avoir permis de partir en mission océanographique aux portes de l'Arctique, ce fut une expérience fantastique et inoubliable. Je vous remercie de m'avoir poussée à communiquer à travers les congrès, malgré mes réticences initiales, ce fut toujours des expériences enrichissantes. Enfin, je tiens à vous remercier de m'avoir permis de découvrir le Québec.

Ma thèse s'étant déroulée en cotutelle, il y a de nombreuses personnes que je tiens à remercier. Chronologiquement, au CRPG je tiens à remercier la Lolotte,...Catherine Zimmermann. Grande prêtresse du Tims, toi la première m'a initié à ses secrets. Je te remercie de m'avoir montré et enseigné tant de choses. Je te remercie aussi de m'avoir humiliée avec tes « zimades », de m'avoir conseillée si souvent, d'avoir partagé mes croissants au Tims, de m'avoir tenu compagnie durant les analyses, et pour ces longues discussions pendant mes innombrables pauses dans ton bureau. Je tiens à remercier Lolo, Laurent Zimmermann pour son aide avec l'échantillon #15, pour ses pâtes bolo, et pour tous ces bons moments de détentes. Je voudrais remercier toute la famille Zimmermann, Thomas, Sophie, Catherine et Laurent pour leur gentillesse et leur accueil lorsque j'étais sans toit.

Je remercie Christophe Cloquet pour son aide et ses conseils. Je remercie également Christiane pour sa gentillesse. Je remercie mes camarades de bureau Johan, Nicolas et Alice pour ces moments bien sympathiques. Je remercie également Mag, Marc-O, Anne-Sophie,

Maxence et Lise pour ces moments hors laboratoires. Enfin je remercie toutes les personnes du CRPG pour leur accueil.

À Montréal je tiens à remercier tout particulièrement Christelle, Benoît et Sandrine. Après tout ce que vous avez fait pour cette thèse, je vous consacre un paragraphe. Dans le désordre. Christelle je te remercie de ton accueil dans les murs du Geotop, de tes conseils sans lesquels j'aurais très certainement beaucoup plus de cheveux blancs, de ta gentillesse et des innombrables relectures que tu as fait sur ma prose. Benoît, je te remercie pour ton accueil, pour toutes ces discussions qui m'ont bien aidée, pour m'avoir accueillie dans le bureau de la joie et pour tous ces moments bien sympa qu'il y a eu. Je te remercie de m'avoir fait découvrir de la bonne musique et iTunes...enfin peut-être pas pour iTunes vu l'argent que j'y ai laissé ! Je te remercie pour toutes ces bières partagées. Sandrine, je te remercie pour toutes les pauses que j'ai faites dans ton bureau, pour m'avoir fait découvrir des perles sur internet, pour m'avoir offert ton porte-monnaie Ziplock, pour avoir si bien coordonné ma fin de thèse et pour avoir approuvé ma décision de laisser un bol de bière sur le bureau de Benoît. Je vous remercie tous les trois pour toutes ces bonnes soirées, pour toutes les pauses café qui, mine de rien, on bien fait avancer cette thèse. Je vous remercie de cette fin semaine dans le Vermont. Je vous remercie tout particulièrement pour votre carte postale qui, je pense, ne sera jamais égalée ! Enfin, je remercie spécialement Sandrine pour nous avoir fait traverser Times Square en auto et pour nous avoir fait passer la frontière avec D'LA BIÈRE !!!!

Je tiens à remercier également Bassam Ghaleb et André Poirier. Je vous remercie pour tous vos conseils, pour avoir toujours répondu à mes questions, et je sais qu'il y en a eu beaucoup. Je vous remercie de m'avoir si souvent aidé au lab ou au spectro.

Je remercie tous les amis du 7e, Émilie et Nico pour les virées dans les Adirondacks, Olivia *my partner in crime*, Laurence, Dimitri, Quentin et Flamoutche pour leur bonne humeur belge, Sky pour les soirées à refaire le monde, et bien sûr Audrey dont la patience et la gentillesse sont sans limites.

Je remercie mes colocataires JS et Gaïdig pour tous ces moments assez fous à l'appart, pour tous ces apéros et repas partagés, pour cette fin de semaine au chalet et tout spécialement pour la soirée ‘Vin Sans Fromage’.

Je remercie Anne de Vernal de m'avoir offert de l'assister comme auxiliaire de cours. Cette première expérience m'a énormément apporté, tant sur le travail effectué que sur la manière de l'aborder.

Je remercie Josée Savard, Diane Brabant et Nicole Turcot de m'avoir si souvent aidée dans toutes les tâches administratives. La cotutelle est une horreur administrative et j'aurais sans doute abandonné sans votre aide. Je voudrais ici exprimer mon incompréhension et ma frustration quant à la lourdeur administrative de la cotutelle. J'ai perdu patience tant de fois face à ces procédures inutiles et au manque d'informations claires et pertinentes. Je remercie donc toutes les personnes qui m'ont écouté râler, fumer, pester et m'apitoyer en raison de cette cotutelle.

Je remercie Chantal Gosselin et Maryse Henry pour tous leurs conseils. Enfin je remercie tous ceux qui, de près ou de loin, ont participé non seulement à cette thèse mais également à mon quotidien: Agnieszka, Raynald, JF, Charlou, Estelle, Ben, Jona, Chip, Arnaud et une bonne partie du personnel du Bénélux.

Je voudrais remercier Nespresso de m'avoir fourni sans jamais défaillir ma drogue de prédilection.

Je voudrais remercier tout spécialement ma famille, la tribu Maccali. Je sais que mon absence n'a pas toujours été évidente alors à mon 'grand' petit frère Romain et mon père Alain, merci. Je remercie également Anne, Nadine, Didier, Mathilde, Tachou, Sonia, Josiane, Pauline, Camille, Christian et Isabelle. Je voudrais remercier particulièrement deux personnes chères à mes yeux, mes grand-parents, dont la gentillesse n'égale que leur générosité. Merci pour tout.

Mon JB, je te remercie pour tellement de choses : pour m'avoir soutenue, pour m'avoir fait rire, pour m'avoir énervée, pour avoir été présent, pour m'avoir laissé râler si souvent, pour le quotidien, pour tous ces petits moments de vie et surtout pour cette vie sans thèse qui nous attend.

Enfin, je tiens à remercier ma mère Delia et mon frère Tony. Mais j'hésite quant à l'ordre. J'entends déjà « Ah tiens tu as remercié ton frère en premier ! ». Alors honneurs aux

dames. Je te remercie d'avoir accepté mon exil mais surtout, je te remercie de ton soutien inconditionnel. Je te remercie de m'avoir toujours encouragée et soutenue.

Tony, je te remercie pour tous ces week-ends passés chez toi, à prendre du bon temps, à en profiter et à oublier pour un moment ce doctorat. Je te remercie pour ton soutien indéfectible et pour toutes ces heures passées au téléphone où l'Atlantique ne semblait plus si grand que ça.

TABLES DES MATIÈRES

AVANT-PROPOS	ii
REMERCIEMENTS	iv
TABLES DES MATIÈRES.....	viii
LISTE DES FIGURES.....	xi
LISTE DES TABLEAUX	xiii
RÉSUMÉ	xiv
INTRODUCTION.....	1
CHAPITRE I	
Pb ISOTOPES AND GEOCHEMICAL MONITORING OF ARCTIC SEDIMENTARY SUPPLIES AND WATER-MASS EXPORTS THROUGH FRAM STRAIT SINCE THE LAST GLACIAL MAXIMUM	21
1. INTRODUCTION.....	22
2. MATERIAL & METHODS.....	24
2.1 Sampling sites and settings.....	24
2.2 Age Model	25
2.3 Analytical methods	26
2.4 Sediment sample heterogeneity.....	29
3. RESULTS.....	30
3.1 ^{137}Cs and ^{210}Pb abundances: definition of the mixed layer.....	30
3.2 The Pb budget in the sediment cores	30
3.3 Surface sediments	32
3.4 Sedimentary time series	33
4. DISCUSSION	34
4.1 The sedimentary domains	34
4.2 Temporal variations	35
4.3 Paleoceanographic implications.....	40
5. CONCLUSIONS.....	43
6. REFERENCES.....	45

7. AUXILIARY MATERIAL	73
CHAPITRE II	
GEOCHEMICAL SIGNATURES OF SEDIMENT TO DOCUMENT SEA-ICE	
AND WATER MASS EXPORTS THROUGH FRAM STRAIT SINCE THE	
LAST GLACIAL MAXIMUM.....	75
1. INTRODUCTION.....	77
2. MATERIAL & METHODS	79
2.1 Sampling sites and settings.....	79
2.2 Sample preparation and isotopic analyses	79
3. RESULTS	82
3.1 Elemental distribution.....	82
3.2 Isotopes: solid residues and coating phases	86
4. DISCUSSION	87
4.1 Elemental distribution among the fractions.....	87
4.2 Sedimentary supplies: influence of eolian material and grain size	90
4.3 Residues - Tracing variations in ice-raftered detritus through time.....	92
4.4 Leachates - The exchangeable Pb and Nd fractions	96
5. CONCLUSION	99
6. REFERENCES.....	102
7. AUXILIARY MATERIAL	127
CHAPITRE III	
CANADIAN RADIOGENIC ISOTOPE SIGNATURE OF YOUNGER DRYAS	
AGE ICE-RAFTED SEDIMENTS IN CORES FROM LOMONOSOV RIDGE AND	
FRAM STRAIT.....	129
1. INTRODUCTION.....	131
2. REGIONAL SETTING	132
3. MATERIAL AND METHODS	134
4. RESULTS	135
4.1 Core MC-18 from Lomonosov Ridge.....	135
4.2 Core MC16 from Fram Strait	136
5. DISCUSSION	136

6. CONCLUSION	138
7. REFERENCES	140
8. AUXILIARY MATERIAL	152
CONCLUSION	156

LISTE DES FIGURES

INTRODUCTION

Figure 1 : Carte bathymétrique de l'océan Arctique	2
Figure 2 : Circulation arctique des eaux a) de surface, b) intermédiaires et c) profondes	5
Figure 3 : Carte bathymétrique du détroit de Fram	6
Figure 4 : Origines et mécanismes de transport des éléments dans l'océan Arctique.	9

CHAPITRE I

Figure 1: Bathymetric map of Fram Strait and surface sample locations.....	65
Figure 2: Age model of depth vs calibrated age for core MC16.....	66
Figure 3: Pb/Al ratios in the bulk sediment and in the detrital residue.....	67
Figure 4: Th/Zr, Th/Pb and $^{206}\text{Pb}/^{204}\text{Pb}$ ratios of surface sample detrital residues and Th/Pb ratios of bulk fractions	68
Figure 5: Th/Zr and $^{206}\text{Pb}/^{204}\text{Pb}$ profiles of cores MC04 and MC16 against depth.....	69
Figure 6: $^{208}\text{Pb}/^{206}\text{Pb}$ vs. $^{206}\text{Pb}/^{204}\text{Pb}$ of leachates and residues from core MC16.....	70
Figure 7: $^{208}\text{Pb}/^{206}\text{Pb}$ vs. $^{206}\text{Pb}/^{204}\text{Pb}$ diagram along with data from the literature.....	72
Figure 8: ^{210}Pb activity (dpm/g) and $^{210}\text{Pb}/^{204}\text{Pb}$ ratio.....	74

CHAPITRE II

Figure 1 : Map of the Arctic during the LGM (Left), bathymetric map of the Fram Strait (top right) and cross section of the Fram Strait (bottom right)	118
Figure 2 : Profiles of Al contents and selected major and trace element contents normalized to Al in residues and bulk fractions	119
Figure 3 : a) Weight % carbon content in the bulk fraction and b) $\delta^{13}\text{C}$ of organic C from the bulk fraction.....	121
Figure 4 : REEs from a.) the leachates ; b.) the residues and c.) the bulk fraction	122
Figure 5 : Isotopic profile of $^{206}\text{Pb}/^{204}\text{Pb}$ ratios, ϵ_{Nd} , $^{87}\text{Sr}/^{86}\text{Sr}$ ratios for residues and leachates from core MC16	123
Figure 6 : a) ϵ_{Nd} vs $^{87}\text{Sr}/^{86}\text{Sr}$ diagram and b) $^{208}\text{Pb}/^{206}\text{Pb}$ vs. $^{206}\text{Pb}/^{204}\text{Pb}$ diagram	124

Figure 7 : a) Map of the Arctic during LGM and b) with the proposed sea-ice conditions after the YD	125
Figure 8 : Nd isotope compositions of leachates.....	126
Figure 9: Analytical procedure followed	127
Figure 10: Average μ grain-size and coarse fraction distribution of core MC16	128

CHAPITRE III

Figure 1: Bathymetric map of the Arctic	147
Figure 2: Nd- and Sr- isotopic composition of bulk samples from the Lomonosov Ridge and of residues from Fram Strait.....	148
Figure 3: Nd- vs Sr-isotopes from core MC-18.....	149
Figure 4: Nd- vs Sr-isotopes from core MC16	150
Figure 5: Nd- vs Sr-isotope data from core MC-18 and core MC16	151
Figure 6 : Nd- vs Sr-isotopes diagram	155

LISTE DES TABLEAUX

CHAPITRE I

Table 1 : Site locations of surface samples	52
Table 2 : ^{210}Pb and ^{137}Cs activity data from the bulk sediment from core MC16	52
Table 3 : Elemental and Pb isotopic data from total, detrital and leachable fractions from core MC16	53
Table 4 : Elemental and Pb isotopic data from total, detrital and leachable fractions from duplicate samples from core MC16	57
Table 5 : Elemental and Pb isotopic data from total, detrital and leachable fractions from core MC04	60
Table 6. Elemental and Pb isotopic data from total, detrital and leachable fractions from surface samples.....	63
Table S7: calibrated age and the corresponding depth	73

CHAPITRE II

Table 1 : Nd- and Sr-isotopic composition of residues.....	114
Table 2 : Nd- and Sr- isotopic composition of second leaching step.....	116

CHAPITRE III

Table 1 : Isotopic composition of bulk samples from the Lomonosov Ridge.....	144
Table 2 : Isotopic composition of residue samples from Fram Strait	145
Table 3: Estimated isotopic composition of residue samples from the Lomonosov Ridge...	154

RÉSUMÉ

La circulation océanique est un élément important du système climatique, notamment via les courants de surface, les *upwellings* et la formation d'eaux profondes. Les flux d'eau douce, glace de mer et courants océaniques, de l'Océan Arctique vers les mers nordiques jouent un rôle critique en ce qui a trait, en particulier, à *l'Atlantic Meridional Overturning Circulation (AMOC)*. Les facteurs contrôlant ces flux, à l'échelle géologique, sont encore partiellement méconnus. Un moyen indirect de retracer l'intensité et les schémas de circulation de la glace de mer est de retracer l'origine des sédiments transportés par la glace de mer, et sédimentés au long des grands courants de glace et d'eau douce vers l'Atlantique Nord. Il s'agit donc de tracer un flux particulaire direct, lié à la matrice des particules détritiques. Un second flux, indirect, provient des éléments dissous dans les masses d'eau, marqués par les processus d'adsorption/désorption le long des marges où les flux particulaires terrigènes sont les plus importants. L'extraction de la phase authigène d'un signal dissous par lessivage spécifique, nous a permis de documenter l'évolution des masses d'eau transitant par le détroit de Fram depuis le dernier maximum glaciaire.

Dans les deux premiers volets de notre étude, nous avons analysé la composition géochimique et les isotopes de Pb, Nd et Sr d'échantillons de surface prélevés le long d'un transect NE-SO dans le détroit de Fram. Ces analyses ont permis de définir trois domaines sédimentaires distincts : l'extrême est du détroit (i.e. la marge continentale du Svalbard), la partie est du détroit et enfin, la partie ouest du détroit. La marge continentale du Svalbard est sous l'influence des apports sédimentaires proximaux du Svalbard. La partie est du détroit reçoit du matériel sédimentaire des mers nordiques et possiblement des marges russes (e.g. mer de Barents et mer de Kara). Enfin, la partie ouest du détroit est sous l'influence des courants océaniques en provenance de l'océan Arctique. La carotte MC16, située dans le centre du détroit, est sous l'influence principale des masses d'eaux et de la glace de mer arctiques malgré et remonte jusqu'au dernier maximum glaciaire. Des recirculations dans la mer du Groenland peuvent influencer le régime courantologique du détroit de Fram, notamment lorsque ces gyres s'étirent vers le nord en période interglaciaire. Les sédiments de cette carotte (MC16) ont été lessivés afin de récupérer les fractions détritique (résidus) et échangeable (lessivats).

La composition élémentaire des sédiments du détroit de Fram a permis de répartir les éléments en trois groupes : terrigènes ; biogéniques et authigènes. La matière organique délivrée de manière discontinue aurait, par modifications des conditions d'oxydo-réduction, entraîné la redistribution de certains éléments tels que le manganèse et le molybdène. Le fer quant à lui, présente une mobilité moins importante que celle du manganèse et ne semble pas avoir subi de redistribution majeure. Le plomb et le néodyme incorporés dans les hydroxydes de fer n'auraient été que peu ou pas redistribués, validant ainsi la pertinence des analyses de lessivats le long de la colonne sédimentaire.

Les rapports $^{206}\text{Pb}/^{204}\text{Pb}$ et $^{208}\text{Pb}/^{206}\text{Pb}$ ainsi que les isotopes de Nd et Sr de la fraction détritique définissent deux tendances (A et B) correspondant respectivement aux intervalles pre- et post-Dryas Récent. Une revue de la littérature nous a permis d'identifier la signature isotopique de trois sources majeures d'*Ice Rafted Detritus (IRD)*, les marges continentales russes, canadiennes et groenlandaises. La tendance A (pré-Dryas Récent) reflète l'influence des marges canadiennes et des marges russes occidentales (mers de Barents et de Kara),

régions occupées alors par de larges calottes de glace : les calottes Laurentienne et Innuitienne en Amérique du Nord et la calotte Eurasienne de la Scandinavie aux mers de Barents et Kara. Une excursion isotopique est enregistrée à ~19.8 ka BP et présente une composition isotopique vers le pôle russe, suggérant quelques instabilités de la calotte Eurasienne. Les échantillons de l'Holocène présentent des compositions isotopiques moins variables provenant de sources plus diverses : les marges canadiennes, les marges des mers Est Sibérienne et de Chukchi ainsi que des marges groenlandaises. L'intervalle du Dryas Récent (~12.9-11.6 ka BP) est marqué par une excursion isotopique vers le pôle canadien suggérant un drainage via l'océan Arctique du lac proglaciaire Agassiz.

La composition isotopique de la fraction lessivable est liée aux processus d'échange de surface (*boundary exchange processes*), aux sites à flux particulaire élevé. Les masses d'eau acquerraient leur signature isotopique par échange avec les flux particulaires le long des marges continentales canadiennes et russes. Cette étude illustre la complémentarité des informations issues de l'analyse des fractions héritées (résidus) et échangeables (lessivats) dans les sédiments du détroit de Fram.

Dans le troisième chapitre, nous nous sommes plus particulièrement intéressés au Dryas Récent, épisode froid de la dernière déglaciation qui s'est produit entre 12.9 et 11.6 ka BP. Cet événement est un des mieux documentés à l'égard de son impact climatique. Un drainage du lac proglaciaire Agassiz dans l'Atlantique Nord, via le Saint-Laurent, est fréquemment évoqué comme cause du Dryas Récent. Cet apport d'eau douce dans l'Atlantique Nord aurait provoqué un ralentissement de l'*AMOC* et donc un refroidissement aux moyennes et hautes latitudes de l'hémisphère nord. Toutefois, un passage par le nord via la rivière Mackenzie aurait été plus efficace pour ralentir l'*AMOC*. L'étude de deux carottes prélevées dans le centre du bassin Arctique (Ride de Lomonosov) et dans le détroit de Fram a mis en évidence une forte augmentation de la sédimentation lors du Dryas Récent. Ce matériel sédimentaire présente une signature similaire à celle des marges canadiennes. Nos résultats confirment l'hypothèse d'un événement paléocéanographique dans l'Arctique durant le Dryas Récent et révèlent également de profonds changements de la circulation arctique suite à cet événement. Le changement de source des *IRD* après le Dryas Récent suggère une modification de la circulation de la glace de mer.

Mots clés : Océan Arctique ; Paleocéanographie ; Sédiments ; Isotopes Radiogéniques

INTRODUCTION

Le climat se définit comme un état moyen de l'atmosphère sur une période de temps donnée, en termes de températures, de précipitations ou encore d'humidité (Deconinck, 2006). Les échanges entre les différents réservoirs thermiques (e.g. atmosphère et océan) régissent le climat, mais leur variabilité temporelle reste cependant encore partiellement inconnue. Sous l'effet de l'insolation, les océans emmagasinent de l'énergie et constituent le plus grand réservoir de chaleur (Cronin, 1999). Ils jouent donc un rôle prédominant dans le système climatique. Cette chaleur est alors redistribuée depuis les basses latitudes, jusqu'aux hautes. L'intensité et les schémas de circulation océanique ont un contrôle direct sur la redistribution de chaleur dans l'océan et les échanges vers l'atmosphère donc, *in fine*, sur le système climatique lui-même.

Ainsi, dans l'Atlantique Nord, après transfert de la chaleur vers l'atmosphère, les eaux de la dérive nord-atlantique se densifient. Par suite, cette masse d'eau de l'Atlantique Nord pénètre par subduction dans l'océan Arctique, sous la masse d'eau superficielle de l'Arctique, moins salée. Le budget d'eau douce exportée de l'Arctique vers l'Atlantique Nord a donc un impact direct sur la stratification de la colonne d'eau de l'Atlantique Nord et sur la formation d'eaux intermédiaires et profondes et donc, sur le climat.

On se réfère généralement à l'*« amplification arctique »* pour exprimer l'amplification de la réponse thermique de l'Arctique par rapport à celle de l'ensemble du monde. De par ses caractéristiques propres (localisation au pôle nord, importance des marges continentales, présence de glace de mer, etc.), l'océan Arctique est sensible aux changements internes du système climatique. La compréhension des boucles de rétroactions, positives et/ou négatives (e.g. l'albédo) ainsi que celle des mécanismes reliés à ces boucles de rétroactions est donc cruciale.

L'océan Arctique



Figure 1 : Carte bathymétrique de l'océan Arctique (<https://sfb574.geomar.de/gmt-maps>). Les noms des mers arctiques sont indiqués en bleu, ceux des principales rivières, en rouges, ceux des bassins océaniques des ridges sous-marins respectivement en gris et en noir.

Principales caractéristiques

L'océan Arctique peut être défini comme étant de type « méditerranéen », c'est à dire comme un océan semi clos et dont les échanges avec l'océan global sont limités (Fig. 1). L'océan Arctique est relié à l'océan Pacifique par le détroit et la mer de Béring, et à l'océan Atlantique, par le détroit de Fram, les mers nordiques, la mer de Barents, et également par la

baie de Baffin via l'archipel arctique Canadien (Darby et al., 2006). L'océan Arctique a une superficie d'environ $9.4 \times 10^6 \text{ km}^2$ dont près du tiers est constitué de marges continentales (Jones, 2001). La ride sous-marine de Lomonosov, qui s'étire de l'Amérique du Nord à la Sibérie, sépare le bassin amérasien (canadien) du côté Pacifique, d'une part, et le bassin eurasien du côté Atlantique, d'autre part. Chacun de ces bassins est lui-même subdivisé par des rides sous-marines. La ride de Nansen-Gakkel sépare les bassins eurasiens d'Amundsen au nord et de Nansen plus au sud. Le bassin de Makarov et le bassin du Canada sont séparés par la ride Alpha-Mendeleev dans le bassin amérasien (Herman, 1974; Stein, 2008a, b).

Propriétés des masses d'eau arctiques

La colonne d'eau de l'océan Arctique se stratifie en eaux i) de surface (Fig. 2a), ii) intermédiaires (Fig. 2b) et iii) profondes (Fig. 2c) :

- La *Polar Mixed Layer* (PML : couche polaire de mélange), de 30 à 50 m de profondeur, est caractérisée par de faibles salinités en raison d'importants apports d'eau douce des rivières sibériennes et de la rivière Mackenzie. Ces apports représentent environ 10% des flux fluviaux mondiaux. L'*halocline arctique*, pouvant atteindre 200 m de profondeur dans le bassin amérasien, comprend des eaux froides peu salées et stratifiées de diverses provenances (Pacifique, Atlantique et glace de mer; Rudels et al., 2004) et limite les échanges avec les masses d'eau plus profondes.
- L'*Atlantic Layer* (AL : couche atlantique, température potentielle $\theta^\circ > 0^\circ\text{C}$; salinité $S \sim 34.85$) est une masse d'eau intermédiaire présente dans l'ensemble du bassin arctique, entre 200 et 800 m de profondeur environ. Cette couche atlantique correspond au prolongement du *North Atlantic Current (NAC)* qui se refroidit légèrement en entrant dans le bassin arctique via l'est du détroit de Fram. Une branche de la même masse d'eau atlantique pénètre via la mer de Barents et rejoint la branche passant par le détroit de Fram. Par la suite, celles-ci longent la marge continentale sibérienne en une boucle cyclonique (Jones, 2001; Rudels et al., 2004).
- Les masses d'eaux profondes représentent près de 60% du volume total de l'océan Arctique (Stein, 2008a, b). La présence de la ride de Lomonosov limite le mélange des eaux profondes entre les deux bassins. Dans le bassin amérasien (canadien) la *Canadian Basin Deep Water (CBDW)* est plus chaude et plus salée ($\theta^\circ \sim 0.5^\circ\text{C}$;

$S>34.95$), que l'*Eurasian Basin Deep Water* (EBDW : $\theta^{\circ}\sim0.7^{\circ}\text{C}$; $S>34.94$) dans le bassin eurasien (Jones et al., 1995).

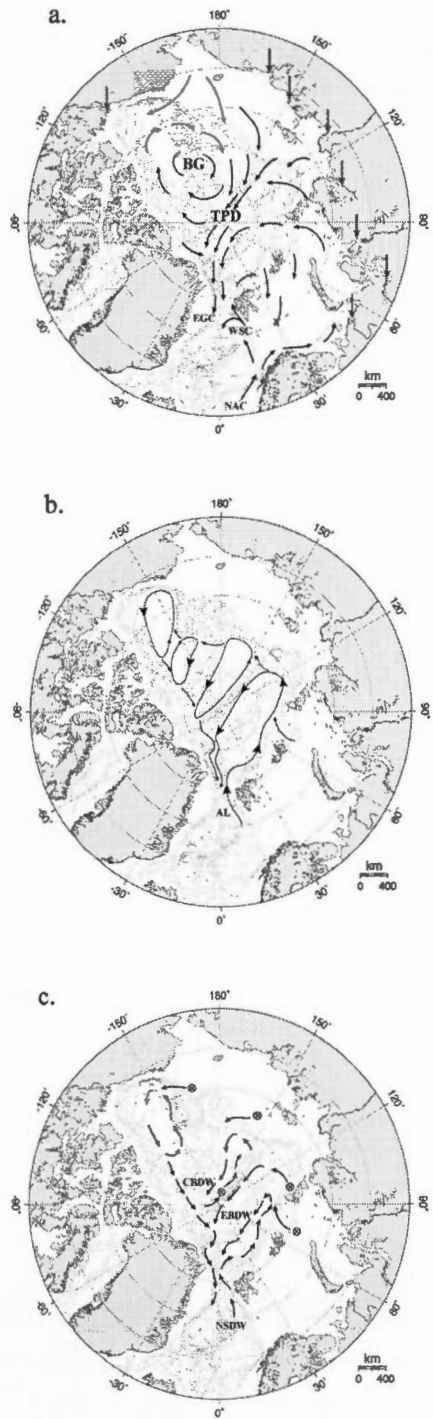


Figure 2 : Circulation arctique des eaux a) de surface, b) intermédiaires et c) profondes. Les cercles croisés indiquent le lieu de plongement des masses d'eau (carte bathymétrique <https://sfb574.geomar.de/gmt-maps>).

En terme de transport, l'océan Atlantique est le principal « échangeur » de masses d'eau avec l'océan Arctique puisqu'en moyenne, plus de 60% des apports océaniques proviennent de l'Atlantique Nord, via le détroit de Fram et la mer de Barents. De même, plus de 50% des flux sortant de l'Arctique transitent via le détroit de Fram (Dickson et al., 2007). Étant le seul passage pour les eaux profondes, entrantes et sortantes, le détroit de Fram constitue une région clé pour déterminer l'échange de masses d'eau entre l'océan Arctique et l'océan mondial.

Le budget sédimentaire de l'Océan Arctique, tel que récemment estimé par Macdonald et Gobeil (2011), montre qu'actuellement, en période interglaciaire, deux tiers des apports sédimentaires sont issus de l'érosion costale et les rivières délivrent le tiers restant. Les autres sources sédimentaires (e.g. apports éoliens, apports pacifiques et atlantiques) sont mineures. En termes de déposition, près de 66% des apports se déposent sur les vastes marge continentales et 24% dans les bassins profonds. Les exports sédimentaires par les courants océanographiques et la glace de mer représentent près de 10% des exports totaux. Compte tenu des caractéristiques physiques de l'Océan Arctique, il est facilement envisageable que ces apports(exports sédimentaires aient pu changer en période glaciaire, où notamment un tiers de l'aire de l'Arctique correspondant aux marge continentales était émergé.

Le détroit de Fram : principale voie de communication entre l'Atlantique Nord et l'océan Arctique

Large de 600 km, le détroit de Fram sépare le Groenland de l'archipel du Svalbard, entre 76°N et 82°N. La région comprend des plateaux continentaux, à la fois sur les marge est du Groenland et ouest du Svalbard, et des pentes continentales qui se poursuivent jusqu'aux plaines abyssales (~2600m; Winter et al., 1997). Les rides de Mohns, de Knipovich et de Gakkel dans le bassin eurasien de l'océan Arctique, correspondent à l'extension vers le nord de la ride médio-Atlantique (Baturin et al., 1994).

Les eaux chaudes et salées ($S>34.9$; $\theta>3^{\circ}\text{C}$) du *NAC* entrent dans l'océan Arctique via la mer de Barents ($1.5\text{-}2 \text{ Sv}$, $1\text{Sv} = 10^6 \text{ m}^3/\text{s}$) et le secteur est du détroit de Fram (1-1.5 Sv). Le *West Spitsbergen Current (WSC)* correspond au prolongement du *NAC* et transite vers le Nord, à l'ouest de l'archipel du Svalbard ($S>34.9$; $\theta>3^{\circ}\text{C}$). Ce sont des eaux froides et salées qui ressortent dans la partie ouest du détroit de Fram (*East Greenland Current, EGC* : $3\text{-}3.5\text{Sv}$; $S\sim34.9$; $\theta<0^{\circ}\text{C}$), puis entrent dans l'Atlantique Nord par le détroit du Danemark où elles forment la partie la plus dense de la *North Atlantic Deep Water (NADW)*. Une partie du *WSC* recircule vers le sud-ouest du détroit, il s'agit du *Return Atlantic Current (RAC)* (Dickson et al., 2007; Fahrbach et al., 2001; Jones, 2001; Jones et al., 1995; Rudels et al., 2005; Rudels et al., 2000).

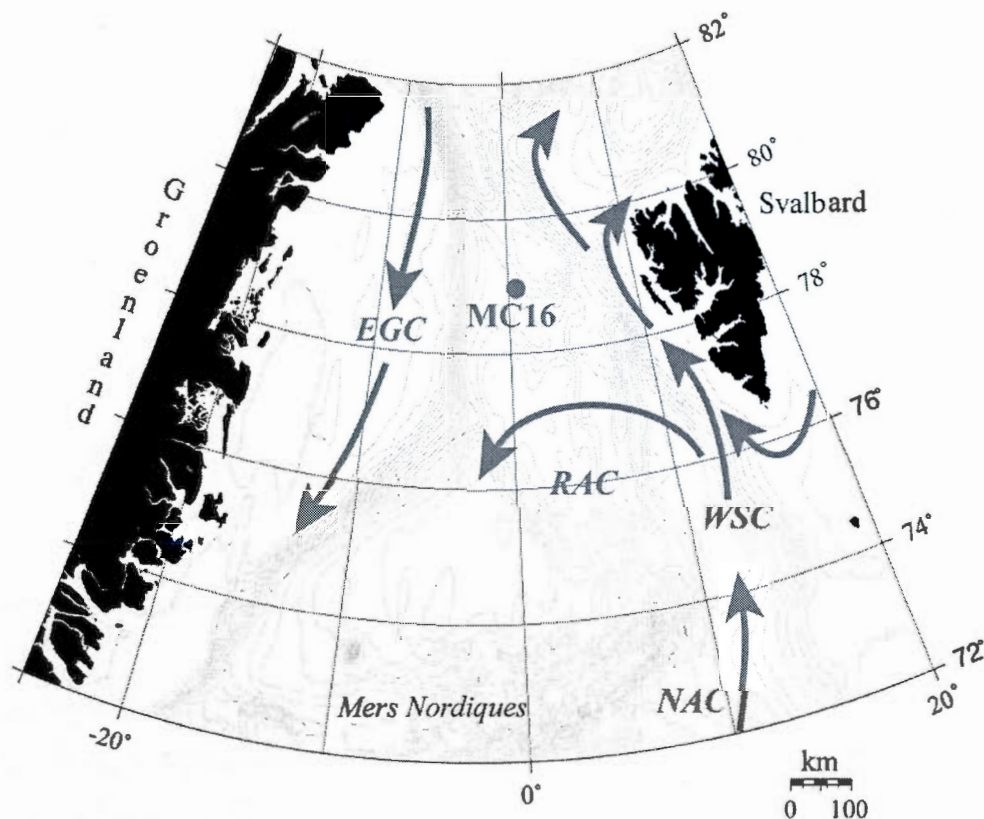


Figure 3 : Carte bathymétrique du détroit de Fram (<https://sfb574.geomar.de/gmt-maps>) avec les principaux courants océaniques : i) Atlantique (rouge) et ii) Arctique (bleu). EGC : East

Greenland Current ; RAC : Return Atlantic Current ; WSC : West Spistbergen Current ; NAC : North Atlantic Current

Les exports d'eau douce Arctiques

Tel que mentionné précédemment, les exports arctiques ont un impact direct sur la circulation océanique et donc sur le climat. Les détroits de Nares, d'Hudson et de Fram sont les trois exutoires de l'Arctique. Cependant en période glaciaire, seul le détroit de Fram permet l'exportation d'eau douce depuis l'Arctique. Celle-ci s'effectue à la fois sous forme d'eau, essentiellement de surface, et de glace de mer. Actuellement, la glace de mer est régie par deux courants principaux : la Gyre de Beaufort et la dérive trans-polaire (ou *Trans-Polar Drift*). La Gyre de Beaufort est une gyre anti-cyclonique, localisée principalement au-dessus du bassin ouest, à l'intérieur de laquelle la glace peut circuler plusieurs années avant d'être prise en charge par la dérive trans-polaire. Cette dernière transporte la glace de mer depuis les marges sibériennes jusqu'aux mers nordiques via le détroit de Fram. Ces courants de glace sont régis par les vents et leur intensité varie en fonction des conditions de pression atmosphérique qui règne aux hautes latitudes (Darby et al., 2006; Serreze and Barry, 2005; Stein, 2008a, b).

Par exemple, en hiver, des zones de basse pression sur l'Islande et sur les îles Aléoutiennes entraînent une Gyre de Beaufort plus active et donc une exportation de glace de mer plus importante qu'en été. En effet, en été, l'Arctique est une zone de basse pression réduisant la vigueur de la Gyre de Beaufort. Cette variabilité, mise en évidence à l'échelle saisonnière, a pu également changer au cours des temps géologiques, notamment entre les périodes glaciaires et inter-glaciaires (Serreze and Barry, 2005).

La glace de mer se forme principalement le long des marges continentales et en particulier dans la zone du plateau continental de la mer de Sibérie (cf. *sea ice factory* ou « usine de glace de mer »). En effet, les faibles profondeurs ainsi que les apports fluviaux importants créent une couche de surface de faible salinité facilitant la formation de la glace. Lors du gel, des particules en suspension, ou arrachées le long du littoral, sont incorporées à la glace de mer et sont transportées jusqu'au lieu de fonte (Darby et al., 2006; Stein, 2008a, b). Ainsi la sédimentation du bassin arctique est-elle directement liée aux décharges de glace de mer et d'icebergs.

Méthode : le traçage isotopique

La paleocéanographie emploie de nombreux outils dont la mesure des compositions chimique, minéralogique, physique et isotopique des sédiments. Toute caractérisation du sédiment donne des indications sur son origine, les mécanismes de transport mis en jeu mais également les altérations subies durant et après la sédimentation (i.e. diagenèse précoce et/ou tardive ; Fig. 4). La détermination des sources sédimentaires renseigne sur les courants océaniques et, dans le cadre de ce projet de thèse, sur les trajectoires de la glace de mer. Le traçage des circulations océaniques par les isotopes radiogéniques fut proposé, dès 1978, par O'Nions et al. (1978), sur la base du système Sm-Nd. Le principe général du traçage isotopique repose sur les rapports spécifiques des compositions isotopiques des roches, en fonction de leur histoire (formation, âge, type, etc.; e.g. Goldstein and Hemming, 2003). La mesure de ces rapports ainsi que la connaissance de la géologie des terrains adjacents permet de relier les sédiments aux roches mères, ou sources, dont ils sont issus.

Les isotopes radiogéniques sont ainsi couramment employés comme traceurs géochimiques dans les sédiments marins (Abouchami et al., 1999; Baskaran, 2001; Bayon et al., 2004; Eisenhauer et al., 1999; Fagel and Hillaire-Marcel, 2006; Fagel et al., 2002; Frank, 2002; Gartside, 1996; Grousset et al., 2001; Haley et al., 2008; Innocent et al., 2000; Land Farmer et al., 2003; McManus et al., 2004; O'Nions et al., 1978; Tütken et al., 2002; Winter et al., 1997). Les processus biologiques et de dissolution ne modifient pas ou peu les abondances des isotopes radiogéniques. Ceux-ci peuvent donc être considérés comme de bons marqueurs de sources et de trajectoires des courants océaniques (Frank, 2002; Goldstein and Hemming, 2003). Les méthodes de séparation, de purification et d'analyse sont maintenant bien établies et décrites dans les chapitres 1 et 2.

Une seconde approche basée sur les isotopes radiogéniques et utilisée en océanographie est la détermination de la composition isotopique d'éléments dissous dans l'eau de mer. Les éléments traces sont introduits dans l'océan via les rivières (sous forme particulière, dissoute et/ou colloïdale), transportés sous forme de fines poussières par les vents (avec dissolution partielle ou totale dans l'océan) et/ou par les vents hydrothermaux (Fig. 4). Le néodyme (Nd) et le plomb (Pb) sont des traceurs paleocéanographiques particulièrement intéressants dans la mesure où leur temps de séjour dans l'océan est inférieur

au temps de mélange global (~ 1500 a; Broecker, 1991) et permettent donc de tracer l'évolution des masses d'eau.

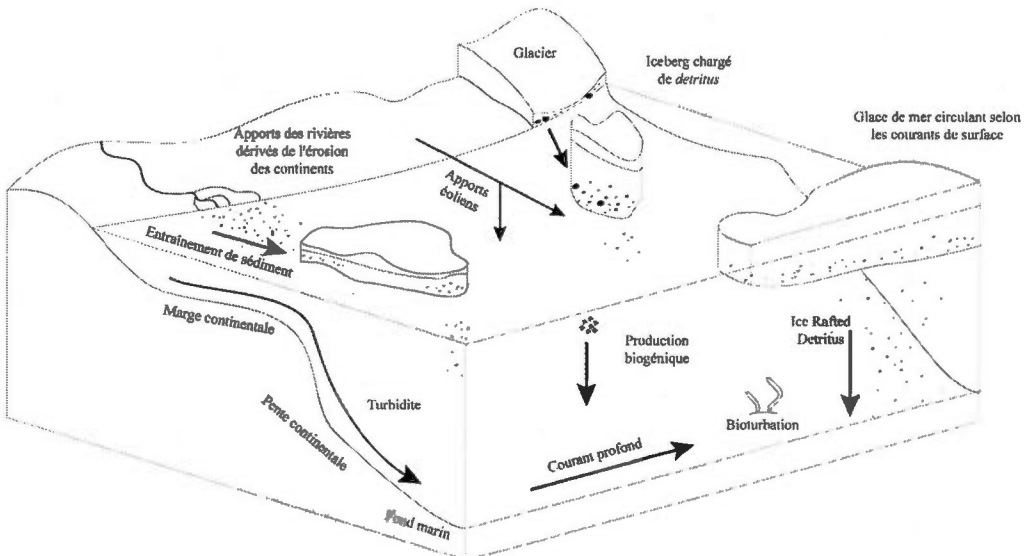


Figure 4 : Origines et mécanismes de transport des éléments dans l'océan Arctique.

Le Nd est réactif aux particules et son temps de séjour dans l'océan est relativement court (quelques centaines d'années; Tachikawa et al., 1999). Le Nd est semi-conservatif dans l'océan et a été largement employé comme traceur océanographique (Andersson et al., 2008; Jeandel et al., 2007; Lacan and Jeandel, 2004a, b, c, 2005a, b; Porcelli et al., 2009) et paleocéanographique (Bayon et al., 2004; Gutjahr et al., 2008; Martin et al., 2010; O'Nions et al., 1978; Piotrowski et al., 2004, 2005; Piotrowski et al., 2008; Piotrowski et al., 2000; Rutberg et al., 2000). Les isotopes du Nd dans l'eau de mer sont propres à une masse d'eau donnée et reflètent en partie la nature des terrains adjacents. Ainsi, l'Atlantique Nord présente les compositions les moins radiogéniques (i.e. ϵ_{Nd} très négatives) reflétant des croûtes continentales anciennes, le Pacifique présente des compositions plus radiogéniques (i.e. ϵ_{Nd} élevées) influencées notamment par le volcanisme, et enfin, l'océan Indien présente des compositions intermédiaires entre les deux bassins précédents. L'absence de corrélation entre les profils de concentration et de composition isotopique a permis de mettre en évidence le « paradoxe du Nd » (Bertram and Elderfield, 1993; Jeandel et al., 1995; Jeandel et al., 1998; Tachikawa et al., 2003; Tachikawa et al., 1999). En effet, alors que les isotopes de Nd

semblent indiquer un mélange binaire entre deux pôles principaux (nord et sud), les teneurs en Nd ne présentent pas le même comportement. Afin de concilier concentration et composition isotopique, l'équipe de Catherine Jeandel a, la première, proposé un échange entre Nd dissout et Nd particulaire, appelé *Boundary Exchange Process* ou processus d'échange de surface. Le Nd acquerrait donc sa signature isotopique au contact de particules détritiques par des processus de dissolution/adsorption (Jeandel et al., 1995; Tachikawa et al., 2003).

Le Pb est plus réactif aux particules (i.e. moins soluble) et son temps de séjour dans l'océan, de moins de 100 a (Henderson and Maier-Reimer, 2002), est plus court que celui du Nd. Cependant, depuis le début de la révolution industrielle, de fortes quantités de Pb ont été émises et incorporées dans les écosystèmes (Hamelin et al., 1990; Veron et al., 1987). Ces apports anthropogéniques rendent malaisée toute analyse de la composition isotopique naturelle du Pb, postérieurement au début de la révolution industrielle. Comme pour le Nd, la composition isotopique du plomb n'est pas affectée par des processus biologiques ou par évaporation. Toutefois, *Harlavan et al.* (2002; 1998) ont montré que l'altération de granitoïdes, par exemple en période glaciaire, larguait du plomb dissous plus radiogénique que la roche mère dont il était issu. L'effet de recul lors de la chaîne de désintégration, ajouté à l'action de l'altération mécanique glaciaire qui augmente la surface d'échange, serait à l'origine de ce phénomène. Le Pb serait donc un bon traceur de l'altération des continents avoisinants (Frank, 2002). Ceci est largement démontré dans le secteur nord-ouest de l'Atlantique nord (Gutjahr et al., 2009; Gutjahr et al., 2008; Kurzweil et al., 2010; Vance et al., 2009; Von Blanckenburg and Nägler, 2001). Cependant, sur la base de deux études (Haley et al., 2008; Maccali et al., 2011), cette caractéristique n'est pas aussi évidente dans l'océan Arctique. La possibilité d'un processus de « *Boundary exchange* » similaire en cela au Nd sera envisagée dans notre étude.

Le Strontium (Sr) quant à lui, a un temps de séjour dans l'océan bien supérieur au temps de mélange océanique global (~Ma; Faure, 1986). Sa composition peut donc être considérée comme constante à l'échelle de temps considérée. Les isotopes de Sr seront utilisés pour estimer la contribution de la fraction détritique lors de l'extraction des fractions échangeables (voir ci-après).

Les isotopes du Nd et, dans une moindre mesure, ceux du Pb, permettent ainsi de tracer les masses d'eaux océaniques. *O'Nions et al.* (1978) ont appliqué ces caractéristiques à la paleocéanographie en déterminant la composition isotopique à partir d'archives de l'eau de mer, tels que les nodules de manganèse. En effet, les terres rares sont en concentration suffisamment élevée (plusieurs $\mu\text{g/g}$) dans les oxydes de manganèse et/ou de fer pour permettre des analyses isotopiques. Toutefois, la croissance de ces nodules, de l'ordre de quelques millimètres par millions d'années (mm/Ma) ainsi que la masse minimale qui peut être physiquement prélevée limite la résolution temporelle de telles archives. La présence d'oxydes mixtes de fer-manganèse (Fe-Mn) dans le sédiment lui-même, avec des concentrations en éléments traces suffisantes, fournit une archive temporelle à plus haute résolution (la résolution étant fonction du taux de sédimentation). En effet, *Tessier et al.* (1979) ont établi une classification des éléments traces dans les sédiments marins : i) adsorbés à la surface des minéraux (i.e. échangeables ou labiles), ii) associés ou incorporés aux carbonates, iii) extraits ou « scavenged » par les oxydes de Fe-Mn, iv) liés aux composés organiques, et enfin, v) liés à la fraction résiduelle détritique. La concentration et la composition isotopique totale du sédiment représentent donc la somme de chacune de ces phases. La fraction détritique est dérivée de l'érosion de la croûte continentale ainsi que d'apports volcaniques. La fraction biogénique reflète l'activité biologique et comprend la matière organique ainsi que des restes minéralisés. La fraction authigène quant à elle correspond aux composés formés lors du dépôt (i.e. dans la colonne d'eau) ou *in situ*, via les réactions chimiques de diagénèse (précoce ou tardive), principalement contrôlées par les conditions potentiel rédox-pH (Eh-pH).

Les oxydes de Fe-Mn sont distribués de manière variable le long de la colonne sédimentaire, incorporant les éléments traces issus des masses d'eaux locales. Le signal enregistré dans cette fraction authigène est donc un "proxy" direct (i.e. un témoin) de la composition isotopique des éléments dissous dans les masses d'eau. La difficulté est cependant de pouvoir extraire spécifiquement ce signal sans induire une dissolution partielle des autres phases, notamment la phase détritique. Pour cela des protocoles de lessivage séquentiels et sélectifs ont été développés, dans un premier temps par *Chester and Hughes* (1967). Par la suite, *Tessier et al.* (1979), *Rutberg et al.* (2000), *Bayon et al.* (2002) et *Gutjahr et al.* (2007) ont proposé d'importantes améliorations.

Dans cette étude, nous avons adapté le protocole de lessivage décrit par *Gutjahr et al.* (2007) afin d'extraire la fraction échangeable principalement issue de la mise en solution des oxyhydroxydes mixtes de Fe-Mn. En effet, les sédiments arctiques présentent de fortes teneurs en oxydes de Fe-Mn (Rusakov et al., 2010).

Objectifs de la thèse

L'émergence récente de protocoles de lessivage sélectif des sédiments marins permet de distinguer les fractions labile et héritée. Ces deux fractions illustrent deux flux particulaires : l'un, direct, est lié à la matrice des particules détritiques; l'autre, indirect, provient des éléments dissous dans les masses d'eau, marqués par les processus d'adsorption/désorption le long des marges où les flux particulaires terrigènes sont les plus importants. Ces deux flux particulaires livrent ainsi des informations sur les sources "terrigène" vs "authigène" des éléments ou isotopes considérés.

Un premier objectif méthodologique de cette thèse a été la validation de l'outil géochimique et isotopique appliqué aux sédiments du détroit de Fram. Les sources terrigènes potentielles ont-elles des signatures géochimiques et isotopiques suffisamment distinctes pour pouvoir les différencier ? Nous démontrerons, dans un premier chapitre, que tel est le cas. La composition géochimique et isotopique en tant que traceur de provenance semble donc tout à fait adaptée à la région d'étude.

Au vue de la teneur élevée en oxydes mixtes de fer et manganèse dans l'océan Arctique, un second objectif méthodologique a été l'extraction sélective des deux signaux "authigène" et "terrigène". La méthode de *Gutjahr et al.* (2007) a été utilisée, mais a requis un temps de lessivage plus élevé que le proposent ces auteurs. En conséquence si le signal détritique issu de l'analyse de la fraction résiduelle est clairement déterminé, le signal « dissous » de la fraction lessivable, beaucoup plus discret, est susceptible d'être légèrement contaminé par la fraction détritique.

D'un point de vue thématique, plusieurs objectifs ont également été retenus. Le premier, surtout traité dans le second chapitre de la thèse, visait à identifier l'évolution des signaux hérité et authigène en relation avec les changements paléogéographiques et

paléocéanographiques importants qui ont marqué l'océan Arctique et les continents qui le délimitent, depuis le dernier maximum. Les implications et reconstructions paleocéanographiques des données géochimiques de l'étude renseignent sur la dynamique de la glace de mer ainsi que son évolution au cours de la déglaciation. Une des conséquences de ces reconstructions paleocéanographiques est de donner un aperçu du rôle des marges glaciaires sur cette circulation.

Enfin, nous nous sommes intéressés à un événement bref de la déglaciation, le *Younger Dryas* (YD, ou Dryas Récent). Le YD (~11.6-12.9 ka) est enregistré dans les carottes de glaces du Groenland (Alley et al., 2010; Alley et al., 1993; Dansgaard et al., 1993; Dansgaard et al., 1989) et correspondrait à un bref retour à des conditions plus froides et un fort ralentissement de la production des eaux profondes de l'Atlantique Nord. L'objectif, ici, a été de tester une hypothèse avancée par Tarasov et Peltier (2005), sur le rôle déclencheur éventuel du drainage d'un grand lac glaciaire de la calotte Laurentienne, le lac Agassiz, vers l'océan Arctique, via la vallée de la rivière Mackenzie. Ce drainage aurait eu trois conséquences notables : i) un événement sédimentaire marqué par une augmentation de la sédimentation, ii) un transport d'eau douce accru à travers le détroit de Fram, vers les mers nordiques, lieu de formation des eaux profondes, et, iii) une déstabilisation de la banquise, rendant la circulation plus dynamique.

Le premier chapitre valide ainsi l'utilisation des isotopes du Pb comme outil paléocéanographique ainsi que les reconstructions interprétées à partir de ces données. Ce chapitre a été accepté dans la revue *Paleoceanography* (doi : 10.1029/2011PA002152).

Le second chapitre détaille la distribution des éléments dans les différentes fractions étudiées et valide notamment le signal extrait de la phase authigène. Il inclut des données isotopiques complémentaires (Sr et Nd) en vue d'une meilleure identification des sources sédimentaires du circum-arctique. Ce chapitre, présenté sous forme d'article est soumis à *Quaternary Science Reviews* (*JQSR-D-11-00441*).

Enfin, le troisième chapitre met l'accent sur le Dryas récent et étaye l'existence d'un signal spécifique issu de la marge glaciaire canadienne, reflétant probablement le drainage du lac glaciaire Agassiz. Ce chapitre est présenté sous forme d'article en vue d'une soumission prochaine dans une revue spécialisée.

- Abouchami, W., Galer, S.J.G., Koschinsky, A., 1999. Pb and Nd isotopes in NE Atlantic Fe-Mn crusts: Proxies for trace metal paleosources and paleocean circulation. *Geochimica et Cosmochimica Acta* 63, 1489-1505.
- Alley, R.B., Andrews, J.T., Brigham-Grette, J., Clarke, G.K.C., Cuffey, K.M., Fitzpatrick, J.J., Funder, S., Marshall, S.J., Miller, G.H., Mitrovica, J.X., Muhs, D.R., Otto-Bliesner, B.L., Polyak, L., White, J.W.C., 2010. History of the Greenland Ice Sheet: paleoclimatic insights. *Quaternary Science Reviews* 29, 1728-1756.
- Alley, R.B., Meese, D.A., Shuman, C.A., Gow, A.J., Taylor, K.C., Grootes, P.M., White, J.W.C., Ram, M., Waddington, E.D., Mayewski, P.A., Zielinski, G.A., 1993. Abrupt increase in Greenland snow accumulation at the end of the Younger Dryas event. *Nature* 362, 527-529.
- Andersson, P.S., Porcelli, D., Frank, M., Björk, G., Dahlqvist, R., Gustafsson, O., 2008. Neodymium isotopes in seawater from the Barents Sea and Fram Strait Arctic-Atlantic gateways. *Geochimica et Cosmochimica Acta* 72, 2854-2867.
- Baskaran, M., 2001. Scavenging of thorium isotopes in the Arctic regions: Implications for the fate of particle-reactive pollutants. *Marine Pollution Bulletin* 42, 16-22.
- Baturin, D., Fedukhina, T., Savostin, L., Yunov, A., 1994. A geophysical survey of the Spitsbergen Margin and surrounding areas. *Marine Geophysical Researches* 16, 463-484.
- Bayon, G., German, C.R., Boella, R.M., Milton, J.A., Taylor, R.N., Nesbitt, R.W., 2002. An improved method for extracting marine sediment fractions and its application to Sr and Nd isotopic analysis. *Chemical Geology* 187, 179-199.
- Bayon, G., German, C.R., Burton, K.W., Nesbitt, R.W., Rogers, N., 2004. Sedimentary Fe-Mn oxyhydroxides as paleoceanographic archives and the role of aeolian flux in regulating oceanic dissolved REE. *Earth and Planetary Science Letters* 224, 477-492.
- Bertram, C.J., Elderfield, H., 1993. The geochemical balance of the rare earth elements and neodymium isotopes in the oceans. *Geochimica et Cosmochimica Acta* 57, 1957-1986.
- Broecker, W.S., 1991. The Great Ocean Conveyor. *Oceanography* 4, 7° - 89.
- Chester, R., Hughes, M.J., 1967. A chemical technique for the separation of ferro-manganese minerals, carbonate minerals and adsorbed trace elements from pelagic sediments. *Chemical Geology* 2, 249-262.

- Cronin, T.M., 1999. Principles of Paleoclimatology, 1st ed. Columbia University Press, New York.
- Dansgaard, W., Johnsen, S.J., Clausen, H.B., Dahl-Jensen, D., Gundestrup, N.S., Hammer, C.U., Hvidberg, C.S., Steffensen, J.P., Sveinbjörnsson, A.E., Jouzel, J., Bond, G., 1993. Evidence for general instability of past climate from a 250-kyr ice-core record. *Nature* 364, 218-220.
- Dansgaard, W., White, J.W.C., Johnsen, S.J., 1989. The abrupt termination of the Younger Dryas climate event. *Nature* 339, 532-534.
- Darby, D.A., Polyak, L., Bauch, H.A., 2006. Past glacial and interglacial conditions in the Arctic Ocean and marginal seas - a review. *Progress in Oceanography* 71, 129-144.
- Deconinck, J.F., 2006. Paléoclimats: l'enregistrement des variations climatiques. Edition Vuibert.
- Dickson, R., Rudels, B., Dye, S., Karcher, M., Meincke, J., Yashayaev, I., 2007. Current estimates of freshwater flux through Arctic and subarctic seas. *Progress in Oceanography* 73, 210-230.
- Eisenhauer, A., Meyer, H., Rachold, V., Tütken, T., Wiegand, B., Hansen, B.T., Spielhagen, R.F., Lindemann, F., Kassens, H., 1999. Grain size separation and sediment mixing in Arctic Ocean sediments: Evidence from the strontium isotope systematic. *Chemical Geology* 158, 173-188.
- Fagel, N., Hillaire-Marcel, C., 2006. Glacial/interglacial instabilities of the Western Boundary Under Current during the last 365kyr from Sm/Nd ratios of the sedimentary clay-size fractions at ODP site 646 (Labrador Sea). *Marine Geology* 232, 87-99.
- Fagel, N., Innocent, C., Gariepy, C., Hillaire-Marcel, C., 2002. Sources of Labrador Sea sediments since the last glacial maximum inferred from Nd-Pb isotopes. *Geochimica et Cosmochimica Acta* 66, 2569-2581.
- Fahrbach, E., Meincke, J., Østerhus, S., Rohardt, G., Schauer, U., Tverberg, V., Verduin, J., 2001. Direct measurements of volume transports through Fram Strait. *Polar Research* 20, 217-224.
- Faure, G., 1986. Principles of isotope geology, Second edit. ed. John Wiley & Sons, NY, USA.

- Frank, M., 2002. Radiogenic isotopes: Tracers of past ocean circulation and erosional input. *Reviews of Geophysics* 40, 1-1 - 1-38.
- Gartside, M., 1996. Sources et inventaire du plomb anthropique dans les sédiments de l'Océan Arctique profond, Département des Sciences de la Terre. Université du Québec à Montréal, Montréal, p. 79.
- Goldstein, S.L., Hemming, S.R., 2003. Long-lived Isotopic Tracers in Oceanography, Paleoceanography, and Ice-sheet Dynamics, In: Holland, H.D., Turekian, K.K. (Eds.), *Treatise on Geochemistry*. Pergamon, Oxford, pp. 453 - 489.
- Grousset, F.E., Cortijo, E., Huon, S., Hervé, L., Richter, T., Burdloff, D., Duprat, J., Weber, O., 2001. Zooming in on Heinrich layers. *Paleoceanography* 16, 240-259.
- Gutjahr, M., Frank, M., Halliday, A.N., Keigwin, L.D., 2009. Retreat of the Laurentide ice sheet tracked by the isotopic composition of Pb in western North Atlantic seawater during termination 1. *Earth and Planetary Science Letters* 286, 546-555.
- Gutjahr, M., Frank, M., Stirling, C.H., Keigwin, L.D., Halliday, A.N., 2008. Tracing the Nd isotope evolution of North Atlantic Deep and Intermediate Waters in the western North Atlantic since the Last Glacial Maximum from Blake Ridge sediments. *Earth and Planetary Science Letters* 266, 61-77.
- Gutjahr, M., Frank, M., Stirling, C.H., Klemm, V., van de Flierdt, T., Halliday, A.N., 2007. Reliable extraction of a deepwater trace metal isotope signal from Fe-Mn oxyhydroxide coatings of marine sediments. *Chemical Geology* 242, 351-370.
- Haley, B.A., Frank, M., Spielhagen, R.F., Fietzke, J., 2008. Radiogenic isotope record of Arctic Ocean circulation and weathering inputs of the past 15 million years. *Paleoceanography* 23.
- Hamelin, B., Grousset, F., Sholkovitz, E.R., 1990. Pb isotopes in surficial pelagic sediments from the North Atlantic. *Geochimica et Cosmochimica Acta* 54, 37-47.
- Harlavan, Y., Erel, Y., 2002. The release of Pb and REE from granitoids by the dissolution of accessory phases. *Geochimica et Cosmochimica Acta* 66, 837-848.
- Harlavan, Y., Erel, Y., Blum, J.D., 1998. Systematic changes in lead isotopic composition with soil age in glacial granitic terrains. *Geochimica et Cosmochimica Acta* 62, 33-46.

- Henderson, G.M., Maier-Reimer, E., 2002. Advection and removal of ^{210}Pb and stable Pb isotopes in the oceans: A general circulation model study. *Geochimica et Cosmochimica Acta* 66, 257-272.
- Herman, Y., 1974. Marine geology and oceanography of the arctic seas. Springer-Verlag, New York.
- Innocent, C., Fagel, N., Hillaire-Marcel, C., 2000. Sm-Nd isotope systematics in deep-sea sediments: Clay-size versus coarser fractions. *Marine Geology* 168, 79-87.
- Jeandel, C., Arsouze, T., Lacan, F., Téchiné, P., Dutay, J.C., 2007. Isotopic Nd compositions and concentrations of the lithogenic inputs into the ocean: A compilation, with an emphasis on the margins. *Chemical Geology* 239, 156-164.
- Jeandel, C., Bishop, J.K., Zindler, A., 1995. Exchange of neodymium and its isotopes between seawater and small and large particles in the Sargasso Sea. *Geochimica et Cosmochimica Acta* 59, 535-547.
- Jeandel, C., Thouron, D., Fieux, M., 1998. Concentrations and isotopic compositions of neodymium in the eastern Indian Ocean and Indonesian straits. *Geochimica et Cosmochimica Acta* 62, 2597-2607.
- Jones, E.P., 2001. Circulation in the Arctic Ocean. *Polar Research* 20, 139-146.
- Jones, E.P., Rudels, B., Anderson, L.G., 1995. Deep waters of the Arctic Ocean: origins and circulation. *Deep-Sea Research Part I* 42, 737-760.
- Kurzweil, F., Gutjahr, M., Vance, D., Keigwin, L., 2010. Authigenic Pb isotopes from the Laurentian Fan: Changes in chemical weathering and patterns of North American freshwater runoff during the last deglaciation. *Earth and Planetary Science Letters* 299, 458-465.
- Lacan, F., Jeandel, C., 2004a. Denmark Strait water circulation traced by heterogeneity in neodymium isotopic compositions. *Deep-Sea Research Part I: Oceanographic Research Papers* 51, 71-82.
- Lacan, F., Jeandel, C., 2004b. Neodymium isotopic composition and rare earth element concentrations in the deep and intermediate Nordic Seas: Constraints on the Iceland Scotland Overflow Water signature. *Geochemistry, Geophysics, Geosystems* 5.
- Lacan, F., Jeandel, C., 2004c. Subpolar mode water formation traced by neodymium isotopic composition. *Geophysical Research Letters* 31, L14306 14301-14305.

- Lacan, F., Jeandel, C., 2005a. Acquisition of the neodymium isotopic composition of the North Atlantic Deep Water. *Geochemistry, Geophysics, Geosystems* 6.
- Lacan, F., Jeandel, C., 2005b. Neodymium isotopes as a new tool for quantifying exchange fluxes at the continent-ocean interface. *Earth and Planetary Science Letters* 232, 245-257.
- Land Farmer, G., Barber, D., Andrews, J., 2003. Provenance of Late Quaternary ice-proximal sediments in the North Atlantic: Nd, Sr and Pb isotopic evidence. *Earth and Planetary Science Letters* 209, 227-243.
- Maccalli, J., Carignan, J., Hillaire-Marcel, C., Reisberg, L.C., 2011. Pb-isotopes and geochemical monitoring of Arctic sedimentary supplies and water-mass export through Fram Strait since the Last Glacial Maximum. *Paleoceanography* In Press.
- Macdonald, R.W., Gobeil, C., 2011. Manganese Sources and Sinks in the Arctic Ocean with Reference to Periodic Enrichments in Basin Sediments. *Aquatic Geochemistry*, 1-27.
- Martin, E.E., Blair, S.W., Kamenov, G.D., Scher, H.D., Bourbon, E., Basak, C., Newkirk, D.N., 2010. Extraction of Nd isotopes from bulk deep sea sediments for paleoceanographic studies on Cenozoic time scales. *Chemical Geology* 269, 414-431.
- McManus, J.F., Francois, R., Gherardi, J.M., Kelgwin, L., Brown-Leger, S., 2004. Collapse and rapid resumption of Atlantic meridional circulation linked to deglacial climate changes. *Nature* 428, 834-837.
- O'Nions, R.K., Carter, S.R., Cohen, R.S., Evensen, N.M., Hamilton, P.J., 1978. Pb, Nd and Sr isotopes in oceanic ferromanganese deposits and ocean floor basalts. *Nature* 273, 435-438.
- Piotrowski, A.M., Goldstein, S.L., Hemming, S.R., Fairbanks, R.G., 2004. Intensification and variability of ocean thermohaline circulation through the last deglaciation. *Earth and Planetary Science Letters* 225, 205-220.
- Piotrowski, A.M., Goldstein, S.L., Hemming, S.R., Fairbanks, R.G., 2005. Temporal relationship of carbon cycling and ocean circulation at glacial boundaries. *Science* 307, 1933-1938.
- Piotrowski, A.M., Goldstein, S.L., Hemming, S.R., Fairbanks, R.G., Zylberman, D.R., 2008. Oscillating glacial northern and southern deep water formation from combined neodymium and carbon isotopes. *Earth and Planetary Science Letters* 272, 394-405.
- Piotrowski, A.M., Lee, D.C., Christensen, J.N., Burton, K.W., Halliday, A.N., Hein, J.R., Günther, D., 2000. Changes in erosion and ocean circulation recorded in the Hf isotopic

- compositions of North Atlantic and Indian Ocean ferromanganese crusts. *Earth and Planetary Science Letters* 181, 315-325.
- Porcelli, D., Andersson, P.S., Baskaran, M., Frank, M., Björk, G., Semiletov, I., 2009. The distribution of neodymium isotopes in Arctic Ocean basins. *Geochimica et Cosmochimica Acta* 73, 2645-2659.
- Rudels, B., Björk, G., Nilsson, J., Winsor, P., Lake, I., Nohr, C., 2005. The interaction between waters from the Arctic Ocean and the Nordic Seas north of Fram Strait and along the East Greenland Current: Results from the Arctic Ocean-02 Oden expedition. *Journal of Marine Systems* 55, 1-30.
- Rudels, B., Jones, E.P., Schauer, U., Eriksson, P., 2004. Atlantic sources of the Arctic Ocean surface and halocline waters. *Polar Research* 23, 181-208.
- Rudels, B., Meyer, R., Fahrbach, E., Ivanov, V.V., Østerhus, S., Quadfasel, D., Schauer, U., Tverberg, V., Woodgate, R.A., 2000. Water mass distribution in Fram Strait and over the Yermak Plateau in summer 1997. *Annales Geophysicae* 18, 687-705.
- Rusakov, V.Y., Levitan, M.A., Roshchina, I.A., Spielhagen, R.F., Gebhardt, K., 2010. Chemical composition of late Pleistocene-Holocene pelagic sediments in Gakkel Ridge, Arctic Ocean. *Geochemistry International* 48, 999-1013.
- Rutberg, R.L., Hemming, S.R., Goldstein, S.L., 2000. Reduced North Atlantic Deep Water flux to the glacial Southern Ocean inferred from neodymium isotope ratios. *Nature* 405, 935-938.
- Serreze, M.C., Barry, R.G., 2005. The Arctic Climate System. Cambridge University Press, Cambridge.
- Stein, R., 2008a. Chapter One Introduction to the Arctic: Significance and History, In: Ruediger, S. (Ed.), *Developments in Marine Geology*. Elsevier, pp. 3-34.
- Stein, R., 2008b. Chapter Two Modern Physiography, Hydrology, Climate, and Sediment Input, In: Ruediger, S. (Ed.), *Developments in Marine Geology*. Elsevier, pp. 35-84.
- Tachikawa, K., Athias, V., Jeandel, C., 2003. Neodymium budget in the modern ocean and paleo-oceanographic implications. *Journal of Geophysical Research C: Oceans* 108, 3254.
- Tachikawa, K., Jeandel, C., Roy-Barman, M., 1999. A new approach to the Nd residence time in the ocean: The role of atmospheric inputs. *Earth and Planetary Science Letters* 170, 433-446.

- Tarasov, L., Peltier, W.R., 2005. Arctic freshwater forcing of the Younger Dryas cold reversal. *Nature* 435, 662-665.
- Tessier, A., Campbell, P.G.C., Blsson, M., 1979. Sequential extraction procedure for the speciation of particulate trace metals. *Analytical Chemistry* 51, 844-851.
- Tütken, T., Eisenhauer, A., Wiegand, B., Hansen, B.T., 2002. Glacial-interglacial cycles in Sr and Nd isotopic composition of Arctic marine sediments triggered by the Svalbard/Barents Sea ice sheet. *Marine Geology* 182, 351-372.
- Vance, D., Teagle, D.A.H., Foster, G.L., 2009. Variable Quaternary chemical weathering fluxes and imbalances in marine geochemical budgets. *Nature* 458, 493-496.
- Veron, A., Lambert, C.E., Isley, A., Linet, P., Grousset, F., 1987. Evidence of recent lead pollution in deep north-east Atlantic sediments. *Nature* 326, 278-281.
- Von Blanckenburg, F., Nägler, T.F., 2001. Weathering versus circulation-controlled changes in radiogenic isotope tracer composition of the Labrador Sea and North Atlantic Deep Water. *Paleoceanography* 16, 424-434.
- Winter, B.L., Johnson, C.M., Clark, D.L., 1997. Strontium, neodymium, and lead isotope variations of authigenic and silicate sediment components from the Late Cenozoic Arctic Ocean: Implications for sediment provenance and the source of trace metals in seawater. *Geochimica et Cosmochimica Acta* 61, 4181-4200.

CHAPITRE I

Pb ISOTOPES AND GEOCHEMICAL MONITORING OF ARCTIC SEDIMENTARY SUPPLIES AND WATER-MASS EXPORTS THROUGH FRAM STRAIT SINCE THE LAST GLACIAL MAXIMUM

Jenny Maccalli^{1,2}, Claude Hillaire-Marcel¹, Jean Carignan³ and Laurie Reisberg²

¹Geotop, Université du Québec à Montréal, C.P. 8888, Montréal, QC, H3C 3P8, Canada

²CRPG, 15 Rue Notre-Dame-des-Pauvres, 54501 Vandoeuvre-lès-Nancy, France

³Takuvik, CNRS, Université Laval-CEN, 2405 rue de la Terrasse, QC, G1V 0A6, Canada

Article accepté à Paleoceanography : doi 10.1029/2011PA002152

ABSTRACT

Elemental and Pb-isotope measurements were performed on leachates and residues from surface sediments and two <50 cm cores (MC04 and MC16) collected along a NE-SW transect through Fram Strait. Geochemical and isotopic properties of residues from surface sediments define three distinct spatial domains within the Strait: i) the easternmost edge of the Strait; ii) the eastern part of the Strait off the Svalbard margins; and iii) the western part of the Strait, influenced respectively by supplies from Svalbard, the Nordic seas with possible contributions from northwestern Siberian margins and sea-ice and water outflow from the Arctic. Core MC16, in domain (iii) beneath the outflowing Arctic waters, spans the LGM-Present interval. Sediments from this core were leached to obtain detrital (residues) and exchangeable (leachates) fractions. Detrital supplies to core MC16 are believed to originate mainly from melting of the overlying sea-ice and thus can be used to document changes in Arctic sedimentary sources. Detrital $^{206}\text{Pb}/^{204}\text{Pb}$ and $^{208}\text{Pb}/^{206}\text{Pb}$ ratios illustrate two mixing trends (*Trend A and B*) corresponding respectively to the pre- and post-Younger Dryas (YD) intervals. These trends represent binary mixtures with a common end-member (Canadian margins) and either a Siberian- (*Trend A*) or Greenland- (*Trend B*) margin end-member. The YD is marked by an isotopic excursion towards the Canadian end-member, suggesting a very active Beaufort Gyre possibly triggered by massive drainage of the Laurentide ice sheet. Pb-isotope compositions of leachates, thought to represent the signature of the overlying water masses, define a unique linear trend coincident with *Trend A*. This suggests that water masses acquired their signature through exchange with particulate fluxes along the Canadian and Siberian continental margins.

1. INTRODUCTION

Freshwater/sea-ice exports from the Arctic into the North Atlantic have a direct impact on the Atlantic Meridional Overturning Circulation (AMOC) and thus on the circum-Atlantic climate [Broecker, 1991; Broecker and Peng, 1992; McManus *et al.*, 2004a; Peltier *et al.*, 2006]. Fram Strait, situated between Greenland and Spitsbergen, the main and westernmost island of the Svalbard Archipelago, is the only deep gateway allowing passage of North Atlantic Water (NAW) as a sub-surface water mass into the Arctic [Rudels *et al.*,

2004]. It is also the major route of freshwater/sea-ice export into the North Atlantic and its marginal basins [Fahrbach *et al.*, 2001; Hebbeln and Wefer, 1997; Jones *et al.*, 1995; Rudels *et al.*, 2005]. Documentation of water mass exchange through this strait, using geochemical and sedimentological records in deep-sea cores, may thus help elucidate the influence of Arctic sea-ice or freshwater export on the AMOC [Birgel and Hass, 2004; Hebbeln and Berner, 1993] (Fig. 1).

Sediments in the Arctic basin are mainly derived from surrounding land masses, and delivered as suspended particulate matter and bedloads from rivers and as wind-transported dust. In shallow margins, suspended particles are incorporated in sea-ice during its formation and are transported over long distances throughout the Arctic Ocean [Darby *et al.*, 2006]. Pb isotopes in bulk sediment from deep-sea cores have proven to be useful tracers of the source areas for such detrital supplies [Fagel *et al.*, 2002; Fagel *et al.*, 2004; Haley *et al.*, 2008; Von Blanckenburg and Nägler, 2001; Winter *et al.*, 1997]. In a complementary manner, the isotopic composition of Pb of exchangeable fractions leached from sediments (i.e. the authigenic sediment fraction) can be used to trace water mass circulation. This is facilitated by the short marine residence time of Pb in its dissolved form (< 100 a) [Henderson and Maier-Reimer, 2002] which allows regional inputs to be identified. Whereas Pb isotopes are not fractionated by biological processes, recent studies have demonstrated that weathering processes can lead to some isotopic fractionation. Physically eroded rocks such as granitoids, in high latitudes, may preferentially release radiogenic Pb from damaged crystal structures [Foster and Vance, 2006; Gutjahr *et al.*, 2009; Harlavan and Erel, 2002; Harlavan *et al.*, 1998; Kurzweil *et al.*, 2010; Von Blanckenburg and Nägler, 2001]. Thus the isotopic composition of exchangeable and dissolved Pb-fractions derived from continental weathering could potentially differ from that of the detrital residue.

Trace metals are precipitated from ambient sea-water onto sinking and sedimented particles by incorporation in authigenic Fe-Mn coatings. Such coatings have been studied in the western North Atlantic [Gutjahr *et al.*, 2009; Gutjahr *et al.*, 2008] and in the Arctic Ocean itself [Haley *et al.*, 2008] following the procedure developed by Gutjahr *et al.* [2007] to specifically leach this phase. The residual detritus left after the leaching procedure is thought to represent the pure terrigenous/detrital fraction of the sediment while leachates provide information concerning water masses.

Here, we document changes in detrital supplies to marine sediments, mostly linked to Ice-Rafting Deposition (IRD), and variations in water mass geochemical properties that occurred since the Last Glacial Maximum (LGM). Our conclusions are based on Pb isotope data and a few trace element ratios, in residues and leachates from two sediment cores and surface sediments taken along a NE-SW transect across Fram Strait (Fig. 1). In a preliminary study of these samples, Carignan et al. [2008] demonstrated that several elemental ratios (e.g. Th/U, Th/Zr) and Pb isotopes in bulk sedimentary fractions from the same area are sensitive tracers of changes in sources and trajectories of Fram Strait sediments. Previously, Gobeil et al. [2001] used Pb-concentrations and -isotopic compositions of surface sediments from several Arctic and sub-Arctic basins, to document anthropogenic Pb-fluxes and -sources. In this study, we use Th/Zr ratios of bulk sediments and residues as a first criterion for identifying the source components of the terrigenous fraction. In addition we use Pb isotopes in leachates and residual sedimentary fractions to document particulate transport (sediment sources and trajectories) and exchange with carrier water masses, as well as mixing processes in surface sediment. The time frames of the two sediment cores, MC04 and MC16, encompass respectively the very late Holocene and the LGM-Present interval, and thus provide time resolution varying from the centennial to the millenial scale. We particularly concentrate our efforts on core MC16, both because this core provides a record since the LGM and because it is composed primarily of ice-rafted detritus, thus allowing reconstruction of sea-ice and water mass exports from the Arctic into the northern North Atlantic over the past ~20 ka.

2. MATERIAL & METHODS

2.1 Sampling sites and settings

The sediment cores were collected during the 2006 *WarmPast* Cruise on the R/V JanMayen along a NE-SW transect across Fram Strait [Husum, 2006a]. Ten sites (Fig. 1, Table 1) provided material that can be used to document modern particulate sources and trajectories. Here, we examine surface samples obtained from eight of these sites using box cores or multi-cores, as well as two long (40-50 cm) multi-cores, JM06-WP-04-MC (MC04) and JM06-WP-16-MC (MC16). MC04 was taken in the east, below the NAW incoming from

the Greenland, Icelandic and Norwegian (GIN) seas, whereas MC16 was taken in the west, below the outflowing Arctic waters (Fig. 1) [Dickson *et al.*, 2007; Husum, 2006a]. These cores were sub-sampled at 1 cm-intervals onboard the JanMayen. Core MC04 illustrates conditions below the West Spitsbergen Current (WSC) that enters the Arctic basin through the eastern Fram Strait area. Core MC16 is under the influence of cold Arctic waters and sea-ice flowing south. The outflowing water masses are i) at the surface, the Modified Atlantic Water (MAW), ii) in the upper subsurface, the Arctic Atlantic Water (AAW), iii) at greater depths, the Arctic Intermediate Water (AIW) and, iv) at the sea-floor, the Canadian Basin Deep Water (CBDW) and Eurasian Basin Deep Water (EBDW), which eventually merge into the North Atlantic Deep Water (NADW) [Fahrbach *et al.*, 2001; Jones, 2001; Rudels *et al.*, 2005; Rudels *et al.*, 2000].

2.2 Age Model

All ages will be presented in calibrated years BP. The age models used for establishing the chronology of the two cores are based primarily on radiocarbon ages calibrated using the Calib 6.0 curve [P. J. Reimer *et al.*, 2009]. In the absence of a consensus regarding reservoir ages within the Arctic, no reservoir age has been added to the MARINE09 calibration (ΔR of 0). MC04 chronology is based on ^{14}C dating of planktonic foraminifera assemblages [see Bonnet *et al.*, 2010 for more details]. Core MC04 (~2.5 ka-Present) displays a mean sedimentation rate of ~18cm/ka. Site MC04 is influenced by productive Atlantic waters [Dokken and Hald, 1996; Hebbeln *et al.*, 1994] and hence has a relatively high microfossil accumulation rate.

Site MC16 is influenced by Arctic waters and remains ice-covered almost all year long [Elverhøi *et al.*, 1998; Hebbeln, 2000]. As a result, most of the sediment is derived from ice-rafting processes and sedimentation rates are much lower than those of core MC04. The age model established for site MC16 is based on three ^{14}C measurements from three planktonic foraminifera assemblages [Zamelczyk *et al.*, 2010], a tephrochronological date [Zamelczyk *et al.*, 2010] and correlations with cores (MC-18 and TC-18) from the Lomonosov Ridge [Hanslik *et al.*, 2010; Not and Hillaire-Marcel, 2011a]. Cores MC-18 and TC-18, located in an intra-basin of the Lomonosov Ridge, are upstream of core MC16, on the

pathway of the merging Beaufort Gyre and Trans-Polar Drift (Fig. 1). MC-18 revealed a 5-fold higher sedimentation rate during the Younger Dryas (YD; ~12-13 ka), compared to the mean Holocene rate, that Not and Hillaire-Marcel [2011a] ascribed to enhanced sea-ice drifting along the Beaufort Gyre which deposited detrital material carrying a strong NW Canadian margin (Mackenzie River area) mineralogical signature.

In core MC16, ash grains found at 16 cm were tentatively identified as belonging to the Vedde Ash event on the basis of their geochemical characteristics. This ash deposit has been dated elsewhere at ~12.1 cal. ka [Thornalley *et al.*, 2011 ; and references therein] and thus falls near the end of the YD event. Slightly lower in the core, at a depth of 20 cm, Pb isotopes display a strong excursion towards compositions similar to that of the Mackenzie River indicating a Canadian margin source area (see below). The onset of the YD has been assigned to this excursion, which we correlate to that observed in the Lomonosov Ridge, though we recognize some circularity in this reasoning.

The age model retained for MC16 (Fig. 2) suggests a mean sedimentation rate of 2.3 cm/ka below 20 cm, i.e. for the LGM-early deglacial interval. The sedimentation rate increased to about 5 cm/ka from 20 to 14 cm, during the YD event itself. Finally, during the Holocene, it has decreased to a mean value of ~1.1 cm/ka. Unfortunately, this poorly constrained age model does not allow us to identify potential intervals of hiatus or short-term changes in sedimentation rates. However, it suggests similar ~5 fold higher sedimentation rates during the YD, compared to the Holocene, as estimated by Not and Hillaire-Marcel [2011a], upstream on the IRD route, in the Lomonosov Ridge area.

2.3 Analytical methods

2.3.1 ^{210}Pb and ^{137}Cs measurements

Bulk fractions from sediment samples were used for ^{210}Pb and ^{137}Cs measurements (Table 2 and supplements), in order to document mixing processes in surface sediments. Pb isotopes in modern sediments (Table 3) carry an anthropogenic signature [Gobeil *et al.*, 2001] and, along with ^{210}Pb and ^{137}Cs measurements, allow assessment of the maximum depth of anthropogenic inputs in the sediment and hence help define the mixed layer. Sediment subsamples were dried and ground. ^{210}Pb activities were determined by measuring the

radioactive decay of its daughter isotope ^{210}Po ($t_{1/2}=138.4$ days; $\alpha=5.30$ MeV) by alpha spectrometry [Ghaleb, 2009]. A ^{209}Po spike was added as a yield and counting efficiency tracer. Po was extracted and purified by chemical treatment and deposited on silver disks following the method of Flynn [1968]. The ^{209}Po and ^{210}Po activities were measured in a silicon surface barrier α spectrometer (EGG and ORTEC type 576A). ^{137}Cs was measured by \square -spectrometry at 66.6 keV, using a low background high-purity Ge well-detector (Canberra). IAEA-300 standard reference material was used as a counting efficiency tracer of the detector and to estimate the reproducibility ($1\square = 1\%$).

2.3.2 Separation of authigenic and residual components

Bulk sediments are composed of distinct fractions: i) exchangeable, ii) bound to carbonates, iii) bound to Fe-Mn oxides, iv) bound to organic matter, and v) the residual detrital fraction [Bayon et al., 2002; Gutjahr et al., 2007; Tessier et al., 1979]. Fe-Mn oxides are leachable phases that are thought to precipitate either during settling of particles within the water column or at the sediment/water interface, incorporating trace metals directly from the water masses. The leachable fractions may thus record properties of overlying deep-water masses, but may also include some soluble/exchangeable elements hosted by detrital phases (e.g. exchangeable metals in clay). Thus it is important to choose a leaching technique that releases "authigenic" fractions, i.e., that exchanged with or formed directly from dissolved fractions in overlying water masses. However, it is necessary to first remove the carbonate fraction, as it may have a mixed detrital-authigenic origin. The methodology we have chosen is based mostly upon techniques developed by Bayon et al. [2002] and Guthjar et al. [2007]. Sediments are first sieved through a nylon mesh with milli-QTM water to obtain fractions with grain sizes $<100\mu\text{m}$. As nearly all of the sediment is in this size range, this step serves to remove stray, unrepresentative large grains. After drying and grinding, aliquots of ca. 300 mg are accurately weighed in TeflonTM beakers. Weighing and all subsequent chemical treatment were performed in a class 100 clean lab. Carbonates are removed by adding 12mL of a Na-acetate buffer (1M - Acetic acid 1M; 52:48) and shaking at room temperature for 3 hours. Samples are centrifuged and the supernatant, containing the carbonate fraction, is removed. Residues are rinsed three times with milli-QTM water, then subjected to repeated centrifugation (typically 3 times), dried, weighed and ground in an agate mortar. 12 mL of a

solution of 0.05 M Hydroxylamine Hydrochloride (HH) - 15% acetic acid - 0.03 M Na-EDTA, buffered to pH 4 with analytical grade NaOH, is added to the residue and shaken at room temperature for 24 hours. The supernatant, which will henceforth be referred to as the leachate, is recovered, and residues are rinsed as previously described and the rinse water is added to the supernatant. The leachate obtained from this procedure is dominated by the Fe-Mn oxyhydroxyde fraction, but we cannot exclude the possibility of a minor contribution from other phases.

2.3.3 Major and trace element analyses

All subsequent analyses were performed on the <100 μm aliquot fractions. After sieving, sediment samples were dried and ground in an agate mortar. The bulk sediment powders, as well as leachates and residues obtained after carbonate and Fe-Mn oxide removal, were analyzed for major and trace elements at the *Service d'Analyse des Roches et Minéraux (SARM-CNRS)*, Nancy, France, following procedures described by Carignan et al. [2008; and references therein]. Calibration curves and accuracy controls were performed using international geological reference materials. Total concentration uncertainties were about 1% for major elements and between 5% and 10% for trace elements, depending on concentration levels.

2.3.4 Pb isotopic analyses

Pb isotopic analyses were performed on residues of the sieved (<100 μm) sediment after carbonate and Fe-Mn oxide removal, as well as on the leachates thought to represent the Fe-Mn oxide fraction. In this respect, they differ from the Pb analyses presented in the preliminary study of Carignan et al. [2008], which were performed on bulk sediment powders. For the residues, approximately 100 mg of powder were weighed and digested with a mixture of HF, HNO₃ and HCl on a hot plate at 110°C. This acid mixture was also added to the leachates, after partial evaporation, to ensure dissolution of any precipitates. Pb was extracted using anion-exchange chromatography, following Manhès et al. [1980]. Measurements were performed on a (MC)-ICP-MS Isoprobe™, at either the CRPG laboratory in Nancy, France or the GEOTOP laboratory in Montreal, Canada. In both cases, the standard reference material NIST 981 was used as a reference. Instrumental mass bias

was corrected internally after addition of SRM NIST 997 Tl solution [White *et al.*, 2000]. Nominal isotopic values used for Pb and Tl ($^{205}\text{Tl}/^{203}\text{Tl}$ of 2.3889) reference materials were taken from Thirlwall [2002]. Analytical uncertainty was estimated by repeated measurement of the Pb-Tl reference material. Calculated NIST 981 Pb-ratios indicate an overall reproducibility better than 150 ppm/amu (2*sd of the mean: $^{208}\text{Pb}/^{206}\text{Pb}$: 2.43380 ± 0.00029 ; $^{206}\text{Pb}/^{207}\text{Pb}$: 1.09308 ± 0.00012 ; $^{207}\text{Pb}/^{206}\text{Pb}$: 0.91485 ± 0.00017 ; $^{208}\text{Pb}/^{204}\text{Pb}$: 36.722 ± 0.011 ; $^{207}\text{Pb}/^{204}\text{Pb}$: 15.4974 ± 0.0047 ; $^{206}\text{Pb}/^{204}\text{Pb}$: 16.9398 ± 0.0053). Blanks for the Pb procedure in detrital residues were under 0.9 ng and represent less than 0.30% of the total amount of Pb present in the samples. Blanks for the leachate fraction represent less than 0.46% of the total Pb present.

2.4 Sediment sample heterogeneity

Before discussing the results, we address the methodological issue of the representativity/heterogeneity of glacial sediment subsamples. As illustrated in Table 4, some variability is observed, not only with varying depth, but even between distinct ~1cc subsamples taken from a single 1 cm-thick core slice. Two explanations can be suggested. The first is procedural. We can rule out biases in the mass spectrometric measurements, since analyses of the same homogenized residue powder performed in the two laboratories yield identical results within standard deviation (Table 4, samples at 19-20 cm and 39-40 cm). Incomplete digestion of certain heavy minerals could also potentially influence the measured isotopic compositions. However, the reproducibility of replicates of the same leached subsamples in different laboratories also argues against this possibility. On the other hand, since different subsamples were sieved and leached in different laboratories, we cannot exclude the possibility of small biases due to subtle procedural differences, particularly in the leaching technique, despite our efforts to use identical techniques. A more likely explanation from our point of view is that the sediments are intrinsically heterogeneous at the sampling level. All of our analyses of duplicate subsamples are from the glacial to late-glacial interval. This time period is marked by large Pb isotopic heterogeneities linked to a rapidly changing sedimentary regime (see below). Therefore, 1 cm³ of material that corresponds to several hundred years may not be representative of the mean sedimentary properties of the

corresponding layer. To get around this issue, in the discussion we use mean values from available measurements for a given layer, and underscore the statistical uncertainties inherent in this type of sampling.

3. RESULTS

3.1 ^{137}Cs and ^{210}Pb abundances: definition of the mixed layer

Previous ^{210}Pb and ^{137}Cs analyses of sediments from core MC04 suggested a thickness of about 10 cm for the modern mixed layer [see *Bonnet et al.*, 2010 for more details]. In core MC16, elevated ^{137}Cs levels extend down to at least the 3-4 cm interval, while above background levels of ^{210}Pb are found to around 6-7 cm (Table 2 and supplements). This indicates that the modern mixed layer in this core is about 6 cm thick. This value is unlikely to represent mixing conditions in the past, especially prior to the Holocene, because primary productivity and benthic mixing were reduced [*Zamelczyk et al.*, 2010]. In particular, foraminiferal abundance presents very sharp peaks (with a significant increase in number) deeper in the core, suggesting that bioturbation was less intense in the past.

3.2 The Pb budget in the sediment cores

Figure 3 presents both bulk and residue Pb/Al ratio profiles in cores MC04 (Fig. 3a, Table 5) and MC16 (Fig. 3b, Table 3). Pb/Al ratios, rather than absolute Pb concentrations are compared because absolute concentrations in bulk samples can be affected by dilution by carbonates. Aluminum was chosen as the normalizing element for several reasons. Al is an immobile element, as shown by the fact that less than 2% is removed during the leaching procedure. Al is derived from terrigenous inputs and represents alumino-silicates, the main group of minerals found in fine sediment fractions. Anthropogenic inputs of Al are negligible. Al is also non-reactive, thus its levels will not change as a consequence of chemical reactions within the sediment [*Fütterer*, 2000]. In addition, Al is a major element and thus does not usually display the ‘nugget’ effects frequently observed for crustal trace elements. Al is hence an excellent choice when normalizing for terrigenous inputs. Comparison of Pb/Al ratios of the bulk and residual fractions allows us to constrain the

relative importance of the various components of the Pb budget (detrital, leachable geogenic and leachable anthropogenic).

In both cores, Pb/Al ratios in residual fractions remain nearly constant with depth. In contrast, Pb/Al ratios of the bulk sediment are significantly higher throughout the profiles, and increase markedly in the mixed layers, most probably because of the addition of Pb of anthropogenic origin. In accordance with this observation, common Pb concentrations in leachates of the upper 6-7 cm of core MC16 are higher than those from deeper in the core (Table 3), thus confirming the above estimate of the mixed layer thickness from ^{210}Pb abundances. Based on the quantities of Pb in the bulk, residual and leachate fractions, we estimate that $59\pm4\%$ and $65\pm5\%$ of the Pb is removed during the leaching procedure in samples from below the mixed layer in cores MC04 and MC16, respectively. (These percentages correspond to the proportion of Pb removed during the final leaching step relative to the total amount of Pb in the decarbonated sediment.) In the mixed layer these proportions increase to $84\pm3\%$ and $74\pm5\%$ respectively. On average, the leaching procedure thus removed 42% (MC04) and 14% (MC16) more Pb in the mixed layer than in the rest of the core. This excess Pb probably represents the anthropogenic contribution (Fig. 3), larger in core MC04 than in MC16. The bulk fractions of the surface samples are thus imprinted by anthropogenic Pb inputs [Gobeil *et al.*, 2001]. Pb concentrations in residual fractions show little difference between samples from the mixed layer and those from deeper sediments. We conclude that the leachable Pb, including anthropogenic Pb, has been efficiently removed during the leaching procedure.

The Pb contained in the fraction removed by Na-acetate leaching is thought to represent the Pb contribution from carbonates. While the Pb content of this fraction was not directly measured, it has been estimated by calculating the difference between bulk sample Pb content and the sum of the Pb contents recovered in i) leachates (from the HH-acetic acid-EDTA leaching step) and ii) residues. In the mixed layer of MC04, almost no Pb was removed by the Na-acetate leachates whereas in deeper sediment, an average of 30% of Pb was apparently removed. However, due to minor losses during each step of the analytical procedure, the missing 30% should be seen as a maximum value for the Pb hosted by carbonates. For comparison, in core MC16, an average of 1% was removed by the Na-acetate solution in mixed-layer samples, whereas an average of 3% was removed downcore. Due to

potential losses mentioned above along with a 10% uncertainty on the analysis itself, this difference may be seen as insignificant.

3.3 Surface sediments

Elemental ratios and Pb isotopes from the surface samples of the transect (Fig. 1) are plotted vs longitude in Figure 4 and corresponding data are listed in Table 6. Th/Zr ratios depend almost entirely on detrital silicate supplies and provide a first criterion for discriminating potential sources. This ratio can be used to define at least three distinct sedimentary fields in the Fram Strait area. The easternmost field, on the west Spitsbergen shelf (core MC07; Fig. 4), displays a Th/Zr value of 0.031. Off the Spitsbergen margin, below the WSC, values ranging from 0.041 to 0.045 are observed. Westward, off the Greenland margin, mostly under the influence of outflowing Arctic water masses and sea-ice, Th/Zr ratios return to lower values (0.035 to 0.028).

Total Th/Pb ratios in surface sediments are influenced by anthropogenic Pb contamination [Carignan *et al.*, 2008; Gobeil *et al.*, 2001]. Th/Pb ratios in the bulk sediment of the surface samples, which contain both natural and anthropogenic Pb, show only limited variability along the transect. In contrast, Th/Pb ratios of residual fractions vary geographically in a manner similar to that of Th/Zr ratios. Residual Th/Pb values of 0.72, 0.81-0.91, and 0.71-0.75 are obtained respectively for each of the sedimentary fields identified above, along the NE to SW transect. This confirms that the detrital-Pb fraction can also be used to discriminate between sediment sources [Fagel *et al.*, 2004 and references therein]. This is further demonstrated by distinct Pb isotope signatures in this fraction, with $^{206}\text{Pb}/^{204}\text{Pb}$ -ratios of ~18.650, 18.744 to 18.837 and ~18.554, respectively over the Spitsbergen Shelf, off the Spitsbergen margin, and along the Greenland margin.

3.4 Sedimentary time series

In the long cores, residual Th/Zr and $^{206}\text{Pb}/^{204}\text{Pb}$ ratios vary with depth within the ranges of respectively, 0.038-0.49 and 18.650-18.958 (MC04; Fig. 5 and Table 5) and 0.026-0.042 and 18.404-18.823 (MC16; Fig. 5 and Table 3). The two cores display different Late Holocene values for these ratios in samples taken just below the mixed layer. Further back in time (LGM to Late Holocene), in the MC16 record, Pb isotope data from the residues display distinct trends, with a change in trend direction between sediments deposited before and after the start of the YD, at \sim 13 ka, located at about 20 cm. Below this depth (i.e., throughout the LGM-early deglacial interval), $^{206}\text{Pb}/^{204}\text{Pb}$ ratios increased erratically with decreasing age, defining a “LGM/late-glacial” trend (*Trend A*). In contrast, above the YD (i.e., since \sim 12 cal. ka), $^{206}\text{Pb}/^{204}\text{Pb}$ ratios decreased rather steadily, defining a “Holocene” trend (*Trend B*). These trends are clearly distinguished in the Pb isotope mixing diagram (Fig. 6). Each reflects a dominantly binary mixing system with a common high $^{206}\text{Pb}/^{204}\text{Pb}$ end-member resulting in a total of three end-members. End-member #1, common to both trends, has isotopic compositions of $^{206}\text{Pb}/^{204}\text{Pb} \geq 18.8$ and $^{208}\text{Pb}/^{206}\text{Pb} \leq 2.06$ (Fig. 7). End-member #2, from *Trend A*, displays $^{206}\text{Pb}/^{204}\text{Pb} \leq 18.4$ and $^{208}\text{Pb}/^{206}\text{Pb} \geq 2.085$. End-member #3, from *Trend B*, has $^{206}\text{Pb}/^{204}\text{Pb} \leq 18.6$ and $^{208}\text{Pb}/^{206}\text{Pb} \geq 2.085$.

Three isotopic excursions are recorded in the residues from MC16. The sample at 20cm (i.e. during the YD interval considering the age uncertainty, Fig. 2) displays higher $^{206}\text{Pb}/^{204}\text{Pb}$ ratios whereas samples at 28 and 36 cm (\sim 16.4 and \sim 19.8 cal. ka respectively) exhibit lower $^{206}\text{Pb}/^{204}\text{Pb}$ ratios (Fig. 5). Particular Pb isotopic compositions were also observed for samples from levels 23 and 38 cm (\sim 14.3 and \sim 20.7 cal. ka respectively) which plot along *Trend B* (Fig. 6) whereas the other samples below the YD layer plot along *Trend A*. This suggests a switch of the source regions to end-members #1 and #3 during the deposition of these two samples. Finally, we note that two extreme excursions, at 25 and 38 cm, were also observed in one of the three analyzed subsamples at each of these levels (Table 4). However these subsamples also displayed unusually high Pb concentrations and the other subsamples failed to reproduce the anomalous results. Thus while we cannot completely exclude the possibility of extreme sample heterogeneity, we believe that the most likely explanation of these surprising results is sample contamination and therefore they are not plotted in the figures and we will not discuss them further.

Below the YD-layer, $^{206}\text{Pb}/^{204}\text{Pb}$ ratios in leachates are similar to those of the corresponding residues (Fig. 5), and both leachates and residues plot along the same mixing trend (*Trend A*) in Fig. 6. In contrast, above the YD-layer, $^{206}\text{Pb}/^{204}\text{Pb}$ ratios in leachates tend to be lower than those of the corresponding residues. Surprisingly, the leachates from this section of the core also plot along *Trend A* in Figure 6, whereas the residues plot along *Trend B*.

4. DISCUSSION

In the following sections we compare Pb isotopic compositions of Fram Strait sediments to those of basalts, marginal crustal rocks and other marine sequences (both bulk and residues). Considering that residues represent the detrital fraction, their compositions should be comparable to those of the eroding continental crust in their source regions. The Arctic Ocean is a semi-enclosed basin and major potential Arctic sources include Greenland, the Arctic Archipelago (Queen Elizabeth Islands), the Mackenzie region, the Chukchi Sea, the East Siberian Sea, the Laptev Sea, the Kara Sea, the Barents Sea and Svalbard. Atlantic sources include Scandinavia, northwestern Europe and the Barents Sea (Fig. 1). Unfortunately, only limited Pb isotopic data are available for many of these areas. Nevertheless, these data provide important constraints on the provenance of material delivered to Fram Strait through IRD.

4.1 The sedimentary domains

Pb isotope compositions coupled with selected geochemical ratios allow distinction between Atlantic and Arctic sedimentary inputs that are controlled by the main active currents in the Strait (Fig. 4). The bidirectional flow through Fram Strait leads to a zonation in the sedimentary supply as a function of longitude within the Strait. Geochemical and Pb isotopic compositions of surface sediments define the sedimentary domains under the present-day current pathways. Pb isotopes of surface samples from cores MC07 and MC04, located on the continental slope off the Spitsbergen margin (Fig. 1, inset), plot along a linear trend defined by Pb isotope compositions of the Svalbard basalts and the Pan-African crust of northwestern Europe [Fagel *et al.*, 2004] (Fig. 7a) suggesting that the North Atlantic Current

(NAC) and the WSC control sedimentary fluxes in this area. Further to the west, under the influence of incoming waters from the GIN seas, distinctly higher $^{206}\text{Pb}/^{204}\text{Pb}$ ratios are observed in surface samples from cores MC10, 12 and 14 (Fig. 4, Table 6). They point to a stronger contribution from the western European Pan-African crust, (Fig. 7a). The central and western parts of Fram Strait are unquestionably influenced by both surface and deep currents from the Arctic Ocean [Darby and Zimmerman, 2008; Darby et al., 2002a; Rudels et al., 2000]. This is evident in the fact that sediments from cores MC21, 24 and 26 have higher $^{208}\text{Pb}/^{206}\text{Pb}$ and lower $^{206}\text{Pb}/^{204}\text{Pb}$ than those from cores further to the east (Fig. 4), possibly reflecting a contribution from the Pan-African Greenland crust (Fig. 7a).

The surface sample from core MC16 displays a Pb isotopic composition very similar to those in cores MC04 and MC07 (Fig. 4). However regarding the difference in sedimentation rates, the first cm of core MC16 would correspond to the top 10 cm of core C04 which, except for the surface, are distinct from core MC16. Cores MC04 and MC16 belong to distinct sedimentary domains and must be fed by different sedimentary source regions.

4.2 Temporal variations

Core MC04 is located on the continental slope off Svalbard and presents a sedimentation rate ~15 times higher than that of core MC16. In addition, the sea-ice cover over core MC04 is much less extensive than that over core MC16 [Müller et al., 2009]. All of these considerations suggest that sediment transport mechanisms should be different between core MC16 and core MC04. Therefore MC16 sedimentation is thought to be mainly derived from Arctic sea-ice. Pb isotopes from core MC04 display few variations suggesting constant supplies over the last two millennia. $^{206}\text{Pb}/^{204}\text{Pb}$ ratios suggest that core MC04 was mostly influenced by sediments derived from the Pan-African crust of western Europe through northward flowing currents. Since core MC16 provides a record since the LGM and because it reflects Arctic and/or proximal Greenland inputs and their variations since the LGM, we will focus the discussion on data from core MC16, in central Fram Strait.

4.2.1 Detrital Residues - Identification of potential source regions

The Pb isotopic compositions of the detrital residues from core MC16 are not randomly distributed within the mixing field delimited by the three end-members defined above. Instead they define two distinct trends, prior to and after the YD interval, with each trend representing a mixture of only two of the end-members. This rather abrupt change in the mixing pattern suggests a major change in sediment sources and thus in ice-drifting pathways.

The three end-members have been tentatively assigned to specific circum-Arctic sources based on (limited) data available in the literature. As illustrated in figure 7b, total and silicate fractions of surface sediments from Alpha-Ridge, in the Canadian basin north of Ellesmere Island, have Pb isotope ratios close to those of end-member #1 [Winter *et al.*, 1997]. Alpha-Ridge sediments are thought to be derived from the Queen Elizabeth Islands. River sediments from the Mackenzie and the Red Arctic rivers [Millot *et al.*, 2004] and marine sediments from the Canadian Basin [Gartside, 1996; Gobeil *et al.*, 2001; Stn 11 & Stn 18; Gueibe, 2009] display $^{206}\text{Pb}/^{204}\text{Pb}$ and $^{208}\text{Pb}/^{206}\text{Pb}$ ratios that plot on or near *Trend A*. Samples from the Arctic Mendeleyev (Stn 26) and Lomonosov (Stn 35) Ridges [Gobeil *et al.*, 2001] plot slightly off *Trend A* but not far from end-member #1, providing further evidence that this end-member indeed corresponds to Canadian Arctic sources.

River sediments from the Lena display Pb isotopic compositions consistent with end-member #2 (Fig. 7b). The Pb isotopic compositions of basalts from the Norilsk region [Lightfoot *et al.*, 1993; Wooden *et al.*, 1993] and of samples from the Siberia region [Winter *et al.*, 1997 and references therein] both define large fields in the top left corners of figures 7a and 7b that could encompass end-member #2. The Kathanga river, which drains the Norilsk region, as well as the above mentioned Lena river, end in the Laptev sea. We thus assign end-member #2 to the Central Siberia/Laptev Sea source area.

The Greenland Pan-African crust appears to be the most likely source matching end-member #3 (Fig. 7b). *Trend B*, which is essentially a mixture between end-members #1 and #3, shows higher variability (R^2 of 0.64 for the linear regression) than *Trend A* (R^2 of 0.85). Some contributions from end-member #2 might explain this higher variability.

Results from previous studies tend to corroborate our source identification. Darby *et al.* [2002a] and Darby and Zimmerman [2008] identified Fe-oxide grains and sediments from IRD-events in a core very close to MC16 (core PS1230, Fig. 1), which they linked to a

Northern Canada and Queen Elizabeth Islands provenance. These authors also provide evidence for sediment inputs from the Siberian margin (e.g. Laptev Sea) region. Thus their results are coherent with the end-members #1 and #2 that we have defined based on Pb isotope compositions.

4.2.2 Isotopic Excursions

Considering the estimated sedimentation rate of core MC16, from 1.1 to 5 cm/ka, each sample represents a time period of a few hundred years, assuming that mixing by bioturbation remained negligible until recent time, when productivity increased drastically [Zamelczyk *et al.*, 2010]. Thus changes in isotopic compositions at the level of the 1 cm sampling slices are considered to illustrate paleogeographical events of a few hundred years duration. Pb isotope ratios measured at 28 cm and 36 cm downcore tend towards end-member #2, thus suggesting enhanced contributions from the Laptev/Siberian source area at ca 16.4 and 19.8 ka, respectively. In contrast, the isotopic composition at 20 cm tends towards end-member #1 suggesting strong contributions from the Canadian Arctic region during the interval assigned to the YD. Unlike the other pre-YD samples, sediment residues at 23 and 38 cm (at ca 14.3 and 20.7 ka respectively) plot along *Trend B* (Fig. 6). This might suggest a pulse from end-member #3, that is, from Greenland, possibly linked to the LGM extreme Greenland Ice advance, or more simply it might correspond to an isolated calved iceberg. However we remain cautious regarding this interpretation since duplicate analyses of the sample at 38 cm produced distinct values that do not agree within analytical uncertainty. Enhanced heterogeneity of the sediment at this level, possibly linked to a large but rapid paleoceanographic event at ~20.7 ka, might explain this lack of reproducibility. Darby *et al.* [2002a] and Darby and Zimmerman [2008] report evidence for a glacial event at about that time. We note that the two results obtained from the sample at 38 cm, though disagreeing beyond analytical uncertainty, both plot along *Trend B*, which would be consistent with a Greenland contribution.

Darby and Zimmerman [2008] also note some features suggestive of contributions from Laptev/Siberian sources in the sediments from 16.4 and 19.8 ka, which would be consistent with the Laptev/Siberian geochemical component that we see in these excursions (Fig. 6, samples at 28 and 36 cm). According to recent paleogeographical reconstructions

[Hubberten *et al.*, 2004b; Siegert and Marsiat, 2001; Siegert *et al.*, 1999; Spielhagen *et al.*, 2004], the extent of the ice-sheet over northern Siberia was limited to the Barents Sea and the eastern part of the Kara Sea during this time interval. Cold and dry conditions would have prevailed over the emerged Laptev Sea. Therefore, transport of material from the Laptev Sea through ice rafting does not seem to be a viable explanation for these isotopic excursions. On the other hand, a freshwater event in the Kara Sea and the Arctic Ocean at ~15.8 ka has been recently reported, resulting from the drainage of the Chuya Katun lake through the Ob river, into the Kara sea [Reuther *et al.*, 2006]. Since we cannot distinguish between the Kara and Laptev Sea source signatures, this event cannot be ruled out as a possible contributor to the 16.4 ka excursion, given the age uncertainties.

4.2.3 Leachates

In the mixed layer, the anthropogenic Pb signal overprints the natural signal as illustrated by the higher Pb content of sediments and lower $^{206}\text{Pb}/^{204}\text{Pb}$ of leachates in this interval. In the following discussion, data from the mixed layer will hence be excluded and only pre-anthropogenic data will be discussed.

Another issue that must be examined is the possibility that the leaching procedure leads to some contamination of leachates by Pb derived from the detrital fraction, in which case the leachates would not represent the purely authigenic component. Two distinct approaches can be used to address this issue. The first, the Al/Ti test, suggested by Bayon *et al.* [2002] to estimate detrital contributions to leachates, is uninformative here, because Ti concentrations in leachates are often below detection limits. Nonetheless, such very low Ti contents (<0.001%) already suggest that detrital contributions to leachates must be small. An alternative approach involves mass balance calculations following the procedure of Gutjahr *et al.* [2007], using Sr isotopic compositions in both the detrital and leached fractions, and assuming that the Sr isotopic composition of the leachate should be that of seawater. Based on our Sr isotope data (that will be published elsewhere) we demonstrate that the detrital phase may contribute an average of 20% of the leachate Sr. Based on the hypothesis that Pb would behave as Sr does, this level of contamination would modify $^{206}\text{Pb}/^{204}\text{Pb}$ values in leachates by up to 0.025. We thus decided to include this uncertainty in the calculation of error bars of leachate Pb isotope ratios. Values reported for leachates can therefore be

considered to represent Pb inherited through exchange with seawater (henceforth referred to as "authigenic" Pb in contrast with the "detrital" Pb), within the shown uncertainty (Fig. 5).

Pb isotopic compositions in the authigenic vs detrital fractions varied differently through time. In the pre-YD section of MC16, they track each other quite well (Fig. 5). In contrast, in the post-YD interval, they diverge increasingly towards core top. Whereas Pb isotopes in detrital fractions follow two distinct trends with one common end-member, as discussed above, those from the authigenic fraction define a single binary mixing system (Fig. 6, R^2 of 0.97), broadly coincident with *Trend A* from the residue data. Potential sources of the authigenic Pb in leachates are thus likely to be the same as those of end-members #1 and #2 defined for the residues ($^{206}\text{Pb}/^{204}\text{Pb} \geq 18.9$ and $^{208}\text{Pb}/^{206}\text{Pb} \leq 2.06$, and $^{206}\text{Pb}/^{204}\text{Pb} \leq 18.3$ and $^{208}\text{Pb}/^{206}\text{Pb} \geq 2.09$ respectively). The similarity between the Pb isotope values of leachate end-members and detrital end-members #1 and #2 suggests that the water masses developed their Pb isotope signature through exchange with particulate and dissolved fluxes from the Canadian/Mackenzie area and/or the Siberian/Lena area. As discussed above, dissolution of Fe-Mn oxyhydroxide precipitates should account for most of the Pb recovered during the second step of the leaching procedure. Such precipitates may partly form in the water column but are mostly generated by early diagenetic effects at the water-sediment interface [Bayon *et al.*, 2002; Gutjahr *et al.*, 2007].

It is perhaps surprising that leachates do not exhibit a more radiogenic Pb signature than the residues, in contrast to what has been observed in the Northwest Atlantic region [Gutjahr *et al.*, 2009; Gutjahr *et al.*, 2008; Kurzweil *et al.*, 2010; Von Blanckenburg and Nägler, 2001]. The pre-YD samples show no coherent pattern as leachates can be either more or less radiogenic than the corresponding residues, while the post-YD leachates are clearly less radiogenic than their residues. In the Arctic Ocean, Haley *et al.* [2008] suggested that the less radiogenic Pb signal found in leachates reflects glacial remobilization of erosional products of the Siberian basalts. Subsequent partial exchange with these particles would have imprinted the water masses in a way similar to that which is thought to occur for Nd [Lacan and Jeandel, 2004b; c]. Indeed, though Pb and Nd are not completely analogous as illustrated by their different marine residence times, Nd isotopic exchange between dissolved and particulate phases along continental margins might shed some light on Pb isotope behaviour (see for example: [Arsouze *et al.*, 2009; Lacan and Jeandel, 2005a; Tachikawa *et al.*, 1999]).

The results of these studies suggest that the isotopic compositions of highly particle-reactive elements such as Th, Pa, Pb and Nd, along continental margins, could be controlled by adsorption/desorption processes through water/particle exchange. Perhaps such exchange processes partially explain the lack of a systematic difference between the Pb isotopic compositions of leachates and residues. The leachate data would hence reflect the ambient water-mass signature, however this signature would be acquired by exchange with particles at sites with high particle flux such as continental margins.

Data from MC16 (pre-anthropogenic) leachates could suggest that Pb isotopic signatures carried by deep-water masses were acquired through such “boundary exchange” processes off the Siberian margin and/or off the Canadian/Mackenzie margin area i.e., at sites where major particulate fluxes from either paleo-ice margins or large river systems occurred. We suggest that the Pb-fractions from MC16 core leachates were inherited from the ambient water masses circulating over the sediment i.e., the Arctic deep-water. Leachate data define a single mixing line suggesting that, unlike for the residues, the two sources thought to imprint the leachate signature have not changed since the LGM period. Nevertheless, changes did occur in the relative contribution of each end-member.

In conclusion, we think that the Pb isotopic composition of the leachates (i.e. exchangeable fraction) precipitates from ambient sea-water, hence recording the properties of dissolved metals in the sediment carrier water mass. However, the water mass itself is thought to acquire this geochemical signature through adsorption/dissolution processes with particles during its trajectory through circum-Arctic sites where high particulate fluxes occur (off major rivers today).

4.3 Paleoceanographic implications

The two trends defining the three sources of particulate material exported through Fram Strait are interpreted in relation to ice-rafting deposition and thus sea-ice and/or iceberg routes. The pre-YD interval sediments originated from the Canadian/Mackenzie (end-member #1) and Siberian (end-member #2) margins. Maximum influence of the Siberian margins occurred during the isotopic excursions at ca. 16.4 and 19.8 ka. During the post-YD interval (*trend B*), particulate supplies seem to have been mostly derived from

Canadian/Mackenzie (end-member #1) and Greenland (end-member #3) sources. The YD itself was apparently an interval with maximum and prominent input from the Canadian/Mackenzie source area (end-member #1).

Recent studies have proposed a northward meltwater pulse from the Laurentide Ice Sheet through the Mackenzie river system during the YD [Murton *et al.*, 2010; Teller *et al.*, 2005]. It has also been suggested that this pulse destabilized the ice-pack and enhanced sea-ice flux through the Beaufort Gyre [Not and Hillaire-Marcel, 2011a]. Two consequences resulting from such a pulse are worth noting: i) an increased flux of sedimentary material along the ice-rafting route notably over the central Lomonosov Ridge [Hanslik *et al.*, 2010; Not and Hillaire-Marcel, 2011a] and western Fram Strait (site MC16), and ii) a probable increased freshwater/sea-ice export through Fram Strait towards the GIN Seas likely to drastically reduce the AMOC [Tarasov and Peltier, 2005; 2006].

In fact, studies of the Northwind Ridge sediment, off the Chukchi Sea [Polyak *et al.*, 2007; Polyak *et al.*, 2009b], have also suggested the presence of i) a gyre type circulation over the western basin of the Arctic Ocean during the LGM/early deglacial period coexisting with ii) a Trans-Polar Drift type circulation from the Eurasian basin [Polyak *et al.*, 2009b; Spielhagen *et al.*, 2004]. This would produce a sea-ice circulation pattern in agreement with our *Trend A* described above. The short Pb isotopic excursions during this interval might relate to events such as ice-surging and/or drainage events from the Siberian margin area [Darby *et al.*, 2002a].

Several events, along with the YD, occurred during the LGM/deglacial intervals and have likely contributed to changes in sea-ice and iceberg routes of the Arctic: i) the final deglaciation of the Svalbard-Barents Sea Ice Sheet which presumably occurred at ~13-15 ka [Elverhøi *et al.*, 1998; Hubberten *et al.*, 2004b], ii) the opening of Bering Strait at ~13.5 ka [H England and Furze, 2008], iii) the sea level rise subsequent to meltwater pulse 1a at ~14.5 ka. Because of the sea level rise and of the new circulation dynamic after the YD, most of the Siberian margins were at least partially submerged notably the Barents Sea area where sea-ice could have been directly exported from the Arctic Ocean, depending on the atmospheric regime [Hilmer *et al.*, 1998].

During the post-YD interval, increasing relative particulate supplies probably from Greenland (vs Canadian sources) are observed at the MC16 site (*Trend B*). As recently

documented by Larsen et al. [2010] and Möller et al. [2010], the Holocene seems to have been characterized by an eastward drift from northern Greenland towards Fram Strait. This may have been responsible for the enhanced supply of detritus from the Greenland margin and the concomitant relative decrease of the Siberian source material.

Deep-water circulation patterns, as illustrated by exchangeable Pb isotopes from leachates (Fig. 6), seem to have been much less variable through time. This is illustrated by the fact that the data fit a single mixing line, indicating that deep water masses were influenced by particulate fluxes from both the Canadian margin (end-member #1) and the Siberian margin (end-member #2). However the relative contributions of the two end-members fluctuated substantially (Fig. 5). This supports the above interpretation that the Pb isotopic signatures of the deep-water masses were acquired by exchange processes in regions with high particulate fluxes.

5. CONCLUSIONS

This study has demonstrated the ability of geochemical tracers and Pb isotopes in deep-sea sediments to provide insights into paleoceanographical events that occurred during the deglaciation of the circum Arctic, and the Holocene. Indeed, leachable fractions (at core depths below anthropogenic influence) have isotopic signatures acquired by deep-water masses near the continental margins of the Arctic Ocean, whereas residual detrital fractions display isotopic compositions inherited from sediment source areas and thus document sedimentary fluxes towards and across the Arctic Ocean.

This detrital fraction, mainly transported by ice, illustrates relative contributions from three end-members (Canada, Siberia and Greenland margins) that varied significantly through time, both gradually and during short events linked to specific ice-margin instabilities. Our data argue for increasing influence of Greenland sediment supplies through the Holocene suggesting deflection of the Trans-Polar Drift westward towards the northern Greenland ice margin (with a weaker Beaufort gyre). The detrital fraction also records a strong isotopic excursion during the YD-interval, pointing to a trigger event in the Canada/Mackenzie area that resulted in enhanced Beaufort Gyre circulation, as is also recorded in sediments from the Lomonosov Ridge [Not and Hillaire-Marcel, 2011a]. This supports the hypothesis of Tarasov and Peltier [2005; 2006] that an Arctic freshwater/sea-ice pulse might have been at the origin of the AMOC collapse of this interval. We suggest that earlier isotopic excursions found in this core from the LGM to the YD-interval are mostly related to paleogeographical events along the Siberian margins. The low sedimentation rate of the studied core nevertheless limits more detailed paleoceanographic reconstructions.

Ongoing complementary radiogenic isotope measurements (Nd, Sr) will provide tighter constraints on sediment sources and on how their relative importance varied through time.

Acknowledgments

The present study is a contribution to the *WarmPast* and *Past4Future* projects. Funding by the *Ministère du Développement Economique, de l'Innovation et de l'Exportation* of Québec and the *Fonds Québécois de Recherche sur la Nature et les Technologies* has been instrumental. JM also acknowledges support from the French *Ministère de l'Education* and

the GEOTOP research network through PhD awards. Complementary funding by NSERC-Canada (Discovery Grant CHM) is also acknowledged. Special thanks are due to Katrin Husum and Morten Hald (University of Tromsø) for their invitation to the 2006-2008 cruises of the Jan Mayen in the Fram Strait Area. Discussions with Katrin Husum and Katarzyna Zamelczyk (both from the University of Tromsø) and with Anne de Vernal (GEOTOP-UQAM) have been very helpful. We are grateful to Marcus Gutjahr, Julian Murton and Natalie Fagel for their constructive suggestions that significantly improved the quality of this manuscript.

6. REFERENCES

- Arsouze, T., J. C. Dutay, F. Lacan, and C. Jeandel (2009), Reconstructing the Nd oceanic cycle using a coupled dynamical- Biogeochemical model, *Biogeosciences*, 6(12), 2829-2846.
- Bayon, G., C. R. German, R. M. Boella, J. A. Milton, R. N. Taylor, and R. W. Nesbitt (2002), An improved method for extracting marine sediment fractions and its application to Sr and Nd isotopic analysis, *Chemical Geology*, 187(3-4), 179-199.
- Birgel, D., and H. C. Hass (2004), Oceanic and atmospheric variations during the last deglaciation in the Fram Strait (Arctic Ocean): A coupled high-resolution organic-geochemical and sedimentological study, *Quaternary Science Reviews*, 23(1-2), 29-47.
- Bonnet, S., A. de Vernal, C. Hillaire-Marcel, T. Radi, and K. Husum (2010), Variability of sea-surface temperature and sea-ice cover in the Fram Strait over the last two millennia, *Marine Micropaleontology*, 74(3-4), 59-74.
- Broecker, W. S. (1991), The great ocean conveyor, *Oceanography*, 4, 79 - 89.
- Broecker, W. S., and T. H. Peng (1992), *Tracers in the Sea*, Lamont-Doherty Geol. Obs., Palisades, N.Y.
- Carignan, J., C. Hillaire-Marcel, and A. De Vernal (2008), Arctic vs. North Atlantic water mass exchanges in Fram Strait from Pb isotopes in sediments, *Canadian Journal of Earth Sciences*, 45(11), 1253-1263.
- Darby, D. A., and P. Zimmerman (2008), Ice rafted detritus events in the Arctic during the last glacial interval, and the timing of the Innuitian and Laurentide ice sheet calving events, *Polar Research*, 27(2), 114-127.
- Darby, D. A., L. Polyak, and H. A. Bauch (2006), Past glacial and interglacial conditions in the Arctic Ocean and marginal seas - a review, *Progress in Oceanography*, 71(2-4), 129-144.
- Darby, D. A., J. F. Bischof, R. F. Spielhagen, S. A. Marshall, and S. W. Herman (2002), Arctic ice export events and their potential impact on global climate during the late Pleistocene, *Paleoceanography*, 17(2), 15-15.
- Dickson, R., B. Rudels, S. Dye, M. Karcher, J. Meincke, and I. Yashayaev (2007), Current estimates of freshwater flux through Arctic and subarctic seas, *Progress in Oceanography*, 73(3-4), 210-230.

- Dokken, T. M., and M. Hald (1996), Rapid climatic shifts during isotope stages 2-4 in the Polar North Atlantic, *Geology*, 24(7), 599-602.
- Elverhøi, A., J. A. Dowdeswell, S. Funder, J. Mangerud, and R. Stein (1998), Glacial and oceanic history of the polar north atlantic margins: An overview, *Quaternary Science Reviews*, 17(1-3), 1-10.
- England, J. H., and M. F. A. Furze (2008), New evidence from the western Canadian Arctic Archipelago for the resubmergence of Bering Strait, *Quaternary Research*, 70(1), 60-67.
- Fagel, N., C. Innocent, C. Gariepy, and C. Hillaire-Marcel (2002), Sources of Labrador Sea sediments since the last glacial maximum inferred from Nd-Pb isotopes, *Geochimica et Cosmochimica Acta*, 66(14), 2569-2581.
- Fagel, N., C. Hillaire-Marcel, M. Humbert, R. Brasseur, D. Weis, and R. Stevenson (2004), Nd and Pb isotope signatures of the clay-size fraction of Labrador Sea sediments during the Holocene: Implications for the inception of the modern deep circulation pattern, *Paleoceanography*, 19(3), PA3002 3001-3016.
- Fahrbach, E., J. Meincke, S. Østerhus, G. Rohardt, U. Schauer, V. Tverberg, and J. Verduin (2001), Direct measurements of volume transports through Fram Strait, *Polar Research*, 20(2), 217-224.
- Flynn, W. W. (1968), The determination of low levels of polonium-210 in environmental materials, *Analytica Chimica Acta*, 43(C), 221-227.
- Foster, G. L., and D. Vance (2006), Negligible glacial-interglacial variation in continental chemical weathering rates, *Nature*, 444(7121), 918-921.
- Fütterer, D. K. (2000), The Solid Phase of Marine Sediments, in *Marine Geochemistry*, edited by H. D. Schulz and M. Zabel, pp. 1-25, Springer, Berlin; Heidelberg; New-York; Barcelona; Hong Kong; London; Milan; Paris; Singapore; Tokyo.
- Gartside, M. (1996), Sources et inventaire du plomb anthropique dans les sédiments de l'Océan Arctique profond, 79 pp, Université du Québec à Montréal, Montréal.
- Ghaleb, b. (2009), Overview of the methods for the measurement and interpretation of short-lived radioisotopes and their limits, *From Deep-Sea to Coastal Zones: Methods – Techniques for Studying Paleoenvironments, IOP Conference Series: Earth and Environmental Science*, 5(012007), doi: 10.1088/1755-1307/1085/1081/012007.

- Gobeil, C., R. W. Macdonald, J. N. Smith, and L. Beaudin (2001), Atlantic water flow pathways revealed by lead contamination in Arctic basin sediments, *Science*, 293(5533), 1301-1304.
- Gueibe, J. (2009), Analyse minéralogiques et isotopiques (Nd, Pb) des sédiments de l'Océan Arctique (Ride de Mendeleev, carottes HOTRAX) en vue d'identifier les agents de transport océanique, 95 pp, Université Libre de Bruxelles, Bruxelles.
- Gutjahr, M., M. Frank, A. N. Halliday, and L. D. Keigwin (2009), Retreat of the Laurentide ice sheet tracked by the isotopic composition of Pb in western North Atlantic seawater during termination 1, *Earth and Planetary Science Letters*, 286(3-4), 546-555.
- Gutjahr, M., M. Frank, C. H. Stirling, L. D. Keigwin, and A. N. Halliday (2008), Tracing the Nd isotope evolution of North Atlantic Deep and Intermediate Waters in the western North Atlantic since the Last Glacial Maximum from Blake Ridge sediments, *Earth and Planetary Science Letters*, 266(1-2), 61-77.
- Gutjahr, M., M. Frank, C. H. Stirling, V. Klemm, T. van de Flierdt, and A. N. Halliday (2007), Reliable extraction of a deepwater trace metal isotope signal from Fe-Mn oxyhydroxide coatings of marine sediments, *Chemical Geology*, 242(3-4), 351-370.
- Haley, B. A., M. Frank, R. F. Spielhagen, and J. Fietzke (2008), Radiogenic isotope record of Arctic Ocean circulation and weathering inputs of the past 15 million years, *Paleoceanography*, 23(1).
- Hanslik, D., M. Jakobsson, J. Backman, S. Björck, E. Sellén, M. O'Regan, E. Fornaciari, and G. Skog (2010), Quaternary Arctic Ocean sea ice variations and radiocarbon reservoir age corrections, *Quaternary Science Reviews*, 29(25-26), 3430-3441.
- Harlavan, Y., and Y. Erel (2002), The release of Pb and REE from granitoids by the dissolution of accessory phases, *Geochimica et Cosmochimica Acta*, 66(5), 837-848.
- Harlavan, Y., Y. Erel, and J. D. Blum (1998), Systematic changes in lead isotopic composition with soil age in glacial granitic terrains, *Geochimica et Cosmochimica Acta*, 62(1), 33-46.
- Hebbeln, D. (2000), Flux of ice rafted detritus from sea ice in the Fram Strait, *Deep-Sea Research Part II: Topical Studies in Oceanography*, 47(9-11), 1773-1790.
- Hebbeln, D., and H. Berner (1993), Surface sediment distribution in the Fram Strait, *Deep-Sea Research Part I*, 40(9), 1731-1745.

- Hebbeln, D., and G. Wefer (1997), Late Quaternary paleoceanography in the Fram Strait, *Paleoceanography*, 12(1), 65-78.
- Hebbeln, D., T. Dokken, E. S. Andersen, M. Hald, and A. Elverhøi (1994), Moisture supply for northern ice-sheet growth during the last glacial maximum, *Nature*, 370(6488), 357-360.
- Henderson, G. M., and E. Maier-Reimer (2002), Advection and removal of ^{210}Pb and stable Pb isotopes in the oceans: A general circulation model study, *Geochimica et Cosmochimica Acta*, 66(2), 257-272.
- Hilmer, M., M. Harder, and P. Lemke (1998), Sea ice transport: A highly variable link between Arctic and North Atlantic, *Geophysical Research Letters*, 25(17), 3359-3362.
- Hubberten, H. W., et al. (2004), The periglacial climate and environment in northern Eurasia during the Last Glaciation, *Quaternary Science Reviews*, 23(11-13), 1333-1357.
- Husum, K. (2006), Marine geological cruise to West Spitsbergen Margin and Fram Strait - RV "Jan Mayen" 11-19 October 2006Rep., 40 pp, University of Tromsø, Tromsø.
- Jones, E. P. (2001), Circulation in the Arctic Ocean, *Polar Research*, 20(2), 139-146.
- Jones, E. P., B. Rudels, and L. G. Anderson (1995), Deep waters of the Arctic Ocean: origins and circulation, *Deep-Sea Research Part I*, 42(5), 737-760.
- Kurzweil, F., M. Gutjahr, D. Vance, and L. Keigwin (2010), Authigenic Pb isotopes from the Laurentian Fan: Changes in chemical weathering and patterns of North American freshwater runoff during the last deglaciation, *Earth and Planetary Science Letters*, 299(3-4), 458-465.
- Lacan, F., and C. Jeandel (2004a), Denmark Strait water circulation traced by heterogeneity in neodymium isotopic compositions, *Deep-Sea Research Part I: Oceanographic Research Papers*, 51(1), 71-82.
- Lacan, F., and C. Jeandel (2004b), Neodymium isotopic composition and rare earth element concentrations in the deep and intermediate Nordic Seas: Constraints on the Iceland Scotland Overflow Water signature, *Geochemistry, Geophysics, Geosystems*, 5(11).
- Lacan, F., and C. Jeandel (2005), Neodymium isotopes as a new tool for quantifying exchange fluxes at the continent-ocean interface, *Earth and Planetary Science Letters*, 232(3-4), 245-257.
- Larsen, N. K., K. H. Kjaer, S. Funder, P. Möller, J. J. M. van der Meer, A. Schomacker, H. Linge, and D. A. Darby (2010), Late Quaternary glaciation history of northernmost Greenland-Evidence of shelf-based ice, *Quaternary Science Reviews*, 29, 3399-3414.

- Lightfoot, P. C., C. J. Hawkesworth, J. Hergt, A. J. Naldrett, N. S. Gorbachev, V. A. Fedorenko, and W. Doherty (1993), Remobilisation of the continental lithosphere by a mantle plume: major-, trace-element, and Sr-, Nd-, and Pb-isotope evidence from picritic and tholeiitic lavas of the Noril'sk District, Siberian Trap, Russia, *Contributions to Mineralogy and Petrology*, 114(2), 171-188.
- Manhes, G., C. J. Allègre, B. Dupré, and B. Hamelin (1980), Lead isotope study of basic-ultrabasic layered complexes: Speculations about the age of the earth and primitive mantle characteristics, *Earth and Planetary Science Letters*, 47(3), 370-382.
- McManus, J. F., R. Francois, J. M. Gherardi, L. Kelgwin, and S. Drown-Leger (2004), Collapse and rapid resumption of Atlantic meridional circulation linked to deglacial climate changes, *Nature*, 428(6985), 834-837.
- Millot, R., C. J. Allègre, J. Gaillardet, and S. Roy (2004), Lead isotopic systematics of major river sediments: A new estimate of the Pb isotopic composition of the Upper Continental Crust, *Chemical Geology*, 203(1-2), 75-90.
- Möller, P., N. K. Larsen, K. H. Kjær, S. Funder, A. Schomacker, H. Linge, and D. Fabel (2010), Early to middle Holocene valley glaciations on the northernmost Greenland, *Quaternary Science Reviews*, 29, 3379-3398.
- Müller, J., G. Massé, R. Stein, and S. T. Belt (2009), Variability of sea-ice conditions in the Fram Strait over the past 30,000 years, *Nature Geoscience*, 2(11), 772-776.
- Murton, J. B., M. D. Bateman, S. R. Dallimore, J. T. Teller, and Z. Yang (2010), Identification of Younger Dryas outburst flood path from Lake Agassiz to the Arctic Ocean, *Nature*, 464(7289), 740-743.
- Not, C., and C. Hillaire-Marcel (2011), A trigger from the Arctic: the most plausible scenario for the Younger Dryas cold spell, *submitted to Nature Geoscience*.
- Peltier, W. R., G. Vettoretti, and M. Stastna (2006), Atlantic meridional overturning and climate response to Arctic Ocean freshening, *Geophysical Research Letters*, 33(6).
- Polyak, L., D. A. Darby, J. F. Bischof, and M. Jakobsson (2007), Stratigraphic constraints on late Pleistocene glacial erosion and deglaciation of the Chukchi margin, Arctic Ocean, *Quaternary Research*, 67(2), 234-245.
- Polyak, L., et al. (2009), Late Quaternary stratigraphy and sedimentation patterns in the western Arctic Ocean, *Global and Planetary Change*, 68(1-2), 5-17.

- Reimer, P. J., et al. (2009), IntCal09 and Marine09 radiocarbon age calibration curves, 0-50,000 years CAL BP, *Radiocarbon*, 51(4), 1111-1150.
- Reuther, A. U., J. Herget, S. Ivy-Ochs, P. Borodavko, P. W. Kubik, and K. Heine (2006), Constraining the timing of the most recent cataclysmic flood event from ice-dammed lakes in the Russian Altai Mountains, Siberia, using cosmogenic in situ ^{10}Be , *Geology*, 34(11), 913-916.
- Rudels, B., E. P. Jones, U. Schauer, and P. Eriksson (2004), Atlantic sources of the Arctic Ocean surface and halocline waters, *Polar Research*, 23(2), 181-208.
- Rudels, B., G. Björk, J. Nilsson, P. Winsor, I. Lake, and C. Nohr (2005), The interaction between waters from the Arctic Ocean and the Nordic Seas north of Fram Strait and along the East Greenland Current: Results from the Arctic Ocean-02 Oden expedition, *Journal of Marine Systems*, 55(1-2), 1-30.
- Rudels, B., R. Meyer, E. Fahrbach, V. V. Ivanov, S. Østerhus, D. Quadfasel, U. Schauer, V. Tverberg, and R. A. Woodgate (2000), Water mass distribution in Fram Strait and over the Yermak Plateau in summer 1997, *Annales Geophysicae*, 18(6), 687-705.
- Siegent, M. J., and I. Marsiat (2001), Numerical reconstructions of LGM climate across the Eurasian Arctic, *Quaternary Science Reviews*, 20(15), 1595-1605.
- Siegent, M. J., J. A. Dowdeswell, and M. Melles (1999), Late Weichselian glaciation of the Russian High Arctic, *Quaternary Research*, 52(3), 273-285.
- Spielhagen, R. F., K. H. Baumann, H. Erlenkeuser, N. R. Nowaczyk, N. Nørgaard-Pedersen, C. Vogt, and D. Weiel (2004), Arctic Ocean deep-sea record of northern Eurasian ice sheet history, *Quaternary Science Reviews*, 23(11-13), 1455-1483.
- Tachikawa, K., C. Jeandel, and M. Roy-Barman (1999), A new approach to the Nd residence time in the ocean: The role of atmospheric inputs, *Earth and Planetary Science Letters*, 170(4), 433-446.
- Tarasov, L., and W. R. Peltier (2005), Arctic freshwater forcing of the Younger Dryas cold reversal, *Nature*, 435(7042), 662-665.
- Tarasov, L., and W. R. Peltier (2006), A calibrated deglacial drainage chronology for the North American continent: evidence of an Arctic trigger for the Younger Dryas, *Quaternary Science Reviews*, 25(7-8), 659-688.

- Teller, J. T., M. Boyd, Z. Yang, P. S. G. Kor, and A. M. Fard (2005), Alternative routing of Lake Agassiz overflow during the Younger Dryas: New dates, paleotopography, and a re-evaluation, *Quaternary Science Reviews*, 24(16-17), 1890-1905.
- Tessier, A., P. G. C. Campbell, and M. Blsson (1979), Sequential extraction procedure for the speciation of particulate trace metals, *Analytical Chemistry*, 51(7), 844-851.
- Thirlwall, M. F. (2002), Multicollector ICP-MS analysis of Pb isotopes using a 207pb-204pb double spike demonstrates up to 400 ppm/amu systematic errors in Ti-normalization, *Chemical Geology*, 184(3-4), 255-279.
- Thornalley, D. J. R., I. N. McCave, and H. Elderfield (2011), Tephra in deglacial ocean sediments south of Iceland: Stratigraphy, geochemistry and oceanic reservoir ages, *Journal of Quaternary Science*, 26(2), 190-198.
- Von Blanckenburg, F., and T. F. Nägler (2001), Weathering versus circulation-controlled changes in radiogenic isotope tracer composition of the Labrador Sea and North Atlantic Deep Water, *Paleoceanography*, 16(4), 424-434.
- White, W. M., F. Albarède, and P. Télouk (2000), High-precision analysis of Pb isotope ratios by multi-collector ICP-MS, *Chemical Geology*, 167(3-4), 257-270.
- Winter, B. L., C. M. Johnson, and D. L. Clark (1997), Strontium, neodymium, and lead isotope variations of authigenic and silicate sediment components from the Late Cenozoic Arctic Ocean: Implications for sediment provenance and the source of trace metals in seawater, *Geochimica et Cosmochimica Acta*, 61(19), 4181-4200.
- Wooden, J. L., G. K. Czamanske, V. A. Fedorenko, N. T. Arndt, C. Chauvel, R. M. Bouse, B. S. W. King, R. J. Knight, and D. F. Siems (1993), Isotopic and trace-element constraints on mantle and crustal contributions to Siberian continental flood basalts, Noril'sk area, Siberia, *Geochimica et Cosmochimica Acta*, 57(15), 3677-3704.
- Zamelczyk, K., K. Husum, M. Hald, A. de Vernal, J. Maccali, and C. Hillaire-Marcel (2010), Changes in water mass distribution and sea ice conditions in central Fram Strait over the last 20,000 years, in *APEX meeting*, edited, Höfn , Iceland.

Table 1 : Site locations of surface samples

Sample Name	Water Depth, m	Latitude	Longitude
BC07	1497	N 78° 52.620'	E 07° 20.459'
MC04	1181	N 78° 54.931'	E 06° 46.005'
BC10	2483	N 78° 56.176'	E 05° 24.075'
BC12	2426	N 78° 54.461'	E 02° 24.919'
BC14	2502	N 78° 55.888'	E 01° 06.460'
MC16	2546	N 78° 53.767'	E 01° 06.460'
MC21	1779	N 77° 00.204'	W 02° 30.173'
MC24	2974	N 74° 38.000'	W 03° 23.662'
MC26	3064	N 74° 53.490'	W 10° 46.100'

Table 2 : ^{210}Pb and ^{137}Cs activity data from the bulk sediment from core MC16.

Sample Depth (cm)	^{210}Pb activity (dpm/g)	^{137}Cs (dpm/g)
0 - 1 cm	29.34	0.38
1 - 2 cm	24.86	0.39
2 - 3 cm	11.42	0.26
3 - 4 cm	8.21	0.13
4 - 5 cm	4.91	-
5 - 6 cm	3.08	-
6 - 7 cm	2.61	-
7 - 8 cm	2.47	-
8 - 9 cm	2.44	-
9 - 10 cm	2.49	-

Table 3 : Elemental and Pb isotopic data from total, detrital and leachable fractions from MC16/ Leachate concentrations are reported relative to the initial bulk sediment mass.

Interval Depth, cm	Age, cal. Ka	Total			
		Al _{tot} , %	Zr _{tot} , µg/g	Th _{tot} , µg/g	Pb _{tot} , µg/g
0 - 1	0.2	7.0	137.9	7.3	28.0
1 - 2	1.1	6.9	161.3	7.8	39.8
2 - 3	2.0	6.9	148.9	7.0	25.3
3 - 4	2.9	7.0	202.7	9.3	35.9
4 - 5	3.8	7.4	160.1	7.5	21.7
5 - 6	4.7	7.3	201.0	9.9	30.2
6 - 7	5.6	7.4	206.9	10.2	20.5
7 - 8	6.5	7.3	216.0	10.3	22.0
8 - 9	7.5	7.2	224.9	9.9	23.6
9 - 10	8.3	7.4	186.0	7.8	22.2
10 - 11	9.2	7.3	205.0	10.2	27.4
11 - 12	10.0	7.5	188.9	10.3	28.2
12 - 13	10.9	7.6	189.9	10.7	28.8
13 - 14	11.8	7.8	191.7	11.3	28.2
14 - 15	12.0	8.0	205.0	10.2	26.6
15 - 16	12.2	8.3	208.0	10.7	30.6
16 - 17	12.4	8.1	221.6	11.1	26.4
17 - 18	12.6	8.0	236.1	10.6	23.7
18 - 19	12.8	8.0	231.3	11.0	26.5
19 - 20 ^a	13.0	8.3	188.9	10.3	21.8
21 - 22	13.9	8.3	189.9	10.7	29.8
22 - 23	14.3	8.3	191.7	11.3	25.1
24 - 25 ^b	15.1	7.8	225±35	10.1±0.7	18.9
26 - 27 ^b	16.0	8.2	228.1±3.3	8.8±0.1	24.9
27 - 28	16.4	8.0	221.6	11.1	23.0

29 – 30 ^b	17.3	8.2	189±13	9.1±1.3	19.2
34 – 35 ^b	19.4	8.2	219.9±5.2	10.0±0.5	20.4
35 – 36 ^b	19.8	7.7	224±35	10.0±0.1	20.0
36 – 37	20.2	8.1	210	10.6	21.4
37 – 38 ^b	20.7	7.6	234±21	9.2±0.3	17.8
39 – 40 ^a	21.5	7.8	174.2	7.9	17.7

^a Isotopic values correspond to the mean of duplicate analyses of the same leached aliquot fraction

^b Isotopic values correspond to the mean of analyses of leached aliquot fractions from different sub-samples at the same level.

Table 3 (suite)

Interval	Age, cal. K _a	Residues						
		Al, % μg/g	Zr, μg/g	Th, μg/g	Pb, μg/g	²⁰⁶ Pb/ ²⁰⁴ Pb	²⁰⁷ Pb/ ²⁰⁴ Pb	²⁰⁸ Pb/ ²⁰⁴ Pb
0 – 1	0.2	6.3	152.5	5.3	7.4	18.633	15.601	38.628
1 – 2	1.1	6.7	182.9	6.5	7.9	18.674	15.596	38.804
2 – 3	2.0	6.7	185.9	6.2	7.5	18.660	15.594	38.773
3 – 4	2.9	6.4	151.6	5.6	7.5	18.684	15.588	38.871
4 – 5	3.8	6.9	192.9	6.1	7.5	18.701	15.602	38.719
5 – 6	4.7	6.9	186.6	5.8	7.1	18.621	15.592	38.771
6 – 7	5.6	7.1	182.0	6.2	7.1	18.711	15.608	38.863
7 – 8	6.5	6.8	199.5	6.5	7.6	18.680	15.592	38.751
8 – 9	7.5	6.7	215.7	6.8	8.0	18.655	15.592	38.871
9 – 10	8.3	6.9	209.8	6.7	8.0	18.714	15.598	38.785
10 - 11	9.2	-	-	-	-	-	-	-
11 - 12	10.0	-	-	-	-	-	-	-
12 - 13	10.9	-	-	-	-	-	-	-

13 - 14	11.8	-	-	-	-	-	-	-
14 - 15	12.0	7.3	189.8	7.0	7.7	18.733	15.601	38.832
15 - 16	12.2	-	-	-	-	-	-	-
16 - 17	12.4	-	-	-	-	-	-	-
17 - 18	12.6	-	-	-	-	-	-	-
18 - 19	12.8	-	-	-	-	-	-	-
19 - 20 ^a	13.0	8.0	181.1	7.7	8.0	18.836±0.019	15.6178±0.0003	38.831±0.054
21 - 22	13.9	7.6	204.4	6.4	7.9	18.684	15.599	38.688
22 - 23	14.3	7.6	221.2	6.8	8.1	18.695	15.593	38.824
24 - 25 ^b	15.1	-	-	-	-	18.65±0.07	15.589±0.008	38.64±0.11
26 - 27 ^b	16.0	7.5	211.6	6.4	7.7	18.611±0.069	15.587±0.017	38.606±0.042
27 - 28	16.4	7.4	202.0	5.2	6.6	18.589	15.581	38.569
29 - 30 ^b	17.3	7.4	199.2	6.1	6.5	18.666±0.016	15.598±0.002	38.650±0.022
34 - 35 ^b	19.4	7.6	221.6	7.0	9.1	18.708±0.057	15.603±0.009	38.696±0.040
35 - 36 ^b	19.8	7.2	217.1	5.6	7.6	18.469±0.093	15.573±0.009	38.45±0.18
36 - 37	20.2	7.7	185.0	5.6	7.7	18.598	15.590	38.621
37 - 38 ^b	20.7	-	-	-	-	18.75±0.13	15.608±0.016	38.806±0.057
39 - 40 ^a	21.5	7.3	230.8	6.7	8.3	18.661±0.021	15.599±0.012	38.623±0.025
39 - 40 ^a		21.5		7.8		174.2	7.9	17.7

^a Isotopic values correspond to the mean of duplicate analyses of the same leached aliquot fraction

^b Isotopic values correspond to the mean of analyses of leached aliquot fractions from different sub-samples at the same level.

Table 3 (suite)

Interval Depth, cm	Age, cal. Ka	Leachates						
		Al, %	Th, μg/g	Pb, μg/g	Removed Pb, %	$^{206}\text{Pb}/^{204}\text{Pb}$	$^{207}\text{Pb}/^{204}\text{Pb}$	$^{208}\text{Pb}/^{204}\text{Pb}$
								$^{208}\text{Pb}/^{204}\text{Pb}$
0 - 1	0.2	0/96	2.3	25.2	77	18.472	15.608	38.403
1 - 2	1.1	0.111	2.1	30.6	79	18.331	15.610	38.288

2 - 3	2.0	0.107	1.9	18.9	72	18.503	15.620	38.485
3 - 4	2.9	0.095	2.4	26.4	78	18.338	15.601	38.298
4 - 5	3.8	0.104	2.4	13.9	65	18.608	15.608	38.573
5 - 6	4.7	0.157	2.0	17.3	71	18.442	15.608	38.405
6 - 7	5.6	0.128	2.2	11.5	62	18.787	15.630	38.771
7 - 8	6.5	0.196	2.9	13.7	64	18.709	15.632	38.701
8 - 9	7.5	0.243	2.5	14.7	65	18.593	15.629	38.589
9 - 10	8.3	0.094	2.8	15.1	66	18.584	15.613	38.3545
10 - 11	9.2	-	-	-	-	-	-	-
11 - 12	10.0	-	-	-	-	-	-	-
12 - 13	10.9	-	-	-	-	-	-	-
13 - 14	11.8	-	-	-	-	-	-	-
14 - 15	12.0	0.238	2.8	15.7	64	18.624	15.620	38.589
15 - 16	12.2	-	-	-	-	-	-	-
16 - 17	12.4	-	-	-	-	-	-	-
17 - 18	12.6	-	-	-	-	-	-	-
18 - 19	12.8	-	-	-	-	-	-	-
19 - 20 ^a	13.0	0.068	2.7	12.3	60	18.831	15.632	38.771
21 - 22	13.9	0.120	3.2	18.7	69	18.569	15.623	38.516
22 - 23	14.3	0.117	3.4	17.0	66	18.647	15.626	38.599
24 - 25 ^b	15.1	-	-	-	-	17.621	15.562	37.532
26 - 27 ^b	16.0	0.154	3.0	16.5	66	18.558	15.618	38.523
27 - 28	16.4	0.118	3.0	15.5	68	18.579	15.616	38.547
29 - 30 ^b	17.3	0.103	3.4	12.9	64	18.728	15.620	38.750
34 - 35 ^b	19.4	0.126	2.8	11.4	58	18.764	15.630	38.794
35 - 36 ^b	19.8	0.012	2.2	9.4	54	18.592	15.618	38.576
36 - 37	20.2	0.136	3.2	17.0	68	18.537	15.620	38.523
37 - 38 ^b	20.7	-	-	-	-	17.953	15.579	37.872
39 - 40 ^a	21.5	0.099	2.9	10.3	74	18.770	15.618	38.742
39 - 40 ^a	21.5			7.8		174.2	7.9	17.7

^a Isotopic values correspond to the mean of duplicate analyses of the same leached aliquot fraction

^b Isotopic values correspond to the mean of analyses of leached aliquot fractions from different sub-samples at the same level.

Table 4 : Elemental and Pb isotopic data from total, detrital and leachable fractions from duplicate samples from core MC16. Leachate concentrations are reported relative to the initial bulk sediment mass.

Interval Depth, cm	Age, cal. Ka	Total		
		Zr _{tot} , µg/g	Th _{tot} , µg/g	Pb _{tot} , µg/g
19 – 20	13.0	188.9	10.3	21.8
Mean ^b ±1*sigma				
24 – 25	15.1	200.3	10.6	47.6
	-	-	-	-
	249.2	9.6	18.9	
Mean±1*sigma		225±35	10.1±0.7	18.9
26 – 27	16.0	230.4	8.9	24.9
	225.7	8.7	17.5	
Mean±1*sigma		228.1±3.3	8.8±0.1	21.2±5.2
29 – 30	17.3	198.5	10.0	19.2
	179.3	8.2	19.6	
Mean±1*sigma		189±13	9.1±1.3	19.4±0.3
34 – 35	19.4	223.6	9.6	20.4
	216.2	10.4	19.4	
Mean ±1*sigma		219.9±5.2	10.0±0.5	19.9±0.8
35 – 36	19.8	198.5	10.0	20.0
	249.2	10.1	18.2	
Mean ±1*sigma		224±35	10.0±0.1	19.1±1.3
37 – 38	20.7	248.4	9.0	42.4

		218.8	9.5	17.8
				17.8
Mean ±1*sigma		234±21	9.2±0.3	
39 – 40	21.5	174.2	7.9	17.7
Mean ^b ±1*sigma				

^a The first set of values of samples at 25 and 38 cm have been rejected due to enhanced concentrations of Pb in the bulk sediments that we have interpreted as a possible contamination effect. The means have been calculated using the two subsequent values.

^b Analyses were performed on the same leached aliquot fraction. (All other duplicate analyses were performed on leached aliquots from different sub-samples of the same level.)

Table 4 (suite)

Interval Depth, cm	Age,				Residues		
	cal. Ka	Zr, μg/g	Th, μg/g	Pb, μg/g	²⁰⁶ Pb/ ²⁰⁴ Pb	²⁰⁷ Pb/ ²⁰⁴ Pb	²⁰⁸ Pb/ ²⁰⁴ Pb
		μg/g	μg/g	μg/g			
19 – 20	13.0	181.1	7.7	8.0	18.823	15.618	38.869
					18.850	15.618	38.793
Mean ^b ±1*sigma					18.836±0.019	15.6178±0.0003	38.831±0.054
24 – 25	15.1	-	-	-	18.236 ^a	15.562 ^a	38.297 ^a
					18.696	15.595	38.713
					18.597	15.584	38.636
Mean±1*sigma					18.65±0.07	15.589±0.008	38.64±0.11
26 – 27	16.0	211.6	6.4	7.7	18.562	15.578	38.577
					18.659	15.596	38.636
Mean±1*sigma					18.611±0.069	15.587±0.017	38.606±0.042
29 – 30	17.3	199.2	6.1	6.5	18.677	15.597	38.666
					18.655	15.3600	38.634
Mean±1*sigma					18.666±0.016	15.598±0.002	38.650±0.022
34 – 35	19.4	221.6	7.0	9.1	18.668	15.596	38.667

					18.749	15.609	38.724
Mean $\pm 1^{\text{sigma}}$					18.708± 0.057	15.603± 0.009	38.696± 0.040
35 – 36	19.8	217.1	5.6	7.6	18.536	15.579	38.580
					18.404	15.566	38.323
Mean $\pm 1^{\text{sigma}}$					18.469± 0.093	15.573± 0.009	38.45± 0.18
37 – 38	20.7	-	-	-	18.027 ^a	15.553 ^a	37.927 ^a
					18.657	15.596	38.766
					18.841	15.619	38.846
Mean $\pm 1^{\text{sigma}}$					18.75± 0.13	15.608± 0.016	38.806± 0.057
39 – 40	21.5	230.8	6.7	8.3	18.647	15.590	38.606
					18.676	15.607	38.641
Mean ^b $\pm 1^{\text{sigma}}$					18.661± 0.021	15.599± 0.012	38.623± 0.025

^a The first set of values of samples at 25 and 38 cm have been rejected due to enhanced concentrations of Pb in the bulk sediments that we have interpreted as a possible contamination effect. The means have been calculated using the two subsequent values.

^b Analyses were performed on the same leached aliquot fraction. (All other duplicate analyses were performed on leached aliquots from different sub-samples of the same level.)

Table 4 (suite)

Interval Depth, cm	Age,						Leachates		
	cal. Ka	Th, μg/g	Pb, μg/g	Removed Pb, %	$^{206}\text{Pb}/^{204}\text{Pb}$	$^{207}\text{Pb}/^{204}\text{Pb}$	$^{208}\text{Pb}/^{204}\text{Pb}$		
		μg/g	μg/g	Pb, %					
19 – 20	13.0	2.7	12.3	60	18.831	15.632	38.771		
Mean ^b $\pm 1^{\text{sigma}}$									
24 – 25	15.1	-	-	-	17.621 ^a	15.562 ^a	37.532 ^a		
					-	-	-		
					18.733	15.612	38.676		
Mean $\pm 1^{\text{sigma}}$									
26 – 27	16.0	3.0	16.5	66	18.558	15.618	38.523		

					18.757	15.604	38.681
Mean±1*sigma					18.657±0.14	15.611±0.009	38.602±0.11
29 – 30	17.3	3.4	12.9	64	18.728	15.620	38.750
					18.724	15.613	38.719
Mean±1*sigma					18.726±0.003	15.616±0.005	38.735±0.02
34 – 35	19.4	2.8	11.4	58	18.764	15.630	38.794
					18.724	15.610	38.697
Mean ±1*sigma					18.744±0.028	15.620±0.14	38.746±0.07
35 – 36	19.8	2.2	9.4	54	18.592	15.618	38.576
					18.608	15.609	38.560
Mean ±1*sigma					18.600±0.011	15.613±0.006	38.568±0.11
37 – 38	20.7	-	-	-	17.953 ^a	15.579 ^a	37.872 ^a
					18.676	15.601	38.620
					18.714	15.605	38.658
Mean ±1*sigma					18.695±0.03	15.605±0.0004	38.639±0.03
39 – 40	21.5	2.9	10.3	11.1	18.770	15.618	38.742

Mean^b±1*sigma

^a The first set of values of samples at 25 and 38 cm have been rejected due to enhanced concentrations of Pb in the bulk sediments that we have interpreted as a possible contamination effect. The means have been calculated using the two subsequent values.

^b Analyses were performed on the same leached aliquot fraction. (All other duplicate analyses were performed on leached aliquots from different sub-samples of the same level.)

Table 5 : Elemental and Pb isotopic data from total, detrital and leachable fractions from MC04. Leachate concentrations are reported relative to the initial bulk sediment mass.

Interval Depth, cm	Total			
	Al _{tot} , %	Zr _{tot} , µg/g	Th _{tot} , µg/g	Pb _{tot} , µg/g
0 – 1	6.1	144.1	7.6	43.1
2 – 3	6.8	130.2	7.1	37.5

4 - 5	6.8	146.0	9.4	58.7
5 - 6	6.9	141.2	9.4	49.0
6 - 7	6.9	154.7	9.6	51.8
7 - 8	6.9	163.8	9.8	50.0
8 - 9	6.8	165.5	9.6	54.3
9 - 10	6.7	131.6	7.3	39.0
10 - 11	6.8	165.0	9.9	41.6
11 - 12	6.8	165.8	9.5	33.8
12 - 13	6.9	167.0	9.7	26.5
13 - 14	7.0	173.1	10.1	37.2
14 - 15	7.0	182.3	9.9	26.4
19 - 20	7.1	136.7	7.6	21.6
24 - 25	7.0	173.2	10.1	23.3
34-35a	7.1	176.0	9.9	26.6
34-35b	7.1	159.8	10.1	26.6
39 - 40	7.2	168.8	9.8	36.0
44 - 45	7.0	157.8	10.5	23.9
49 - 50	7.3	144.1	7.6	35.8

Table 5 (suite)

Depth, cm	Residues						
	Al, %	Zr, μg/g	Th, μg/g	Pb, μg/g	$^{206}\text{Pb}/^{204}\text{Pb}$	$^{207}\text{Pb}/^{204}\text{Pb}$	$^{208}\text{Pb}/^{204}\text{Pb}$
0 - 1	6.8	130.7	5.3	7.8	18.650	15.583	38.554
2 - 3	8.1	134.4	5.5	6.8	18.835	15.621	38.736
4 - 5	8.3	122.2	6.0	8.0	18.835	15.616	38.755
5 - 6	-	-	-	-	-	-	-
6 - 7	-	-	-	-	-	-	-
7 - 8	-	-	-	-	-	-	-
8 - 9	-	-	-	-	-	-	-

9 - 10	8.1	127.9	5.3	5.8	18.958	15.638	38.886
10 - 11	-	-	-	-	-	-	-
11 - 12	-	-	-	-	-	-	-
12 - 13	-	-	-	-	-	-	-
13 - 14	-	-	-	-	-	-	-
14 - 15	8.1	195.1	7.5	8.4	18.924	15.633	38.815
19 - 20	8.3	141.8	6.0	7.6	18.660	15.594	38.773
24 - 25	8.2	191.5	7.6	8.2	18.956	15.632	38.829
34-35a	7.9	144.9	6.1	7.1	18.926	15.627	38.867
34-35b	7.9	151.0	5.8	7.0	18.914	15.627	38.843
39 - 40	8.5	128.3	6.2	8.0	18.895	15.631	38.811
44 - 45	8.2	132.9	5.5	6.7	18.921	15.630	38.835
49 - 50	8.4	119.9	5.9	8.2	18.890	15.631	38.800

Table 5 (suite)

Interval Depth, cm	Leachates						
	Al, μg/g	Th, μg/g	Pb, μg/g	Removed Pb, %	$^{206}\text{Pb}/^{204}\text{Pb}$	$^{207}\text{Pb}/^{204}\text{Pb}$	$^{208}\text{Pb}/^{204}\text{Pb}$
0 - 1	99	1.8	31.4	80	18.262	15.576	38.128
2 - 3	117	2.2	32.9	83	18.407	15.613	38.303
4 - 5	141	2.4	48.3	86	18.275	15.604	38.193
5 - 6	-	-	-	-	-	-	-
6 - 7	-	-	-	-	-	-	-
7 - 8	-	-	-	-	-	-	-
8 - 9	-	-	-	-	-	-	-
9 - 10	136	2.3	37.1	86	18.498	15.620	38.444
10 - 11	-	-	-	-	-	-	-
11 - 12	-	-	-	-	-	-	-
12 - 13	-	-	-	-	-	-	-
13 - 14	-	-	-	-	-	-	-

14 – 15	1	1.9	11.9	58	18.655	15.635	38.597
19 – 20	218	2.3	9.7	56	18.709	15.626	38.626
24 – 25	2	2.3	9.7	54	18.792	15.649	38.734
34–35a	165	2.5	10.2	59	18.572	15.604	38.474
34–35b	169	2.5	10.5	60	18.544	15.581	38.415
39 – 40	139	2.7	15.2	66	18.403	15.575	38.286
44 – 45	161	2.5	8.4	56	18.490	15.463	38.191
49 - 50	128	2.9	14.1	63	18.435	15.581	38.300

Table 6. Elemental and Pb isotopic data from total, detrital and leachable fractions from surface samples. Leachate concentrations are reported relative to the initial bulk sediment mass.

Sample name	Total			
	Al _{tot} , %	Zr _{tot} , µg/g	Th _{tot} , µg/g	Pb _{tot} , µg/g
BC07	6.1	129.0	6.4	29.5
MC04	6.1	144.1	7.6	43.1
BC10	6.9	164.1	8.1	29.8
BC12	7.2	134.6	8.1	30.7
BC14	7.2	139.7	8.1	33.1
MC16	7.0	137.9	7.3	28.0
MC21	6.7	177.6	7.1	24.8
MC24	6.7	171.4	7.8	24.6
MC26	6.5	191.7	7.0	25.4

Table 6 (suite)

Sample name	Residues						
	Al,	Zr, µg/g	Th, µg/g	Pb, µg/g	$^{206}\text{Pb}/^{204}\text{Pb}$	$^{207}\text{Pb}/^{204}\text{Pb}$	$^{208}\text{Pb}/^{204}\text{Pb}$
BC07	6.7	156.4	4.8	6.7	18.643	15.603	38.547

MC04	6.8	100.6	4.1	6.0	18.650	15.583	38.554
BC10	7.9	164.5	6.7	7.4	18.837	15.617	38.800
BC12	8.4	154.3	6.2	7.8	18.823	15.613	38.817
BC14	8.3	133.5	6.0	7.0	18.744	15.602	38.739
MC16	7.9	152.5	5.3	7.4	18.633	15.601	38.628
MC21	7.5	164.5	5.2	7.0	18.556	15.582	38.553
MC24	7.6	161.2	5.3	7.4	18.553	15.581	8.657
MC26	7.4	190.3	5.3	7.0	18.545	15.581	38.580

Table 6 (suite)

Sample name	Al, g/g	Leachates					
		Th, μg/g	Pb, μg/g	Removed Pb, %	$^{206}\text{Pb}/^{204}\text{Pb}$	$^{207}\text{Pb}/^{204}\text{Pb}$	$^{208}\text{Pb}/^{204}\text{Pb}$
BC07	14	1.9	24.0	78	18.430	15.610	38.325
MC04	10	1.4	24.1	80	18.262	15.576	38.128
BC10	113	2.0	24.4	77	18.391	15.619	38.347
BC12	16	2.4	21.1	73	18.481	15.603	38.417
BC14	15	2.6	26.7	79	18.457	15.612	38.399
MC16	12	2.3	25.2	77	18.472	15.608	38.403
MC21	12	2.5	18.4	72	18.466	15.599	38.427
MC24	12	2.4	18.3	71	18.457	15.606	38.420
MC26	12	2.0	17.6	71	18.407	15.602	38.369

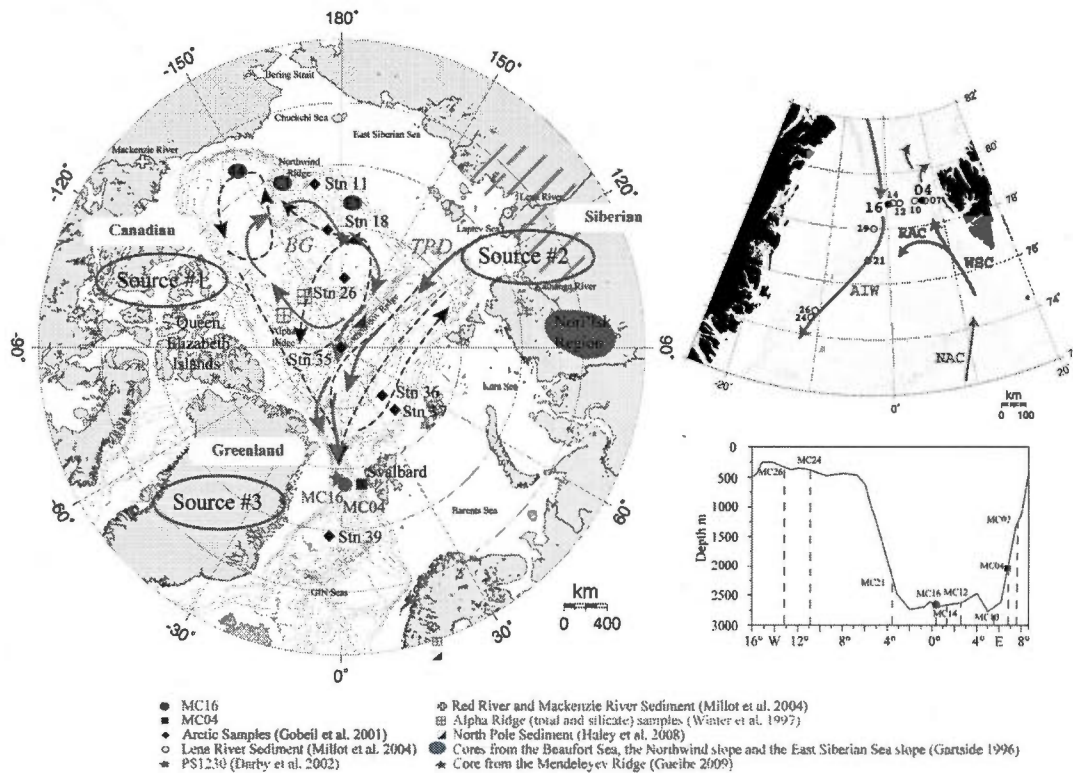


Figure 1: Bathymetric map of Fram Strait and surface sample locations.

Left: map of the Arctic Ocean, light-blue arrows represent main surface currents and dark-blue dashed arrows represent deep currents. BG: Beaufort Gyre; TPD: Trans-Polar Drift [Jones, 2001; Rudels et al., 2004; Rudels et al., 2005]

Top right: Open and full circles represent respectively surface and core samples along the transect. Red arrows illustrate warm Atlantic waters and blue arrows represent cold Arctic waters. NAC: North Atlantic Current, WSC: West Spitsbergen Current, RAC: Return Atlantic Current, AIW: Arctic Intermediate Waters.

Bottom right: Localisation of surface samples vs water depth.

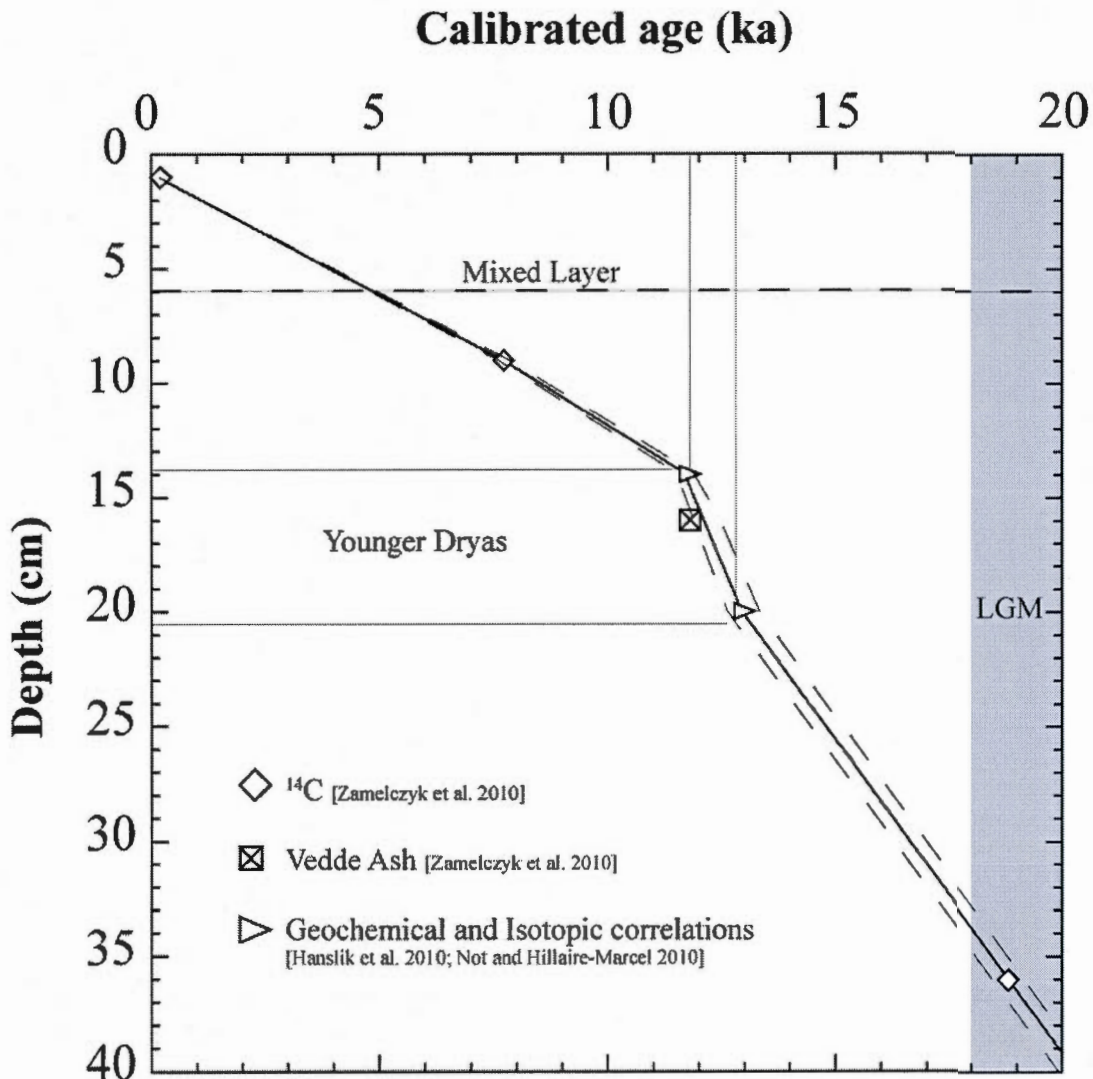


Figure 2: Age model of depth vs calibrated age for core MC16 using ^{14}C dates, tephrochronological layer identification and geochemical correlations with nearby sediment cores. Dashed lines above and below the age model curve represent the estimated uncertainty. The mixed layer, down to 6 cm, is represented by a dashed line.

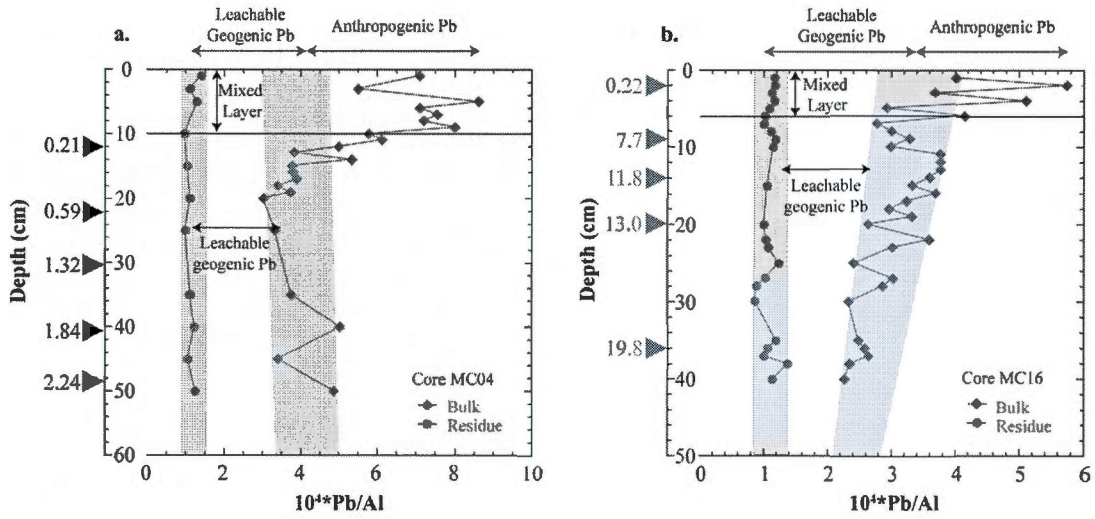


Figure 3: Pb/Al ratios in the bulk sediment (green diamonds) and in the detrital residue (red circles) illustrating the Pb budget in a) core MC04 and b) core MC16. Grey fields represent the crustal, non-leachable Pb. Green fields represent the geogenic Pb determined from the bulk sediments and include all values below the mixed layer defined by ^{137}Cs and ^{210}Pb data. The difference between the grey and green fields represents the leachable geogenic Pb. Pb concentrations were measured on more bulk samples than on residues, hence all bulk samples do not have a corresponding residue. Specific calibrated ages (in ka) are indicated by arrows on the depth axes.

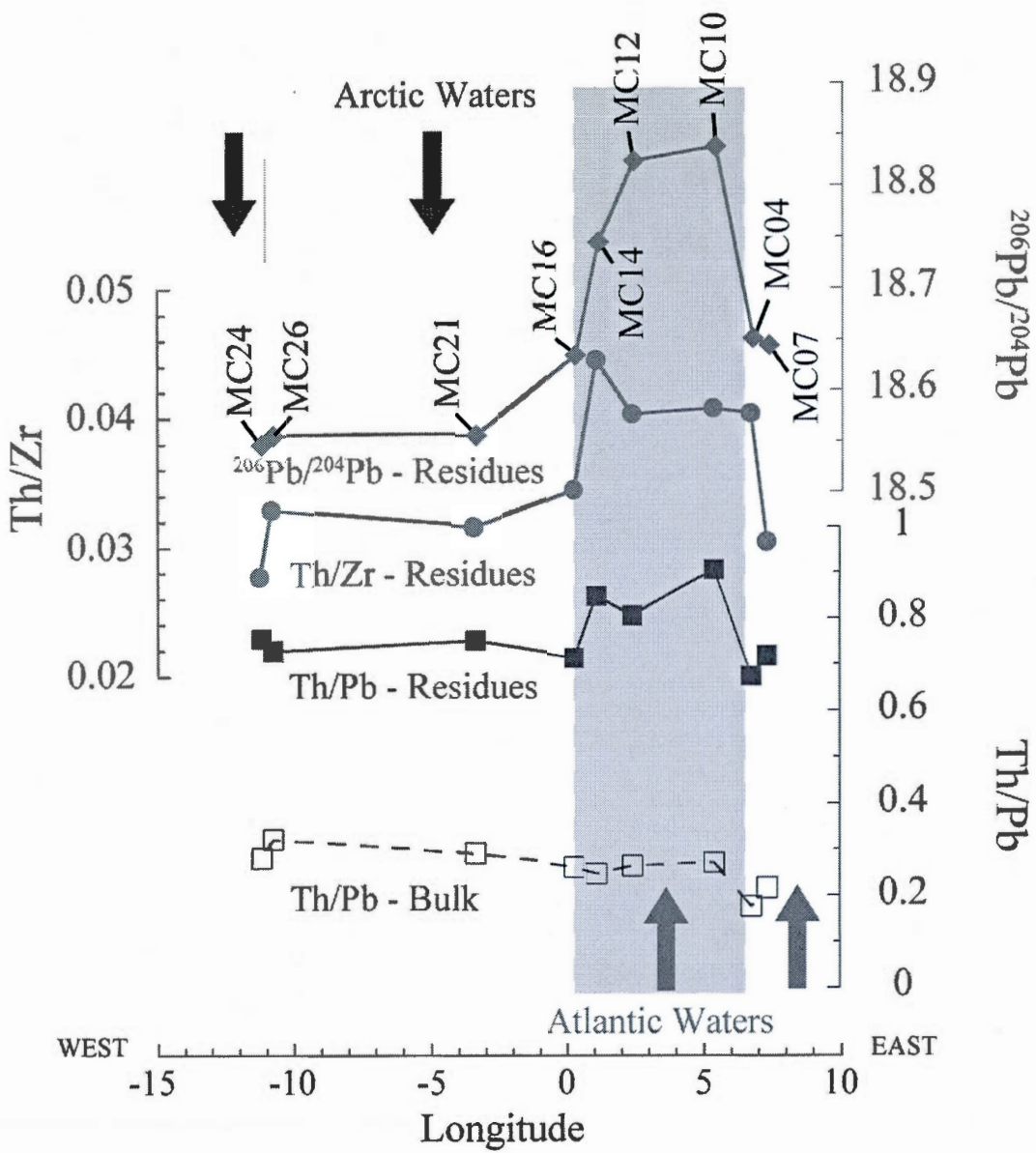


Figure 4: Th/Zr (red), Th/Pb (blue) and $^{206}\text{Pb}/^{204}\text{Pb}$ (green) ratios of surface sample detrital residues and Th/Pb ratios of bulk fractions. Sample sites follow the transect illustrated in figure 1 and their geochemical and isotopic compositions display a spatial zonation in the Strait. Arrows illustrate the main active currents.

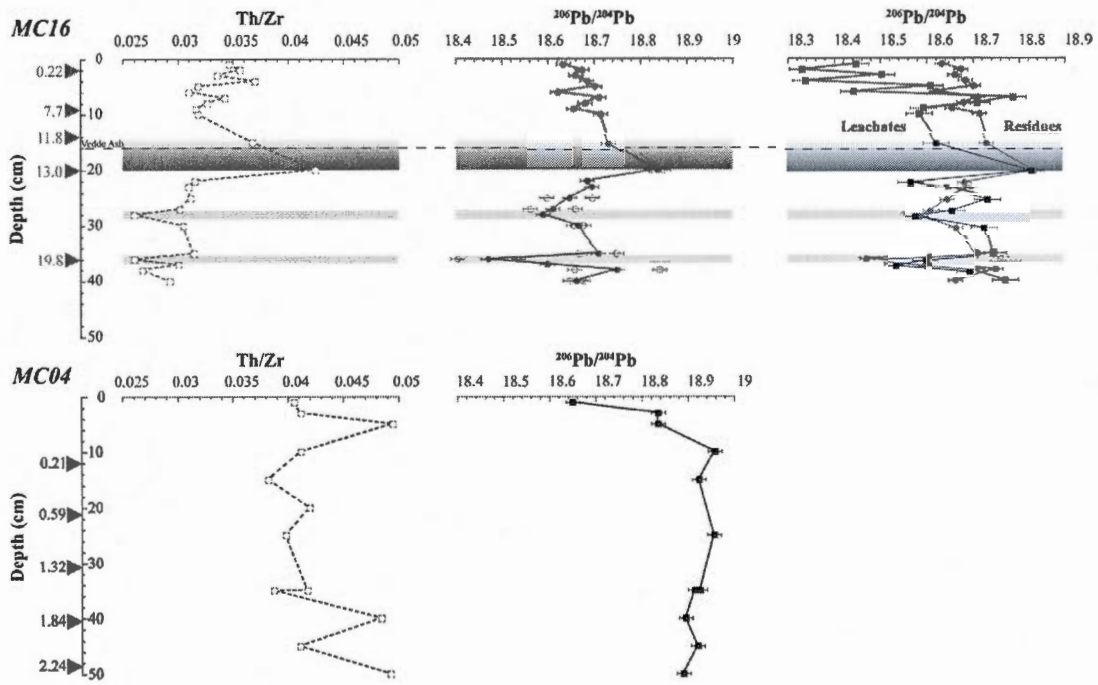


Figure 5: Th/Zr and $^{206}\text{Pb}/^{204}\text{Pb}$ profiles of cores MC04 and MC16 against depth. Red and black arrows represent calibrated ages (ka) in cores MC16 and MC04 respectively. Note the difference in sedimentation rate between the two cores. Graded grey bar represents the Younger Dryas event, thin light grey bars the 16.4 ka (28 cm) and 19.8 ka (36 cm) excursions.

Left panel: Th/Zr ratios in cores MC16 (top; open red squares) and MC04 (bottom; open black squares).

Middle panel: $^{206}\text{Pb}/^{204}\text{Pb}$ ratios in residues from cores MC16 (top; red circles) and MC04 (bottom; black squares). Open red circles represent replicate analyses of residues from core MC16, full circles represent the mean value.

Right panel: $^{206}\text{Pb}/^{204}\text{Pb}$ ratios in residues (red circles) and leachates (blue squares) from core MC16. Blue open squares represent leachate replicates. Full symbols represent the mean values of both residues and leachates.

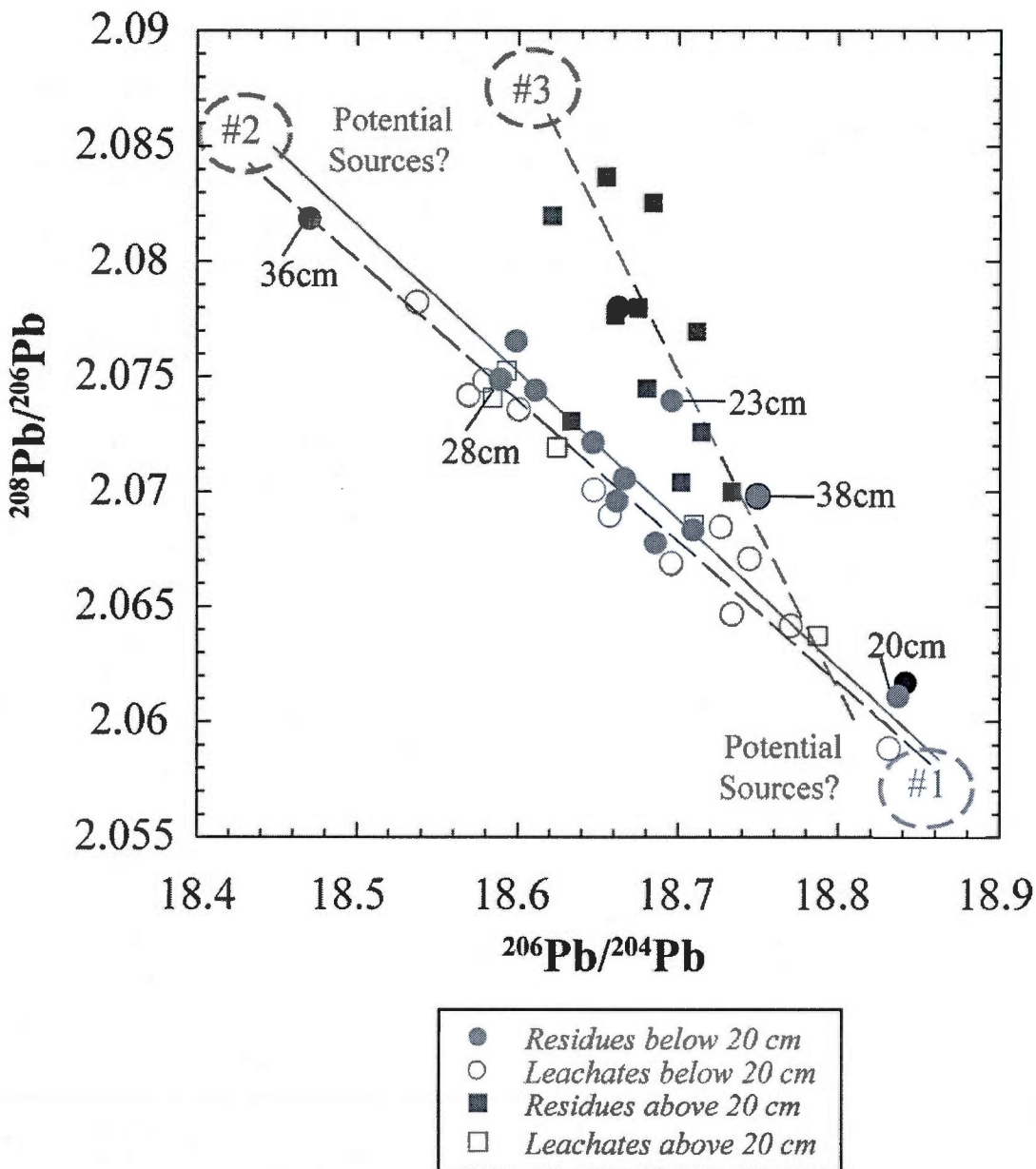


Figure 6: $^{208}\text{Pb}/^{206}\text{Pb}$ vs. $^{206}\text{Pb}/^{204}\text{Pb}$ of leachates (open symbols) and residues (full symbols) from core MC16. Due to the strong anthropogenic contribution, leachate samples from the mixed layer are not represented. Red circles: leachates and residues of samples below 20 cm, the onset of the YD. Blue squares: leachates and residues of samples above 20 cm. Fields for the three main potential sources are identified in green dashed circles. Indicated samples correspond to the isotopic excursions discussed in the text (numbers refer to depths). Black

circles represent the replicate values from the sample at 38 cm and highlight the heterogeneity of this sample although both analyses plot on the same trend. The red circle outlined in black represents the average of these two analyses.

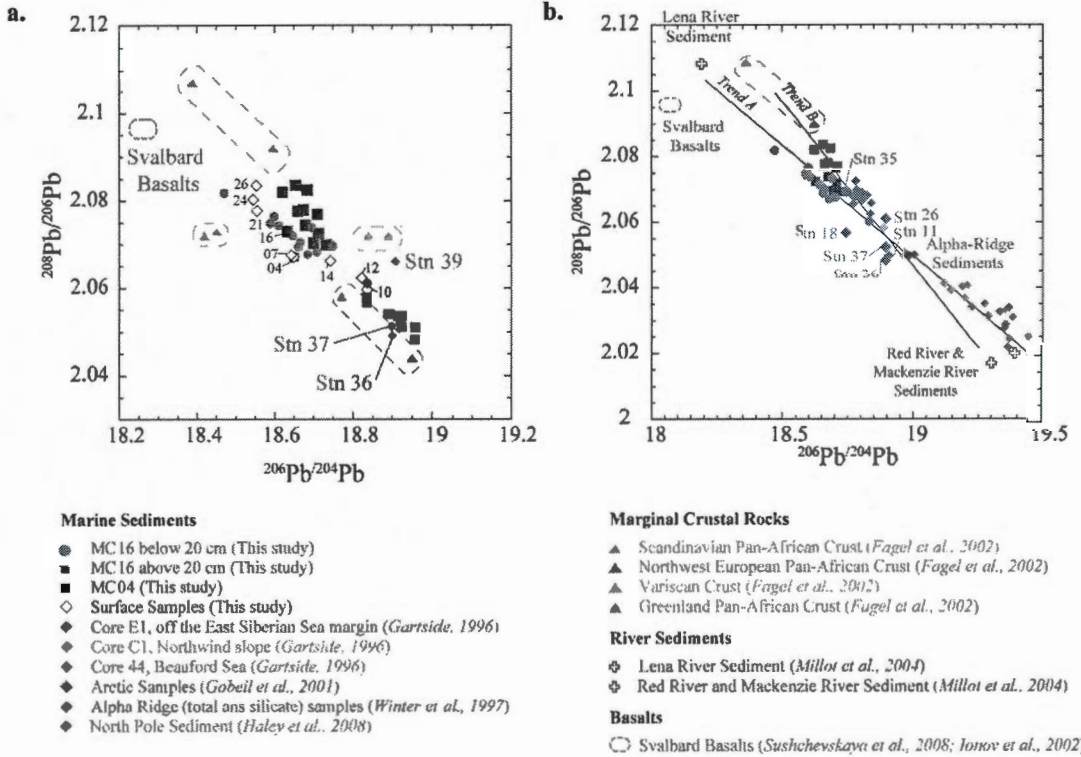


Figure 7: $^{208}\text{Pb}/^{206}\text{Pb}$ vs. $^{206}\text{Pb}/^{204}\text{Pb}$ diagram illustrating the detrital trends defined in Fig. 7 along with data from the literature for marine sediments and potential source regions a.) GIN Seas and European sources along with residues from cores MC04 and MC16 and surface sediments b.) Arctic sources and sediments along with residues from core MC16.

7. AUXILIARY MATERIAL

Table S7: calibrated age and the corresponding depth with the method used to establish the age model (2*sigma uncertainty).

Method	Depth (cm)	Age ^{14}C	Age cal (ka)
^{14}C ^a	1	0.22±0.07	0.22±0.07
^{14}C ^a	9	7.25±0.06	7.7±0.13
Geochemical correlations ^b	14	-	11.8
Vedde Ash ^a	16	10.8	12.1±0.2
Geochemical correlations ^b	20	-	13.0
^{14}C ^a	36	17.10±0.13	19.8±0.4

^a Zamelczyk et al. 2010

^b Hanslik et al. 2010 ; Not and Hillaire-Marcel 2011

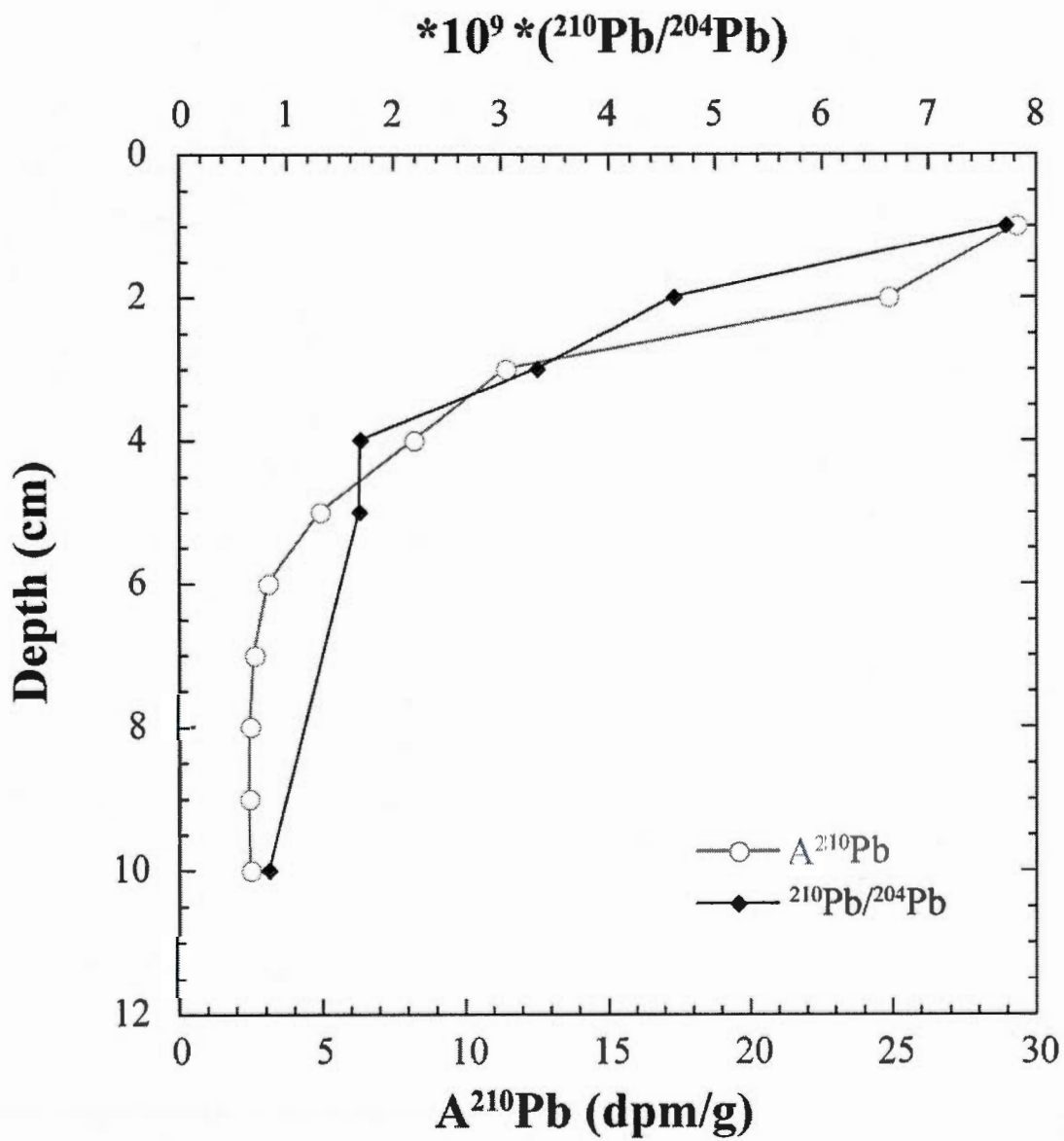


Figure 8: ^{210}Pb activity (dpm/g) and $^{210}\text{Pb}/^{204}\text{Pb}$ ratio highly correlate and illustrate the depth of the mixed layer. Note that ^{210}Pb measurement were performed on the bulk sediment with an alpha-spectrometer and that ^{204}Pb measurement were performed on the $<100\ \mu\text{m}$ sieved fraction with a MC-ICP-MS.

CHAPITRE II

GEOCHEMICAL SIGNATURES OF SEDIMENT TO DOCUMENT SEA-ICE AND WATER MASS EXPORTS THROUGH FRAM STRAIT SINCE THE LAST GLACIAL MAXIMUM

Jenny Maccali^{1,2}, Claude Hillaire-Marcel¹, Jean Carignan³ and Laurie Reisberg²

¹Geotop, Université du Québec à Montréal, C.P. 8888, Montréal, QC, H3C 3P8, Canada

²CRPG, 15 Rue Notre-Dame-des-Pauvres, 54501 Vandoeuvre-lès-Nancy, France

³Takuvik, CNRS, Université Laval-CEN, 2405 rue de la Terrasse, QC, G1V 0A6, Canada

Article Soumis à Quaternary Science Reviews (JQRS-D-11-00441)

ABSTRACT

Elemental (Ca, Zr, Th, etc.) and radiogenic isotope (Pb, Nd, Sr) measurements in leachates and residues from deep-sea sediments of core MC16 (WarmPast Program) in central Fram Strait were used to document the geochemical signatures of outflowing Arctic water masses and ice rafted debris (IRD) since the Last Glacial Maximum. In addition, the elemental distribution among the three main sedimentary fractions (terrigenous, biogenic and authigenic) was quantified. Elements dominated by the terrigenous fraction display a change at ~13ka assigned to an early Younger Dryas (YD) event. In the authigenic fraction, migration of the redox front, perhaps spurred by discontinuous delivery of organic matter to the sediment, has led to the mobility of elements such as Mn. Fe contents display lesser variability within the sediment suggesting that Fe experienced only minor redox-related redistribution. Authigenic Pb and Nd, thought to be hosted primarily by Fe-oxihydroxides, also show little evidence of mobility, suggesting that their isotopic compositions should reliably record the isotopic compositions of past bottom water.

We have broadly identified the isotopic signatures of the three major source areas of IRD, the Russian, Canadian and Greenland margins. The elemental and isotopic residue records from core MC16 display distinct trends prior to and after the YD. The pre-YD interval, with ϵ_{Nd} values between -10.1 and -13.2, and $^{87}\text{Sr}/^{86}\text{Sr}$ ratios from 0.715 to 0.721, reflects a mixture of IRD from the Russian and Canadian margins. The YD episode stands out with sediments originating mostly from the Canadian end-member, displaying the lowest ϵ_{Nd} values and highest $^{87}\text{Sr}/^{86}\text{Sr}$ ratios. This suggests enhanced sea-ice production and/or drifting along the Beaufort Gyre at that time. The post-YD interval, i.e. the Holocene, is characterized by a less variable mixture of IRD material, with ϵ_{Nd} values and $^{87}\text{Sr}/^{86}\text{Sr}$ ratios centered at -12.2 and 0.718 respectively. This material was derived from several sources including northwestern Canada (Mackenzie River), the western Arctic, the East Siberian/Chukchi Seas, and the more proximal Greenland margin.

The isotopic compositions of leachates are mostly linked to boundary exchange processes near major meltwater and freshwater source areas. Due to its longer residence time relative to Pb, Nd preserves the isotopic signature of more distal areas where high-density particulate fluxes may occur. In the studied core, Nd-isotope leachate data illustrate the influence of the western Russian margins prior to the YD event and that of the East Siberian

and Chukchi Sea margins following this event. This study illustrates that complementary information on IRD sources and water-mass histories can be obtained from isotopic analyses of inherited (residual) and exchangeable (leachable) fractions in deep Arctic Ocean sediments. Higher resolution cores are now needed to illustrate more rapid variations of paleo sea-ice and water mass circulation.

1. INTRODUCTION

The Arctic Ocean, though of small size, has a disproportionately large influence on the world's climate system (Holland et al., 2010; Jakobsson et al., 2010; Koenigk et al., 2011; Miller et al., 2010). Exports of freshwater and sea-ice may influence deep-water formation in the Greenland, Iceland and Norwegian (GIN) Seas and consequently the Atlantic Meridional Overturning Circulation (AMOC), which in turn strongly affects heat exchange with the atmosphere (Broecker, 1991; McManus J. F., 2004; Peltier et al., 2006). Sea-ice is a key feature of the Arctic climatic system notably because of its strong albedo which provides a positive feedback mechanism by reflecting solar irradiation and hence preventing heat transfer to the ocean surface, maintaining a highly stratified water column (Miller et al., 2010; Polyak et al., 2010). The role of the Arctic with respect to changes in the AMOC can be examined by documenting water mass exchanges through Fram Strait using geochemical and sedimentological records from deep-sea cores (Birgel and Hass, 2004; Carignan et al., 2008; Darby et al., 2002; Fagel and Hillaire-Marcel, 2006; Fagel et al., 2004; Fagel et al., 1997; Fagel et al., 2002; Gutjahr et al., 2008). Fram Strait is the major Arctic gateway for freshwater and sea-ice export and the only gateway for deep-water mass exchange between the Arctic and the North Atlantic (Fahrbach et al., 2001; Jones, 2001; Jones et al., 1995; Rudels et al., 2004). During glacial times, Fram Strait was also the only passage permitting exchange between the Arctic Ocean and the GIN Seas (Darby et al., 2006; Tütken et al., 2002). Atlantic waters enter the Arctic as the West Spitsbergen Current, in the eastern Fram Strait, and form the subsurface Atlantic waters present throughout the Arctic ocean. In the western part of Fram Strait, the outflowing water masses are i) at the surface, the Modified Atlantic Water; ii) in the upper subsurface, the Arctic Atlantic Water; iii) at greater depths, the Arctic intermediate Water; and iv) at the seafloor, the Canadian Basin Deep Water and

Eurasian Basin Deep Water (Figure 1) (Dickson et al., 2007; Langehaug and Falck, 2011; Rudels et al., 2005; Rudels et al., 2000). Changes in freshwater and sea-ice supplies within the Arctic are primarily linked to river discharge and to ice-sheet margin dynamics, related to the drainage of glacial lakes and/or ice-surges, calving and release of icebergs (Darby and Zimmerman, 2008; Tarasov and Peltier, 2005; Tütken et al., 2002). In addition, the inception of low-salinity water inflow from the Pacific through Bering Strait during deglaciation likely played a role that still remains poorly understood. Our aim is to document paleo sea-ice circulation and water mass exchange from late glacial to modern times.

The geochemical compositions of deep-sea sediments are indicative of their sources, transport mechanisms, and in some cases, of diagenetic processes. Marine sediments are composed of three distinct fractions: detrital, biogenic and authigenic (which includes syn-depositional and early diagenetic components). The detrital fraction is derived from weathering of continental crust, including mechanical erosion by ice-sheets, as well as from volcanic material. River transport are usually the main mechanisms that provide sediment to the ocean, but under the specific conditions of the modern Arctic, wind-transport of fine particles, iceberg-transport and sea-ice rafting can also provide a substantial amount of detrital material derived from coastal erosion (Macdonald and Gobeil, 2011). The biogenic fraction consists of fossil material, organic matter and mineralized remains. The authigenic fraction corresponds to components formed *in situ* via post-depositional chemical processes, mainly controlled by Eh-pH conditions at or below the water-sediment interface (Fütterer, 2000; Sageman and Lyons, 2003). Arctic Ocean sediments have low organic matter content and are mainly terrigenous (Rusakov et al., 2010). However, the abundance of Fe- and Mn-oxides indicates that diagenesis has had some impact on the geochemical properties of these sediments (Jakobsson et al., 2000; Löwemark et al., 2008).

In the Arctic Ocean, detrital sediments can be used to trace paleo sea-ice source areas and circulation (Darby et al., 2002; Winter et al., 1997). In addition, Fe-Mn oxyhydroxyde coatings on detrital particles, which incorporate trace elements (e.g. Pb, Rare Earth Element) as they precipitate from ambient seawater, have isotopic compositions that can provide information on the circulation history of deep-water masses (Bayon et al., 2002; Gutjahr et al., 2007). In a previous study of sediments from core MC16 in central Fram Strait (Maccalini et al., 2012), we demonstrated that certain elemental ratios and Pb-isotopes of leachates trace

exchanges with ambient waters, while the residues display detrital geochemical signatures inherited from IRD. Here we use complementary tracers (i.e., Nd- and Sr-isotopes) in samples from the same core to further document and refine source area signatures and to evaluate their implications for sea-ice circulation through Fram Strait since the last glacial maximum (LGM). We also discuss the distribution of major and trace elements among the various sedimentological fractions (detrital, biogenic and authigenic).

2. MATERIAL & METHODS

2.1 Sampling sites and settings

The studied sediment core was collected in 2006 during a WarmPast Program cruise on board the R/V Jan Mayen, along a NE-SW transect through Fram Strait (Husum, 2006). Core JM06-WP-16-MC (henceforth MC16; 79°53.767'N; 16.916'E; 2546 m water depth) is 40 cm long, and was raised in central Fram Strait below the outflowing Arctic waters (Fig. 1) (Dickson et al., 2007; Husum, 2006). The core was sub-sampled at 1 cm intervals.

The adopted age model is based on three AMS-¹⁴C measurements on planktonic foraminifera assemblages (Zamelczyk et al., 2012). The online software Calib 6.0 was used for calibration, with a standard 400-year reservoir age correction (R) and a DR value of 0 (MARINE09 calibration curve; Reimer et al., 2009). Ages are reported as calibrated years before present (BP; 2s uncertainties). In addition, tephrochronological investigations by Zamelczyk et al. (2012) established the presence of the Vedde Ash layer (~12.1 ka; Thornalley et al., 2011), thus confirming the position of the YD-Holocene transition in the core. Core MC16 spans the LGM to present, with a poorly constrained sedimentation rate before the YD (mean sedimentation rate of ~2.3 cm/ka), enhanced sedimentation during the YD (~ 5 cm/ka) and a steadier sedimentation regime during the Holocene (mean sedimentation rate of ~1.2 cm/ka). For convenience, ages will be followed by the corresponding depths downcore in cm throughout the manuscript.

2.2 Sample preparation and isotopic analyses

2.2.1 Major and trace element concentrations

The bulk fraction consists of sub-samples (~300mg) wet-sieved to <100µm, dried and ground in an agate mortar. Major and trace element analyses of residues, leachates and bulk samples were performed at the *Service d'Analyse des Roches et Minéraux*, Nancy, France, of the French *Centre National de la Recherche Scientifique*, following procedures described by Carignan et al. (2008). Full digestion of refractory phases was assured through the use of alkaline fusion. Calibration and accuracy controls were performed using international geological reference materials with relative uncertainties of approximately 1% for major element concentrations and between 5% and 10% for trace elements depending on concentration levels.

2.2.2 Carbon content and organic carbon isotopes

Organic and inorganic carbon contents were measured on bulk (~1g non sieved) samples with a Carlo Erba™ elemental analyzer. A first aliquot was dried and analyzed as evolved CO₂ for its total carbon content. A second aliquot was acidified twice with HCl (1M) to dissolve carbonates and analyzed in a similar fashion for its residual carbon content, which was considered to represent organic carbon (Hélie, 2009). Inorganic carbon was then calculated as the difference between the two measurements. Inorganic and organic carbon fractions are both expressed in dry weight percent of total sediment and represent the mean of two analyses. These values are approximate since the HCl treatment may alter many secondary minerals besides calcite and dolomite as well as mobilize soluble organic matter. The carbon isotopic composition ($\delta^{13}\text{C}$) of organic matter (decarbonated bulk fractions) was measured by continuous-flow mass spectrometry using a Carlo Erba™ elemental analyzer connected to an Isoprime™ mass spectrometer. Results are presented in the standard δ notation versus the VPDB reference value. A precision of $\pm 0.1\text{‰}$ ($\pm 1\sigma$) is estimated based on replicate analyses of standards.

2.2.3 Leaching procedure

In order to analyse specific phases from the bulk sediment, we adapted a leaching procedure based mainly on those of Bayon et al. (2002) and Guthjar et al. (2007), and more precisely described in Maccali et al. (2012) (see supplement). The bulk fraction was leached with a Na-acetate buffer (1M - acetic acid 1M; 52:48) to remove calcium carbonates from the sediment. We note that this procedure may not have removed dolomite, which is more difficult to dissolve (Rosenbaum and Sheppard, 1986). Carbonate leachates were recovered but not analysed. After rinsing, drying and grinding, the residual powder was leached with a solution of 0.05M hydroxylamine hydrochloride (HH) - 15% acetic acid - 0.03M Na-EDTA, then buffered to pH 4 with analytical grade sodium hydroxide (NaOH). This second leach was designed to specifically dissolve Fe-Mn oxides. Henceforth, the recovered supernatant will be referred to as the Fe-Mn leachate. Both the Fe-Mn leachates and residues were independently analysed for their major and trace element contents as described above in section 2.2.1, and for Pb- (presented in Maccali et al., 2012), Nd- and Sr-isotopes (see below).

2.2.4 Nd- and Sr-isotopes

Aliquots of each fraction (residues and leachates) were weighed (~100mg) and digested in a HF, HNO₃, HCl mixture on a hot plate at 130°C. After drying and redissolution, samples were loaded on a column of TRU Spec® resin, and REE and Sr-Rb were separated using dilute HNO₃. Nd was then isolated from other REE using LN Spec® resin with dilute HCl. Sr was purified through two elutions on Sr Spec® resin. Total Nd blanks for both leachates and residues were under 140 pg and represent less than 0.07% of the total Nd present in the sample. Blanks for Sr were below the detection limits of our ICP-MS (equivalent of 0.2 mg/L in solution; about 200 pg as blank samples were retrieved in a 10 ml solution).

Sr-isotopes were measured on both a MAT262 TIMS in static mode at CRPG-CNRS in Nancy, and a VG sector 54 in dynamic mode at GEOTOP in Montreal. ⁸⁷Sr/⁸⁶Sr ratios were normalized to ⁸⁶Sr/⁸⁸Sr = 0.1194. Repeated analyses of the NIST-987 standard yielded values of 0.710258 (\pm 0.000026, 2 σ reproducibility) and 0.710294 (\pm 0.000022, 2 σ

reproducibility) at CRPG and GEOTOP respectively. We have corrected the results for both laboratories to the accepted value for NIST-987 of 0.710248.

Nd-isotopes were analysed as Nd+ using the standard double filament mounting procedure (Ta filament for Nd evaporation, Re filament for ionisation). Mass fractionation was corrected to $^{146}\text{Nd}/^{144}\text{Nd} = 0.7219$. Replicate analyses of the international reference material LaJolla yielded a $^{143}\text{Nd}/^{144}\text{Nd}$ value of 0.511837 (± 0.000016 ; 2σ reproducibility) at CRPG, while the standard JNdI-1 yielded a $^{143}\text{Nd}/^{144}\text{Nd}$ value of 0.512101 (± 0.000013 ; 2σ reproducibility) at GEOTOP. Since the JNdI-1 value should be $\sim 1.000503 * \text{La Jolla}$ (Tanaka et al., 2000), these standard values are coherent, and no corrections are applied.

The Nd isotopic composition will be expressed as follows:

$$\epsilon_{\text{Nd}} = \{(^{143}\text{Nd}/^{144}\text{Nd})_{\text{Sample}} / (^{143}\text{Nd}/^{144}\text{Nd})_{\text{CHUR}} - 1\} * 10^4$$

where CHUR stands for *Chondritic Uniform Reservoir* and represents the present day average earth value $(^{143}\text{Nd}/^{144}\text{Nd})_{\text{CHUR}} = 0.512638$ (Jacobsen and Wasserburg, 1980).

The largest 1σ standard deviations of sample replicates, processed through the entire procedure, were used to quantify the uncertainty (see Tables S9 and S10 in supplements). This uncertainty includes that due to the leaching procedure, chemical separation and purification, as well as the analytical error. Values of 0.3 and 0.4 ϵ_{Nd} unit ($\pm 1\sigma$) were obtained for residues and Fe-Mn leachates respectively. An uncertainty of 0.0004 ($\pm 1\sigma$) for $^{87}\text{Sr}/^{86}\text{Sr}$ was obtained for both residues and leachates. The 1σ uncertainty calculated from replicate measurements is not much larger than the 1σ reproducibility of the standards in the case of Nd. However, uncertainties estimated from replicate measurements are more than one order of magnitude higher than those of the standards in the case of Sr. Sample inhomogeneity combined with the large differences of Sr isotope composition between minerals (Eisenhauer et al., 1999; Tütken et al., 2002) are likely the cause of the variability of replicate Sr analyses.

3. RESULTS

3.1 Elemental distribution

3.1.1 Elemental budget

Major and trace element results from residues, leachates and bulk samples ($<100 \mu\text{m}$) are presented in supplements (Tables S1-S8). Concentrations for both residues and leachates

were calculated relative to the initial mass, before both leaching steps, and were used to estimate the elemental distribution between the various fractions (detrital, authigenic, biogenic) for each sample. The authigenic fraction of each element (i.e. hosted by Fe-Mn oxides) is taken to be the fraction in the Fe-Mn leachate relative to the calcite/aragonite-free sediment (i.e. the sum of the Fe-Mn leachate and residue). The biogenic fraction (i.e. Ca-carbonate leachate) was estimated by subtracting the total content of the residue and the Fe-Mn leachate from the bulk sediment content for each element. However due to the large propagated uncertainties of the analytical errors, elemental proportions in the low-abundance carbonate fraction are discussed in only a qualitative manner.

The following elemental groups were defined: i) those displaying a nearly exclusively terrigenous behaviour (less than 10%wt are leached), ii) those for which a large fraction is related to carbon (C) and hence to biogenic phases, iii) Fe, Mn and elements for which $\geq 20\%$ wt was removed during the Fe-Mn oxide leaching step. Examples of each of these groups are plotted in Fig. 2, with elemental concentrations in the bulk sediment and the residual fraction normalized to those of aluminium, a proxy for alumino-silicate content. Aluminium is derived almost exclusively from terrigenous inputs, has a negligible anthropogenic component and is non reactive, thus its concentration should not be modified through diagenetic chemical reactions within the sediment. It is therefore frequently used to estimate terrigenous inputs and mineralogical variability.

3.1.2 The terrigenous fraction

The presence of minor Al in leachates suggests some dissolution of alumino-silicate minerals during the leaching procedure. However, less than 2% of the total Al is found in leachates on average. Comparatively, up to 7% Mg was recovered in the leachates, suggesting its presence in sites and/or compounds more readily affected by leaching procedures (e.g. dolomite from the Canadian Arctic : Bischof and Darby, 1997). Nonetheless, Al and Mg primarily illustrate properties of terrigenous fractions. From 21.5 to 13.0 ka (40 to 20 cm downcore), Al contents of bulk sediment and residual fractions vary little (Fig. 2). From ~ 13.0 ka (20 cm) on, the Al content decreased, especially in the bulk fraction (blue squares in Fig. 2), probably reflecting dilution by carbonates. Mg/Al ratios in both residues and bulk sediments vary little, except for two "excursions" at ~ 15.1 and ~ 13.0 ka (25 and 20

cm respectively; Fig. 2). In fact, the terrigenous fraction of the geochemical record of Fram Strait changes markedly at ~13.0 ka (20 cm). Other elements (not shown in figure 2; e.g. Si, Ti, Zr) show a similar change at this horizon. Even though these chemical excursions are seen in both the bulk and detrital fractions, they are more pronounced in the latter. In addition to Al and Mg, several other elements, Si, Ti, Zr, Na, K, Th, and to some extent Fe, are hosted primarily by detrital minerals and hence are particularly sensitive to changes in sediment sources.

3.1.3 The biogenic fraction

The biogenic fraction is estimated using the organic (C_{org}) and inorganic (C_{inorg}) carbon contents. As illustrated in Figure 3a, C_{org} contents were constant at ~0.5% until ~8.3 ka (10 cm) and then started to increase. The C_{inorg} content is negligible in the section from ~21.5 to ~12.0 ka (40-15 cm), then increased sharply, reaching a maximum value of ~1% at ~9.2 ka (11 cm). The $d^{13}C$ values of C_{org} (Fig. 3b) increase steadily from -25.5 ‰ V-PDB at the bottom of the core to -24.0 ‰ V-PDB at the core top except for a large excursion with a value of -23.4 ‰ at ~14.3 ka (23 cm). The bulk Ca-fraction correlates with C_{tot} (R^2 of 0.97) and with C_{inorg} (R^2 of 0.97). Ca (mole/g) and C_{inorg} (mole/g) correlate with a slope of ~1 suggesting that the C_{inorg} is primarily hosted by Ca-carbonate. Thus the bulk profile of Ca/Al (Fig. 2b) closely resembles that of C_{inorg} (Fig 3a). Ca/Al remained stable prior to ~13.0 ka (from the core bottom to 20 cm), then increased sharply at ~12.4 ka (17 cm), remained constant from ~8.3 to ~3.8 ka (10-5 cm), then increased again from ~3.8 ka (5 cm) to the surface. Sr/Al and the Ba/Al profiles in bulk sediments display similar patterns, with increasing concentrations after ~13.0 ka (from 20 cm towards the surface), consistent with the fact that both Sr and Ba may substitute for Ca in carbonates. In contrast, Sr, Ba and Ca in residues display little variation throughout the sequence. The Ca/Al and Sr/Al ratios in residues (average values of 0.09 and 0.0020 respectively) are much lower than the mean continental crust values (0.37 and 0.0044 respectively; Taylor and McLennan, 1985), perhaps because much of the Ca and Sr contents in the upper crust is found in carbonates. The carbonate phase contained, respectively, 20%, 9% and 1% of the Ca, Sr and Ba present in the bulk sediments prior to ~13.0 ka (20 cm), and 54%, 46% and 11% of these elements in the younger, more carbonate-rich sediments.

Estimated masses of CaCO_3 calculated from C_{inorg} are comparable to those that would be expected from stoichiometry (assuming all non-detrital Ca is hosted by calcite) in the upper half of the core except for one sample at ~ 12 ka (15 cm). As for Mg, the quantity that could be hosted by dolomite (MgCO_3) is minor, as CaCO_3 can account for almost all of the available C_{inorg} . Dolomite is less easily dissolved than calcite so our results might reflect the non-dissolution of dolomite with the acetate solution. In addition the method used to estimate C contents might have not dissolved dolomite as only fumigation (Hélie personal communication) seems to significantly attack this phase. Thus we cannot accurately discuss dolomite content in our sediments.

3.1.4 The authigenic fraction

Fe and Mn are contained in both the terrigenous fraction and in Fe-Mn oxides, which are among the most important authigenic components in marine sediments. The Fe/Al ratio of the bulk sediment increased from ~ 19.4 to ~ 17.3 ka (35-30 cm) and then remained constant up to the present (Fig. 2c). In the residue profile, Fe/Al increases gradually moving upwards, with both low and high Fe concentration excursions at ~ 15.1 and ~ 13.0 ka (25 and 20 cm), respectively. Thus, detrital Fe, like other elements linked to the terrigenous fraction, peaked at ~ 13.0 ka (20 cm). The Fe-Mn leachates contained an average of 6% of the Fe in sediments older than ~ 19.4 ka (35cm) and approximately twice as much ($\sim 13\%$) in sediments younger than ~ 17.3 ka (30 cm). P and As, and to a lesser extent V, correlate with Fe and are thus thought to be adsorbed onto, or incorporated into Fe-hydroxides.

The Mn/Al profiles differ from those of Fe/Al (Fig. 2). The bulk Mn/Al-profile shows a sharp excursion at ~ 16.4 ka (28 cm) followed by steady, slightly increasing values till ~ 8.3 ka (10 cm), then by a nearly constant value afterwards. The residue profile displays low, nearly constant Mn/Al ratios. These observations are consistent with the fact that up to 90% of the Mn from the ~ 16.4 ka-excursion layer was leached, whereas an average of 70% was leached in sediment younger than ~ 15.6 ka (upper 26 cm). The Mo/Al (Fig. 2) bulk profile resembles that of Mn/Al and displays a similar major excursion at ~ 16.4 ka (28 cm). The Mo/Al residue profile is again similar to that of Mn/Al, showing very little variation with depth. Thus Mo, as well as Ni, which displays a similar profile (not shown), is thought to have a high affinity for Mn oxides.

Particle reactive elements such as Rare Earth Elements (REE) and Pb are also hosted by both the detritic and authigenic fractions. An average of 20-25% of the Nd is removed during the leaching step that dissolves Fe-Mn oxides. Due to the overall similarity of their chemical properties, all REE display similar depth profiles, and Nd is shown as an example in Fig. 2. Bulk REE/Al values show some variations but no clear trend. Residues show relatively constant REE/Al with negative excursions at ~20.2, ~16.4 and ~13.0 ka (37, 28 and 20 cm), and a positive excursion at ~5.6 ka (9 cm). *Post-Archean Australian Shale* (PAAS) (Taylor and McLennan, 1985) normalized REE spectra of the measured leachate compositions display some Middle REE (MREE) enrichment (Fig. 4).

Finally, bulk Pb/Al ratios (Fig. 2) were about constant in the ~21.3 to ~17.3 ka (40-30 cm) interval, increasing slightly between ~17.3 and ~8.3 ka (30-10 cm). A slight decrease then prevailed from ~8.3 ka (10 cm) to the lower limit of the mixed layer at ~4.7 ka (6 cm). In contrast, Pb/Al values in residues are constant throughout the record. Through most of the profile, about 60% of the Pb is contained in the Fe-Mn oxide leachates. This relatively high value might be explained by readsoption of some of the Pb-acetate complex formed during the first leaching step onto Fe-Mn oxides (Shen et al., 2001), thus we might overestimate the amount of Pb that is truly leached during the removal of Fe-Mn oxides.

3.2 Isotopes: solid residues and coating phases

3.2.1 Residues

The Sr- and Nd-isotopic compositions in residues vary with depth (Table 1) and show distinct trends before and after the ~ 13 ka excursion assigned to the Younger Dryas (YD; Fig. 5). Prior to the YD (*Trend A*), supplies were quite variable, at least with respect to Sr-isotopes, as illustrated by the isotopic excursions towards lower $^{87}\text{Sr}/^{86}\text{Sr}$ ratios dated at ~16.4 and ~19.8 ka (28 and 36 cm). After the YD, Sr isotopes displayed lesser variability (*Trend B*), with $^{87}\text{Sr}/^{86}\text{Sr}$ ratios centred at 0.718. In contrast, Nd isotopes, which varied gradually prior to the YD (LGM to 13.0 ka), depict a "noisier" record in younger sediments. The Sr isotopic excursions at ~16.4 and ~19.8 ka have no equivalent in the Nd record.

3.2.2 Leachates

Before discussing the geochemical properties of the leachate fraction, we consider the possibility that our leaching procedure may have partly dissolved the detrital fraction, in which case the leachates would not represent a purely hydrogenous component. We tested this possibility using mass balance calculations as suggested by Gutjahr et al. (2007), from whom we adapted the leaching procedure. Using the Sr isotopic compositions of each fraction (Table 1 and 2), and assuming that the authigenic $^{87}\text{Sr}/^{86}\text{Sr}$ ratio is that of seawater (essentially constant over the time period considered), it follows that the detrital phase contributed an average of 20% of the Sr found in leachates. Assuming a similar detrital proportion for Pb and Nd, $^{206}\text{Pb}/^{204}\text{Pb}$ ratios and ϵ_{Nd} values in leachates could have been shifted by up to ~ 0.005 and ~ 0.25 respectively. In both cases, this effect is within the conservative error bars estimated above. Since the potential effect is minor and the validity of the correction is uncertain, we use uncorrected values with adjusted error bars in the following discussion. The leachates can therefore be considered to represent the authigenic component, from a Pb and Nd perspective.

The Pb-isotope record from leachates is noisy, even if one excludes the mixed layer (upper 6 cm) which shows a strong anthropogenic imprint (Maccali et al., 2012). Nd isotopes of the three bottom samples have an average ϵ_{Nd} value of -8.6 ± 0.1 . ϵ_{Nd} then decreases to values as low as -10.6 (at ~ 12 ka, 9 cm) before increasing again to -9.5, near the core top.

4. DISCUSSION

4.1 Elemental distribution among the fractions

4.1.1 Terrigenous fraction

The concentrations of several elements in the residual fraction show a change at ~ 13.0 ka (20cm; e.g. Al, Mg, Fe and Si, Zr, Na), indicating a short-lived event during the YD followed by a long-term change in the supply of terrigenous material. The Pb-isotope results (Maccali et al., 2012) suggest a strong pulse of material from the Canadian Arctic during this YD event.

4.1.2 Biogenic fraction

Organic matter flux from the continents as well as primary productivity account for C_{org}-concentrations. The relatively steady increase in d¹³C values towards the core-top (Fig. 3b) reflects an increase in the proportion of ¹³C-enriched marine organic material, suggesting a progressive increase in marine productivity and/or a decrease in the relative supply of terrestrial organic carbon (Meyers, 1997). A brief excursion towards heavier C_{org} isotope values is recorded below the YD interval and might be related to a peak in biogenic productivity during late Bölling-(Older Dryas)-Alleröd time (Aagaard-Sørensen et al., 2010). The increase in C_{tot} starting at ~12.0 ka (15cm) is controlled by the C_{inorg} fraction (Fig. 3a), thus to enhanced relative supplies of detrital carbonates and/or enhanced marine productivity (mostly planktic foraminifers here; see Zamelczyk et al., 2012). Assigning a mean weight of 10 µg to shells of the most abundant planktonic foraminifera *Neogloboquadrina pachyderma* (Hillaire-Marcel et al., 2004; Zamelczyk et al., 2012), and assuming that C_{inorg} is 100% hosted by CaCO₃, a mean abundance of 2000 to 9000 planktonic foraminifera per gram of sediments would be required to account for the observed C_{inorg} concentrations. Foraminiferal abundances reported by Zamelczyk et al. (2012) are significantly lower than these estimates, thus suggesting the presence of detrital carbonates. The largest shift in the C_{inorg} content is observed towards the end of the YD-interval (Fig. 3a). This might be linked to a meltwater pulse that occurred during the YD, in the Mackenzie estuary area (Murton et al., 2010; Peltier et al., 2006; Tarasov and Peltier, 2005, 2006), and the subsequent enhancement of ice-rafting deposition observed "upstream" in the Trans-Polar Drift, on Lomonosov Ridge, by Not and Hillaire-Marcel (2012). A much slighter increase in both C_{org} and C_{inorg}, seen at ~3.8 ka (5cm), might be related to an increase in marine productivity and thus, possibly, a decrease in the sea-ice cover.

Elements associated with the biogenic fraction, like those dominated by the terrigenous fraction, display a change at the YD interval (20-14 cm), coeval with the increases in C_{tot} and C_{inorg} (Fig. 3a). Elements involved in the relevant biochemical and biogeochemical cycles can modify the Eh-pH conditions within the sediment, thus possibly inducing precipitation/dissolution reactions among organic and inorganic compounds. C_{org} delivery has been suggested to vary seasonally (Link et al., 2011; Rysgaard et al., 1998) and hence could have affected the Eh-pH conditions in the sediments and thus the distribution of redox sensitive elements (Fütterer, 2000; Sageman and Lyons, 2003). Since we have

specifically leached Fe-Mn oxides, and because Fe and Mn speciation vary with redox condition, we discuss briefly below their behaviour within the sedimentary column.

4.1.3 Authigenic fraction

Gobeil et al. (1997) and later Katsev et al. (2006) have shown that a pulse of C_{org} delivered to sediments of ordinarily low organic content, may lead to the redistribution of both dissolved and particulate Mn within the sedimentary column. The Arctic Ocean is characterized by relatively low fluxes of organic matter, especially during periods of thick sea-ice cover, i.e., during glacial times. However during deglacial intervals, pulses of organic matter, provided for example by spring melting, may force the redox front to migrate upwards and redistribute redox sensitive elements such as Mn. Fe and Mn both have several valence states and easily form oxides and hydroxides (oxyhydroxides). Fe-Mn oxyhydroxides have a high adsorption capacity resulting in the removal of various metals from seawater/pore-water (e.g. Mo, Pb, Th and REE) (Haese, 2000; Koschinsky and Hein, 2003; Maynard, 2003; Rusakov et al., 2010; Sageman and Lyons, 2003). Whereas Mn is more readily "redissolved" than Fe, Fe is more reactive and precipitates more easily than Mn (Glasby, 2000). As a consequence, while Fe has a tendency to remain immobile, Mn migrates upwards until it reprecipitates at the redox boundary (Anschutz P., 2005; Belzile N., 1989; Gobeil C., 1997; Koschinsky and Hein, 2003). This difference in the behaviours of Fe and Mn is clearly seen in the Mn/Al excursion at ~16.4 ka (28cm) in the bulk sediment profile, which reflects an increase in the authigenic Mn component. A strong excursion in the bulk Mo profile is observed at the same level. Mo, like Mn, is highly sensitive to redox conditions and is easily remobilized (März et al., 2011), then restabilized, possibly through its linkage with Mn oxides (Glasby, 2000). It is apparent that the excursion at ~16.4 ka (28 cm) is absent in the Fe profile, suggesting a comparatively minor redistribution of Fe and of elements incorporated or adsorbed on Fe-hydroxides within the sedimentary column.

PAAS normalized REE spectra of the leachates display the MREE bulge and the positive Ce anomaly (Fig. 4) typical of authigenic material (Gutjahr et al., 2007; Haley et al., 2004; Martin et al., 2010). Haley et al. (2004) suggested that the MREE bulge in pore water is linked to Fe²⁺ dissolved from Fe-hydroxides. Assuming this is true for our samples, the

REE leachates are preferentially carried by Fe-hydroxides and would therefore not be significantly redistributed within the sedimentary column as Fe seems to have a reduced mobility. Unlike Mn and Mo, the REE show little or no change at ~16.4 ka (28 cm) in the bulk sediment profiles. Similarly, the absence of a peak in the Pb bulk fraction at ~16.4 ka (28 cm), coupled with the correlation of Pb with Fe (R^2 of 0.49) and the near lack of correlation with Mn (R^2 of 0.15), suggests that Fe-hydroxides are a more important host of authigenic Pb than Mn-oxides. We suggest here two possible explanations to explain the low diagenetic mobility of Pb and Nd within the sedimentary column. The first hypothesis is that conditions are not sufficiently reducing to dissolve and mobilize Fe oxides. As Pb and Nd seem to be preferentially hosted within Fe oxides they also would remain immobile. Nevertheless, though Fe oxides are more stable than Mn oxides, several studies have shown that Fe is indeed mobile under certain circumstances (Neffke et al., 2012; Scholz et al., 2011). Therefore we also suggest a second hypothesis, which is based on the highly particle reactive behaviour of both Pb and Nd. Thus even if Pb and Nd are released into the pore water through Fe oxide reduction, they may be then re-adsorbed onto the surfaces of some still unidentified phases.

These considerations suggest that Pb and Nd are not prone to extensive redistribution within the sediment, and are thus suitable for documenting the isotopic compositions of paleo water masses. Therefore our leachate Nd- and Pb-isotopic data can be viewed as reliable paleo-proxies of ancient water masses.

4.2 Sedimentary supplies: influence of eolian material and grain size

Changes in transport mechanisms may result in changes in sediment grain-size, which could be linked to changes in the isotopic composition of the sediment, particularly for Sr and Pb isotopes (Eisenhauer et al., 1999; Tütken et al., 2002). Changes in eolian supplies, in sea-ice/iceberg rafting routes or the flooding of continental shelves due to sea-level rise, and in oceanic currents, are likely to leave an imprint on the geochemical signature of marine sediments. We demonstrate below that eolian contributions and changes in sedimentary transport mechanisms probably had only minor effects on the sediment composition at site MC16. Indeed, only small particles (<5 μm) such as dust can be wind-transported over long

distances (Biscaye et al., 1997). This wind-carried material represents a small fraction (10 to 15 wt% at most) of the total sediment in the modern Arctic (Lisitzin, 2010). Previous studies have reported the presence of dust in ice-cores (Biscaye et al., 1997; Lupker et al., 2010 and references therein; Svensson et al., 2000). Contrary to inland peatbogs whose Pb isotopes reflect a local to regional composition (Kylander et al., 2010), dust in ice cores has a more distal origin (Biscaye et al., 1997; Lupker et al., 2010). Unfortunately, dust cannot be distinguished by grain-size from sea-ice carried sediments (i.e. glacial flour). Moreover, due to possible partial dissolution of fine air-transported particles in the water column (Bayon et al., 2002; Bayon et al., 2004), a fraction of the eolian signal might be recorded in the dissolved phase. To evaluate the importance of the eolian contribution to Fram Strait sediment during the YD event, we consider a meltwater flux of $\sim 1\text{dSv}$ (Tarasov and Peltier, 2006) during the YD event (equivalent to 10^{15} cubic meters or 2.9×10^{18} kg of ice over 1000a). The Arctic basin area is $14 \times 10^6 \text{ km}^2$, however, as it is unlikely that material from a meltwater pulse from the Laurentide ice sheet could reach Siberian margins, we considered two-thirds of this area ($\sim 10 \times 10^6 \text{ km}^2$). Assuming a dust concentration of 0.1 mg/kg as reported in Lupker et al. (2010) from the analysis of a Greenland ice-core, an average flux of $\sim 4 \text{ mg/cm}^2/\text{ka}$ of reworked eolian material can be estimated during the YD which represents less than 1% of the sedimentary flux in Fram Strait core MC16 during the YD event ($\sim 11.5 \text{ g/cm}^2/\text{ka}$). This is a rough estimate that assumes a homogenous distribution of the dust load over the considered two-thirds of the Arctic basin; nevertheless it suggests that the dust contribution to the Fram Strait core can be neglected.

In addition, analyses of the %wt of the $>106\mu\text{m}$ fraction display no variations ($\sim 6\%$ wt on average) except for the surface samples (16%wt). The grain-size distribution of the fine fraction shows little variation with depth. The mean distribution (illustrated in supplements) exhibits two modes, at $\sim 2\mu\text{m}$ and $\sim 8\mu\text{m}$. The constancy in the percentage of the coarse fraction and the near uniformity of the fine fraction distribution with depth suggest that sedimentary transport mechanisms have probably not significantly changed since $\sim 21\text{ka}$. Sediments at the site of core MC16 are hence believed to be mainly ice-rafted since the LGM as the dust influence has been estimated to be negligible. The small variations in grain-size distribution throughout the core are therefore thought to have only a minor impact on the isotopic composition, which can thus be used to trace source areas.

4.3 Residues - Tracing variations in ice-rafterd detritus through time

As discussed above, it is likely that the eolian contribution to the fine fraction of the sediment is negligible, compared with that of terrigenous material, trapped where sea-ice forms and distributed through IRD processes. Terrigenous-IRD can thus be considered to be the main detrital transport and deposition mechanism of core MC16 sediments. Potential sources of ice rafted deposits and their variations with time will be examined below.

4.3.1 Defining potential source regions

Since the Arctic Ocean is a semi-enclosed basin, terrigenous source regions for the Arctic are limited to the adjacent terrains. These include: Pan-African terrains of Northern Greenland; the Canadian Arctic Archipelago; the Mackenzie delta region; Northern Alaska; the Chukchi Sea with Pacific influences; the East Siberian Sea; the Laptev Sea; the Kara Sea; the Barents Sea; Pan-African crust of Svalbard. Unfortunately the radiogenic isotope compositions of each of these regions are at best only partially documented. In addition, the circum-Arctic terrains display a mosaic of lithologies. As the isotopic composition provided by each source depends on its lithology (e.g. rock type, age) and its weathering rate, no easy estimations can be made of the average composition delivered to the ocean by each region. We will nevertheless use data from the literature (e.g. marine sediment, crustal material, basalts) to try to define the isotopic compositions of potential sources. The discussion will be based mostly on margin sediments, both because they are much easier to characterize than the average bedrock lithology of the adjacent continents and because coastal erosion currently delivers about two-thirds of total sedimentary supply to the Arctic Ocean (Macdonald and Gobeil, 2011).

The most abundant literature is on Nd- and Sr-isotopes. It has allowed us to define a few source areas more precisely than can be done on the basis of Pb-isotopes alone, in particular the Siberian source. Data from the Barents Sea, Kara Sea, West Laptev Sea, East Laptev Sea and the outer Laptev margin are represented in Fig. 7a. The Lena/East Laptev region displays lower ϵ_{Nd} values and can thus be distinguished from the Barents-Kara-West Laptev Sea (BKWLS) area. Sediments from the outer margins of the Laptev Sea have

intermediate compositions illustrating the combined influence of both east and west Laptev sources (Fig. 6a). The lower ϵ_{Nd} values displayed in the East Laptev Sea relative to the West Laptev Sea might reflect the presence of relatively old exposed craton upstream, in the Lena catchment basin (Gladkochub et al., 2006; Gladkochub et al., 2010; Reichow et al., 2009; Vovna et al., 2009). This is also true for the Mackenzie river sediment that display ϵ_{Nd} value similar to that of the Lena. However, their Pb isotopic ratios are significantly different. The lower $^{208}\text{Pb}/^{206}\text{Pb}$ ratios of the Mackenzie river sediment might reflect the more granitic nature of the North American Craton. We also note that Lena sediment plots off the Noril'sk area (i.e. Putorana plateau) in the Sr-Nd diagram while it plots right into it in the Pb-Pb diagram. This highlights the usefulness of a multi-isotopic approach to characterize sediment sources.

4.3.2 Last Glacial Maximum to Younger Dryas (Trend A)

As can be seen in the geochemical and isotopic profiles (Fig. 2 and 5.), a "turning point" in the nature of the sediments deposited in core MC16 occurred at ~13.0 ka (20 cm), that is, at the time of the YD. Two distinct temporal trends, prior to (*Trend A*) and after (*Trend B*) the YD were previously defined on the basis of Pb isotopic data (Maccalli et al., 2012) and correspond to a change in source region (Fig. 6b). Below, we use Sr and Nd isotopic results to more clearly identify the nature of these source regions.

Based on Pb-isotope data, Maccalli et al. (2012) defined the mixing end-members of *Trend A* as the Canadian Arctic margins (end-member #1) and Russian margins (end-member #2). The Sr and Nd isotopes data allow end-member #2 to be more tightly defined as the BKWLS area, as illustrated in Fig. 6a. Interestingly, surface sediments from the Lomonosov Ridge (Eisenhauer et al., 1999), located "upstream" in the Trans-Polar Drift (TPD) relative to the Fram Strait site, plot near *Trend A* between end-members #1 and #2. The TPD includes sea-ice from the Beaufort Gyre (BG) (Darby et al., 2006 ; and references therein) and hence, material from the western (i.e. Canadian) basin (excluding Greenland) which is roughly equivalent to end-member #1, and sediments from central Siberia which are similar to end-member #2.

Ignoring isotopic excursions, the steady trends characterizing the interval below the YD layer illustrate a gradual change from predominantly BKWLS to predominantly

Canadian Arctic IRD material. This change is particularly striking in the Nd-isotope record (Fig. 5). This trend may reflect the earlier disintegration of the Eurasian Ice Sheet relative to that of the Laurentide Ice Sheet (Andrews and Dyke, 2007; Svendsen et al., 2004). The end of the *Trend A* period is marked by a large isotopic excursion at the base of the layer assigned to the YD. A similar large amplitude excursion was observed ‘upstream’ in the TPD, on Lomonosov Ridge (Not and Hillaire-Marcel, 2012). Both sites record a geochemical and isotopic event that may have been linked to a major meltwater pulse from the Laurentide Ice Sheet that passed via the Mackenzie river outlet into the Beaufort Sea (Murton et al., 2010; Not and Hillaire-Marcel, 2012; Teller et al., 2005). This meltwater pulse is thought to have triggered enhanced sea-ice circulation along the BG carrying a Canadian isotopic signature. The YD event thus appears to be a turning point in the MC16 sedimentary sequence, marking a drastic change in sea-ice export rates and drift routes.

Below the YD layer, two other excursions towards compositions closer to the Siberian end-member (#2) are observed in the Pb and Sr isotopic records at 28 and 36 cm (Fig. 5). The older of these is dated at ~19.8 ka, suggesting a paleogeographical event in this area at this time. In core PS1230, located a few hundred nautical miles NNW of site MC16, Darby and Zimmerman (2008) observe a peak in Fe oxides-grains dated at ca 19 ka to which they assign a Laptev Sea provenance. Similarly, an IRD event of the same age, was identified in the Yermak plateau area (Knies et al., 1999), and assigned to a short meltwater event on the northern margin of the Svalbard-Barents Sea ice sheet. This excursion in the studied core might thus be linked to Eurasian Ice Sheet dynamics. Excursion 1 dated at ~16.4 ka is concomitant with the Mn and Mo peak in the authigenic fraction discussed above while excursion 2 dated at ~19.8 ka corresponds to a relative decrease in Mn in this fraction. Despite the similar isotopic compositions, these two excursions might have been caused by different triggers. Indeed, the isotopic excursion seen in the residual fraction at ~16.4 ka may reflect processes that also caused changes in the redox conditions at that time during the Eurasian Ice Sheet deglaciation.

4.3.3 Younger Dryas to Present (*Trend B*)

Residues from sediments overlying the YD event plot in a distinct cluster in Sr-Nd isotope space (Fig. 6a). Pb isotopes, on the other hand, define a rough trend (*Trend B*, Fig.

6b), that includes practically no significant contributions from the western Russian margins, but maintains inputs from the Canadian Arctic and probably from the Chukchi Sea/Bering Strait area (Maccali et al., 2012). The latter (end-member #1 defined above) are mixed with a new component (end-member #3) with Pb isotopic compositions suggesting a Pan-African terrain source region, which might plausibly be located in northern Greenland and/or Svalbard. Sr and Nd isotopes do not provide further constraints, but they are not in contradiction with this interpretation. Sediments from the Lomonosov Ridge (Eisenhauer et al., 1999; Haley et al., 2008b), located ‘upstream’ of our study site on the TPD trajectory, do not display any Pan-African affinities (Fig. 7), suggesting that the post YD Fram Strait sediments have incorporated material from a more proximal source. Both NE Greenland and Svalbard could be considered since they both contain Pan-African material. However, as discussed in Maccali et al. (2012), modern ocean current pathways rule out any significant contributions from Svalbard, and the relatively uniform geochemical responses observed throughout the Holocene sequence suggest that this circulation pattern likely prevailed throughout the whole interval. Therefore, we tentatively assign end-member #3 to the proximal NE Greenland margin which could also be responsible for the measured increase in detrital carbonates (Fig. 3a) as this region contains abundant carbonate rocks (Andrews and Eberl, 2011 and references therein ; Parnell et al., 2007).

The lack of sedimentary inputs carrying a Siberian-Pb isotopic signature during the Holocene deserves further examination. Modern sea-ice drifting follows two distinct patterns (Fig. 7): i) under strong Arctic cyclonic conditions a prominent BG accompanied with a West-East trend along northern Greenland; ii) under anti-cyclonic conditions a weak gyre and a relative stronger vector from the Siberian margins towards Fram Strait (Serreze and Barry, 2005). Clearly, the Holocene geochemical signature of core MC16 corresponded mostly to the first of these patterns: a strong supply of material from the Canadian margin carried by the BG, accompanied by some material from northern Greenland, evacuated eastwards with the multi-year ice accumulated in this area, under cyclonic conditions (Larsen et al., 2010; Möller et al., 2010; Serreze and Barry, 2005). Finally, unlike the older Holocene samples, the surface sediment sample includes some Siberian-derived IRD-material (Fig. 6b), suggesting a recent shift towards prominent anti-cyclonic conditions. Sea-ice carried IRD from Siberian margins could be evacuated through the Barents sea route towards the GIN seas.

4.4 Leachates - The exchangeable Pb and Nd fractions

As discussed above, sediment leachates are composed mostly of Fe-Mn oxyhydroxides, and their isotopic compositions reflect those of the water masses from which they form, either at the sediment-water interface or within the water column during settling. Tachikawa (2003; 1999) and Lacan and Jeandel (2007; 2004, 2005a, b) have discussed isotopic exchange between particles and water masses, a process known as boundary exchange. The isotopic composition of sea-water would equilibrate through dissolved/particulate exchange in regions with high particulate fluxes such as river mouths and continental margins.

However, before using leachate isotopic compositions to try to trace water masses that acquired their isotopic signatures through boundary exchange processes, we must consider the potential influence of terrigenous (or pre-formed) oxides, as mentioned by Bayon et al. (2004). These oxides would be formed on continents and transported towards the ocean where they could interfere with the authigenic signal (Bayon et al., 2004). As we leached the Fe-Mn oxide phase, our method does not allow us to distinguish between pre-formed vs *in situ*-formed oxides. Under glacial conditions, river runoff would have been decreased compared with modern conditions. Ice-streams would have transported mechanically eroded particles from the bedrock and hence the input of terrestrial oxides to the oceans is expected to have been lower during glacial intervals. During deglaciation, it has been suggested that redox elements undergo several cycles of reduction/oxidation (Macdonald and Gobeil, 2011) in the shallow part of the basin (i.e. continental margins). As sediments are thought to be incorporated into sea-ice above margins, the amount of terrigenous oxides that would be transported to the deep basins could be expected to be relatively low. In addition, Pb-isotopes from leachates plot on a single trend while those of the residues plot on two distinct trends. Pre-formed oxides should carry a signature similar to that of the continental source and hence to that of the residues. The distinct isotopic patterns observed for leachates and residues argue for only a minor contribution from terrigenous oxides, but the exact size of this contribution cannot be quantified.

Pb-isotope compositions of leachates plot on a single trend (*Trend A* of the residue data), throughout the whole sequence (Maccali et al., 2012), rather than on the two temporally distinct trends displayed by the residue data. This was interpreted to mean that the deep water Pb was derived from only the Russian and Canadian margins, in varying proportions. The influence of northern Greenland during the Holocene inferred from the detrital fraction is not obvious in the exchangeable Pb of the leachates. Dissolved Pb has a short residence time in the ocean (Henderson and Maier-Reimer, 2002), and is thus strongly influenced by exchange between water masses and suspended particulate matter in continental margins where high particulate fluxes occur. Hence, the exchangeable Pb record of MC16 indicates that the two major particulate sources that contributed to dissolved Pb in the Arctic Ocean during the studied interval were rivers and meltwaters from the Russian and the Canadian margins. Two causes may account for the lack of any clear imprint from the Greenland margins in this exchangeable Pb: i) the absence of any major river flowing from northern Greenland into Fram Strait (thus reduced particulate fluxes from this source); ii) the continental margin topography of northern Greenland in the Amundsen basin, which leads to deep water circulation far away from the Greenland coastline (Björk et al., 2010). Thus whereas multi-year sea-ice which accumulates in this area may carry particulate matter with a northern Greenland Pb-isotope signature to Fram Strait, deep water preserves the Pb-isotope signature acquired earlier during its course along the Russian and Canadian margins.

Dissolved Nd has a significantly longer residence time in the ocean (Tachikawa et al., 1999) than Pb. This might explain the fact that the dissolved Nd record seems much less variable than that of dissolved Pb (Fig. 8). The dissolved Nd isotopic composition is thought to result from the superimposition of the regional Nd signature linked to particulate fluxes in the Arctic over an imprint of more distal Nd sources (North Atlantic waters) modified within the gyre of Arctic waters. Andersson et al. (2008) published a map showing the main sources of dissolved Nd isotopes in the Arctic. At present, deep-waters exiting from the Arctic through Fram Strait have ϵ_{Nd} values of -9.5, which are higher than those of waters entering from the North Atlantic (ϵ_{Nd} of -10.7) (Andersson et al., 2008). These authors interpreted the higher values of the exiting waters as reflecting the influence of the western Arctic basin and more specifically of Pacific waters. Indeed, measurements of Chukchi and East Siberian Sea waters indicate ϵ_{Nd} values of -6 and -5 respectively (Andersson et al., 2008; Porcelli et al.,

2009). In the Eurasian basin (Amundsen and Nansen basins), recorded ϵ_{Nd} values are distinctly lower ($\epsilon_{\text{Nd}} \sim -10.7$ in the Nansen; Haley et al., 2008a; $\epsilon_{\text{Nd}} \sim -12.3$ in the Amundsen; Porcelli et al., 2009) and have been suggested to reflect the influence of the Lena and Laptev Sea.

Values of ϵ_{Nd} in the leachates from core MC16 decrease between 19.8 and 16.8 ka and increase from 5 ka to the present (Fig. 8). Changes in the Nd isotopic composition of seawater are due to: i) addition or removal of a source; ii) change in the source composition and; iii) changes in particulate fluxes (and hence of isotopic exchange with particles). Sources of dissolved Nd in the Arctic ocean have likely changed as conditions changed from glacial to deglacial. During glacial times the area of the Arctic Ocean was about half of its current size, ice-sheets covered North America and northwestern Europe and produced glacial streams (Stokes and Clark, 2001; Stokes et al., 2009; Stokes and Tarasov, 2010). Bering Strait was closed and dry conditions prevailed over central and eastern Siberia. Changes in precipitation and atmospheric conditions must have modified weathering rates and runoff though it is difficult to quantify the influence on dissolved Nd isotopes. The relatively high ϵ_{Nd} values measured at core bottom might suggest some influence of the Kara Sea ($\epsilon_{\text{Nd}} \sim -5$ to -7 ; ($\epsilon_{\text{Nd}} \sim -5$ to -7 ; Andersson et al., 2008) through the melting of the Eurasian ice sheet, at a time when the Bering Strait was closed and the East Siberian Sea shelf was mostly emerged. The decrease of ~ 1.5 ϵ_{Nd} units after 19.8 ka might reflect the increasing influence of the Canadian margins and/or the simultaneous decrease of that of the Kara Sea margins. This decrease in the ϵ_{Nd} value might also be attributed to the progressive decay of the southern part of the Eurasian ice sheet along the Scandinavian margins, which might have modified the particulate flux and hence the isotopic composition of the incoming signal. The ϵ_{Nd} value of -10.7 reported by Andersson et al. (2008) might have been higher during glacial times, when particulate fluxes were lower along the Scandinavian margins in the GIN seas. Finally, the recent return to higher values might correspond to the increasing influence of more radiogenic Pacific waters (Andersson et al., 2008; Porcelli et al., 2009). Nd isotopes thus seem more sensitive than Pb isotopes for tracing changes in incoming water masses, probably due to the longer residence time of Nd in the ocean (i.e. lower reactivity to particles).

5. CONCLUSION

This study has demonstrated the ability of geochemical composition and radiogenic isotopes in deep-sea sediments to provide insights into paleoceanographical events that occurred during the deglaciation of the circum-Arctic and the Holocene. We have highlighted the use of a complementary approach using detrital residues and leachates. Residual fractions inherited from sediment source areas document ice/continental sedimentary fluxes towards the Arctic Ocean and Fram Strait, and help to reconstruct sea-ice circulation patterns. Leachable fractions illustrate the history of water-masses that exit through Fram Strait.

The sediment is composed of three fractions: terrigenous, biogenic and authigenic (i.e. early diagenetic and syn-depositional). Elements that are primarily hosted by the terrigenous fraction are barely removed during the leaching procedure and present a change/excursion at ~13ka assigned to an early YD drainage event in the Beaufort Sea area.

C_{inorg} is thought to be primarily hosted by Ca-carbonates and presents an initial increase at ~12.4 ka (17 cm), interpreted to result from enhanced productivity and influx of detrital carbonate. A second increase at ~3.9 ka (5cm) is concomitant with an increase in C_{org} and is thought to correspond to an increase in productivity, probably linked to a reduced sea-ice cover.

Organic matter delivered discontinuously to Fram Strait, is thought to have caused the redox front to migrate within the sedimentary column. Such migration might have redistributed some redox sensitive elements such as Mn and Mo, as illustrated by a marked peak in the bulk Mn profile at ~16.4 ka (28 cm). Fe on the other hand presents a lower mobility and is thought to have hosted Pb and Nd. Thus these elements should not have undergone major redistribution within the sedimentary column, suggesting that their leachate isotopic compositions provide useful information.

Sr and Nd isotopic results from the residues allow further definition of the mixing end-members of the trends defined in an earlier study on the basis of Pb isotopes (Maccali et al., 2012). Fram Strait samples from the pre-YD interval, received sedimentary supplies from both the Canadian margins and the Barents-Kara-West Laptev Sea region. During this time interval, the Laurentide and Innuitian Ice Sheets covered North America and the Arctic Archipelago, while the Eurasian Ice Sheet covered the Barents Sea and part of the Kara Sea.

Ice sheets would have strongly influenced the sedimentary dynamics by releasing material either through sea-ice or calved icebergs (Fig. 7a).

Fram Strait samples from the post-YD interval, received sedimentary supplies from the western basin and northern Greenland margins. The western basin reflects contributions from Canadian margins and possibly the Chukchi/East Siberian Seas regions, implying that the Barents-Kara-West Laptev Sea region had been largely cut off. The relatively minor influence by the Laptev Sea with regards to sea-ice formation suggests that sea-ice from the Laptev Sea melted and released its IRD elsewhere. This situation may have changed very recently, as the uppermost sample shows a Siberian margin signature. The other valid outlet for Laptev Sea sediments would be through the Barents Sea. This requires a TPD deflected towards the Eurasian basin (Fig. 7b).

The leachate data illustrate the overprinting of Arctic sources on the incoming North Atlantic Water through its gyres in the Arctic basin. Nd isotopes reveal the major influence of the western basin on exiting Arctic waters. Prior to ~16.8ka, the western Russian margins imprinted the water mass signature, likely due to the high particulate flux along the nearby Eurasian Ice Sheet. More recently, Nd isotopes likely reflect the influence of the Pacific waters entering through Bering Strait. Contrary to the residues, the leachates do not record any influence of the Greenland margins, either because there are no major particulate fluxes off northern Greenland or because the water masses circulate far from these margins.

Acknowledgments

The present study is a contribution to the *WarmPast* and *Past4Future* projects. Funding by the *Ministère du Développement Economique, de l'Innovation et de l'Exportation* of Québec and the *Fonds Québécois de Recherche sur la Nature et les Technologies* has been instrumental. JM also acknowledges support from the French *Ministère de l'Education* and the GEOTOP research network through PhD awards. Complementary funding by NSERC-Canada (Discovery Grant CHM) is also acknowledged. Special thanks are due to Katrin Husum and Morten Hald (University of Tromsø) for their invitation to participate in the 2006-2008 cruises of the Jan Mayen in the Fram Strait Area. We are grateful to the three anonymous reviewers for their constructive suggestions that significantly improved the quality of this manuscript.

6. REFERENCES

- Aagaard-Sørensen, S., Husum, K., Hald, M., Knies, J., 2010. Paleoceanographic development in the SW Barents Sea during the Late Weichselian-Early Holocene transition. *Quaternary Science Reviews* 29, 3442-3456.
- Andersson, P.S., Porcelli, D., Frank, M., Björk, G., Dahlqvist, R., Gustafsson, O., 2008. Neodymium isotopes in seawater from the Barents Sea and Fram Strait Arctic-Atlantic gateways. *Geochimica et Cosmochimica Acta* 72, 2854-2867.
- Andrews, J.T., Dyke, A.S., 2007. Late Quaternary in North America. *Encyclopedia of Quaternary Science*, 1095-1101.
- Andrews, J.T., Eberl, D.D., 2011. Surface (sea floor) and near-surface (box cores) sediment mineralogy in Baffin Bay as a key to sediment provenance and ice sheet variations. *Canadian Journal of Earth Sciences* 48, 1307-1328.
- Anschutz P., D.K., Desmazes F., Chaillou G., 2005. Speciation, oxidation state, and reactivity of particulate manganese in marine sediments. *Chemical Geology* 218, 265 - 279.
- Bayon, G., German, C.R., Boella, R.M., Milton, J.A., Taylor, R.N., Nesbitt, R.W., 2002. An improved method for extracting marine sediment fractions and its application to Sr and Nd isotopic analysis. *Chemical Geology* 187, 179-199.
- Bayon, G., German, C.R., Burton, K.W., Nesbitt, R.W., Rogers, N., 2004. Sedimentary Fe-Mn oxyhydroxides as paleoceanographic archives and the role of aeolian flux in regulating oceanic dissolved REE. *Earth and Planetary Science Letters* 224, 477-492.
- Belzile N., L.P., Tessier A., 1989. In situ collection of diagenetic iron and manganese oxyhydroxides from natural sediments. *Nature* 340, 376 - 377.
- Birgel, D., Hass, H.C., 2004. Oceanic and atmospheric variations during the last deglaciation in the Fram Strait (Arctic Ocean): A coupled high-resolution organic-geochemical and sedimentological study. *Quaternary Science Reviews* 23, 29-47.
- Biscaye, P.E., Grousset, F.E., Revel, M., Van der Gaast, S., Zielinski, G.A., Vaars, A., Kukla, G., 1997. Asian provenance of glacial dust (stage 2) in the Greenland Ice Sheet Project 2 ice core, Summit, Greenland. *Journal of Geophysical Research* 102, 26765-26781.
- Bischof, J.F., Darby, D.A., 1997. Mid- to late Pleistocene ice drift in the western Arctic Ocean: Evidence for a different circulation in the past. *Science* 277, 74-78.

- Björk, G., Anderson, L.G., Jakobsson, M., Antony, D., Eriksson, B., Eriksson, P.B., Hell, B., Hjalmarsson, S., Janzen, T., Jutterström, S., Linders, J., Löwemark, L., Marcussen, C., Anders Olsson, K., Rudels, B., Sellén, E., Sølvsten, M., 2010. Flow of Canadian basin deep water in the Western Eurasian Basin of the Arctic Ocean. Deep-Sea Research Part I: Oceanographic Research Papers 57, 577-586.
- Broecker, W.S., 1991. The great ocean conveyor. *Oceanography* 4, 79 - 89.
- Carignan, J., Hillaire-Marcel, C., De Vernal, A., 2008. Arctic vs. North Atlantic water mass exchanges in Fram Strait from Pb isotopes in sediments. *Canadian Journal of Earth Sciences* 45, 1253-1263.
- Darby, D.A., Bischof, J.F., Spielhagen, R.F., Marshall, S.A., Herman, S.W., 2002. Arctic ice export events and their potential impact on global climate during the late Pleistocene. *Paleoceanography* 17, 1025.
- Darby, D.A., Polyak, L., Bauch, H.A., 2006. Past glacial and interglacial conditions in the Arctic Ocean and marginal seas - a review. *Progress in Oceanography* 71, 129-144.
- Darby, D.A., Zimmerman, P., 2008. Ice rafted detritus events in the Arctic during the last glacial interval, and the timing of the Innuitian and Laurentide ice sheet calving events. *Polar Research* 27, 114-127.
- Dickson, R., Rudels, B., Dye, S., Karcher, M., Meincke, J., Yashayaev, I., 2007. Current estimates of freshwater flux through Arctic and subarctic seas. *Progress in Oceanography* 73, 210-230.
- Dyke, A.S., Andrews, J.T., Clark, P.U., England, J.H., Miller, G.H., Shaw, J., Veillette, J.J., 2002. The Laurentide and Innuitian ice sheets during the Last Glacial Maximum. *Quaternary Science Reviews* 21, 9-31.
- Eisenhauer, A., Meyer, H., Rachold, V., Tütken, T., Wiegand, B., Hansen, B.T., Spielhagen, R.F., Lindemann, F., Kassens, H., 1999. Grain size separation and sediment mixing in Arctic Ocean sediments: Evidence from the strontium isotope systematic. *Chemical Geology* 158, 173-188.
- England, J., Atkinson, N., Bednarski, J., Dyke, A.S., Hodgson, D.A., vi Cofaigh, C., 2006. The Innuitian Ice Sheet: configuration, dynamics and chronology. *Quaternary Science Reviews* 25, 689-703.

- Fagel, N., Hillaire-Marcel, C., 2006. Glacial/interglacial instabilities of the Western Boundary Under Current during the last 365kyr from Sm/Nd ratios of the sedimentary clay-size fractions at ODP site 646 (Labrador Sea). *Marine Geology* 232, 87-99.
- Fagel, N., Hillaire-Marcel, C., Humbert, M., Brasseur, R., Weis, D., Stevenson, R., 2004. Nd and Pb isotope signatures of the clay-size fraction of Labrador Sea sediments during the Holocene: Implications for the inception of the modern deep circulation pattern. *Paleoceanography* 19, PA3002 3001-3016.
- Fagel, N., Hillaire-Marcel, C., Robert, C., 1997. Changes in the Western Boundary Undercurrent outflow since the Last Glacial Maximum, from smectite/illite ratios in deep Labrador Sea sediments. *Paleoceanography* 12, 79-96.
- Fagel, N., Innocent, C., Gariepy, C., Hillaire-Marcel, C., 2002. Sources of Labrador Sea sediments since the last glacial maximum inferred from Nd-Pb isotopes. *Geochimica et Cosmochimica Acta* 66, 2569-2581.
- Fahrbach, E., Meincke, J., Østerhus, S., Rohardt, G., Schauer, U., Tverberg, V., Verduin, J., 2001. Direct measurements of volume transports through Fram Strait. *Polar Research* 20, 217-224.
- Fütterer, D.K., 2000. The Solid Phase of Marine Sediments, In: Schulz, H.D., Zabel, M. (Eds.), *Marine Geochemistry*. Springer, Berlin; Heidelberg; New-York; Barcelona; Hong Kong; London; Milan; Paris; Singapore; Tokyo, pp. 1-25.
- Gladkochub, D., Pisarevsky, S., Donskaya, T., Natapov, L., Mazukabzov, A., Stanevich, A., Sklyarov, E., 2006. The Siberian Craton and its evolution in terms of the Rodinia hypothesis. *Episodes* 29, 169-174.
- Gladkochub, D.P., Pisarevsky, S.A., Donskaya, T.V., Ernst, R.E., Wingate, M.T.D., Söderlund, U., Mazukabzov, A.M., Sklyarov, E.V., Hamilton, M.A., Hanes, J.A., 2010. Proterozoic mafic magmatism in Siberian craton: An overview and implications for paleocontinental reconstruction. *Precambrian Research* 183, 660-668.
- Glasby, G.P., 2000. Manganese: Predominant Role of Nodules and Crusts, In: Schulz, H.D., Zabel, M. (Eds.), *Marine Geochemistry*. Springer, Berlin; Heidelberg; New-York; Barcelona; Hong Kong; London; Milan; Paris; Singapore; Tokyo, pp. 335-372.

- Gobeil, C., Macdonald, R.W., Sundby, B., 1997. Diagenetic separation of cadmium and manganese in suboxic continental margin sediments. *Geochimica et Cosmochimica Acta* 61, 4647-4654.
- Gobeil C., M.R.W., Sundby B., 1997. Diagenetic separation of cadmium and manganese in suboxic continental margin sediments. *Geochimica et Cosmochimica Acta* 61, 4647 - 4654.
- Groussset, F.E., Cortijo, E., Huon, S., Hervé, L., Richter, T., Burdloff, D., Duprat, J., Weber, O., 2001. Zooming in on Heinrich layers. *Paleoceanography* 16, 240-259.
- Guo, L., Semiletov, I., Gustafsson, O., Ingri, J., Andersson, P., Dudarev, O., White, D., 2004. Characterization of Siberian Arctic coastal sediments: Implications for terrestrial organic carbon export. *Global Biogeochemical Cycles* 18, GB1036 1031-1010.
- Gutjahr, M., Frank, M., Stirling, C.H., Keigwin, L.D., Halliday, A.N., 2008. Tracing the Nd isotope evolution of North Atlantic Deep and Intermediate Waters in the western North Atlantic since the Last Glacial Maximum from Blake Ridge sediments. *Earth and Planetary Science Letters* 266, 61-77.
- Gutjahr, M., Frank, M., Stirling, C.H., Klemm, V., van de Flierdt, T., Halliday, A.N., 2007. Reliable extraction of a deepwater trace metal isotope signal from Fe-Mn oxyhydroxide coatings of marine sediments. *Chemical Geology* 242, 351-370.
- Haese, R.R., 2000. The Reactivity of Iron, In: Schulz, H.D., Zabel, M. (Eds.), *Marine Geochemistry*. Springer, Berlin; Heidelberg; New-York; Barcelona; Hong Kong; London; Milan; Paris; Singapore; Tokyo, pp. 233-261.
- Haley, B.A., Frank, M., Spielhagen, R.F., Eisenhauer, A., 2008a. Influence of brine formation on Arctic Ocean circulation over the past 15 million years. *Nature Geoscience* 1, 68-72.
- Haley, B.A., Frank, M., Spielhagen, R.F., Fietzke, J., 2008b. Radiogenic isotope record of Arctic Ocean circulation and weathering inputs of the past 15 million years. *Paleoceanography* 23.
- Haley, B.A., Klinkhammer, G.P., McManus, J., 2004. Rare earth elements in pore waters of marine sediments. *Geochimica et Cosmochimica Acta* 68, 1265-1279.
- Hélie, J.-F., 2009. Elemental and stable isotopic approaches for studying the organic and inorganic carbon components in natural samples. *Deep-sea to Coastal Zones: Methods and*

Techniques for Studying Paleoenvironments IOP Conf. Series: Earth and Environmental Science 5.

Henderson, G.M., Maier-Reimer, E., 2002. Advection and removal of ^{210}Pb and stable Pb isotopes in the oceans: A general circulation model study. *Geochimica et Cosmochimica Acta* 66, 257-272.

Hillaire-Marcel, C., De Vernal, A., Polyak, L., Darby, D., 2004. Size-dependent isotopic composition of planktic foraminifers from Chukchi Sea vs. NW Atlantic sediments - Implications for the Holocene paleoceanography of the western Arctic. *Quaternary Science Reviews* 23, 245-260.

Holland, M.M., Serreze, M.C., Stroeve, J., 2010. The sea ice mass budget of the Arctic and its future change as simulated by coupled climate models. *Climate Dynamics* 34, 185-200.

Hubberten, H.W., Andreev, A., Astakhov, V.I., Demidov, I., Dowdeswell, J.A., Henriksen, M., Hjort, C., Houmark-Nielsen, M., Jakobsson, M., Kuzmina, S., Larsen, E., Lunkka, J.P., Lyså, A., Mangerud, J., Möller, P., Saarnisto, M., Schirrmeister, L., Sher, A.V., Siegert, C., Siegert, M.J., Svendsen, J.I., 2004. The periglacial climate and environment in northern Eurasia during the Last Glaciation. *Quaternary Science Reviews* 23, 1333-1357.

Husum, K., 2006. Marine geological cruise to West Spitsbergen Margin and Fram Strait - RV "Jan Mayen" 11-19 October 2006. University of Tromsø, Tromsø, p. 40.

Jacobsen, S.B., Wasserburg, G.J., 1980. Sm-Nd isotopic evolution of chondrites. *Earth and Planetary Science Letters* 50, 139-155.

Jakobsson, M., Long, A., Ingólfsson, Ó., Kjær, K.H., Spielhagen, R.F., 2010. New insights on Arctic Quaternary climate variability from palaeo-records and numerical modelling. *Quaternary Science Reviews* 29, 3349-3358.

Jakobsson, M., Lovlie, R., Al-Hanbali, H., Arnold, E., Backman, J., Mört, M., 2000. Manganese and color cycles in Arctic Ocean sediments constrain Pleistocene chronology. *Geology* 28, 23-26.

Jeandel, C., Arsouze, T., Lacan, F., Téchiné, P., Dutay, J.C., 2007. Isotopic Nd compositions and concentrations of the lithogenic inputs into the ocean: A compilation, with an emphasis on the margins. *Chemical Geology* 239, 156-164.

Jones, E.P., 2001. Circulation in the Arctic Ocean. *Polar Research* 20, 139-146.

- Jones, E.P., Rudels, B., Anderson, L.G., 1995. Deep waters of the Arctic Ocean: origins and circulation. *Deep-Sea Research Part I* 42, 737-760.
- Katsev, S., Sundby, B., Mucci, A., 2006. Modeling vertical excursions of the redox boundary in sediments: Application to deep basins of the Arctic Ocean. *Limnology and Oceanography* 51, 1581-1593.
- Knies, J., Vogt, C., Stein, R., 1999. Late Quaternary growth and decay of the Svalbard/Faeroe Sea ice sheet and paleoceanographic evolution in the adjacent Arctic Ocean. *Geo-Marine Letters* 18, 195-202.
- Koenigk, T., Döschner, R., Nikulin, G., 2011. Arctic future scenario experiments with a coupled regional climate model. *Tellus, Series A: Dynamic Meteorology and Oceanography* 63, 69-86.
- Koschinsky, A., Hein, J.R., 2003. Uptake of elements from seawater by ferromanganese crusts: Solid-phase associations and seawater speciation. *Marine Geology* 198, 331-351.
- Kylander, M.E., Klaminder, J., Bindler, R., Weiss, D.J., 2010. Natural lead isotope variations in the atmosphere. *Earth and Planetary Science Letters* 290, 44-53.
- Lacan, F., Jeandel, C., 2004. Neodymium isotopic composition and rare earth element concentrations in the deep and intermediate Nordic Seas: Constraints on the Iceland Scotland Overflow Water signature. *Geochemistry, Geophysics, Geosystems* 5.
- Lacan, F., Jeandel, C., 2005a. Acquisition of the neodymium isotopic composition of the North Atlantic Deep Water. *Geochemistry, Geophysics, Geosystems* 6.
- Lacan, F., Jeandel, C., 2005b. Neodymium isotopes as a new tool for quantifying exchange fluxes at the continent-ocean interface. *Earth and Planetary Science Letters* 232, 245-257.
- Langehaug, H.R., Falck, E., 2011. Changes in the properties and distribution of the intermediate and deep waters in the Fram Strait. *Progress in Oceanography*.
- Larsen, N.K., Kjaer, K.H., Funder, S., Möller, P., van der Meer, J.J.M., Schomacker, A., Linge, H., Darby, D.A., 2010. Late Quaternary glaciation history of northernmost Greenland-Evidence of shelf-based ice. *Quaternary Science Reviews* 29, 3399-3414.
- Lightfoot, P.C., Hawkesworth, C.J., Hergt, J., Naldrett, A.J., Gorbachev, N.S., Fedorenko, V.A., Doherty, W., 1993. Remobilisation of the continental lithosphere by a mantle plume: major-, trace-element, and Sr-, Nd-, and Pb-isotope evidence from picritic and tholeiitic lavas

- of the Noril'sk District, Siberian Trap, Russia. Contributions to Mineralogy and Petrology 114, 171-188.
- Link, H., Archambault, P., Tamelander, T., Renaud, P.E., Piepenburg, D., 2011. Spring-to-summer changes and regional variability of benthic processes in the western Canadian Arctic. *Polar Biology* 34, 2025-2038.
- Lisitzin, A.P., 2010. Marine ice-rafting as a new type of sedimentogenesis in the Arctic and novel approaches to studying sedimentary processes. *Russian Geology and Geophysics* 51, 12-47.
- Löwemark, L., Jakobsson, M., Mört, M., Backman, J., 2008. Arctic Ocean manganese contents and sediment colour cycles. *Polar Research* 27, 105-113.
- Lupker, M., Aciego, S.M., Bourdon, B., Schwander, J., Stocker, T.F., 2010. Isotopic tracing (Sr, Nd, U and Hf) of continental and marine aerosols in an 18th century section of the Dye-3 ice core (Greenland). *Earth and Planetary Science Letters* 295, 277-286.
- Maccali, J., Hillaire-Marcel, C., Carignan, J., Reisberg, L.C., 2012. Pb-isotopes and geochemical monitoring of Arctic sedimentary supplies and water-mass export through Fram Strait since the Last Glacial Maximum. *Paleoceanography* 27, PA1201.
- Macdonald, R.W., Gobeil, C., 2011. Manganese Sources and Sinks in the Arctic Ocean with Reference to Periodic Enrichments in Basin Sediments. *Aquatic Geochemistry*, 1-27.
- Martin, E.E., Blair, S.W., Kamenov, G.D., Scher, H.D., Bourbon, E., Basak, C., Newkirk, D.N., 2010. Extraction of Nd isotopes from bulk deep sea sediments for paleoceanographic studies on Cenozoic time scales. *Chemical Geology* 269, 414-431.
- März, C., Stratmann, A., Matthiessen, J., Meinhardt, A.K., Eckert, S., Schnetger, B., Vogt, C., Stein, R., Brumsack, H.J., 2011. Manganese-rich brown layers in Arctic Ocean sediments: Composition, formation mechanism, and diagenetic overprint. *Geochimica et Cosmochimica Acta*, doi: 10.1016/j.gca.2011.1009.1046.
- Maynard, J.B., 2003. Manganiferous Sediments, Rocks, and Ores, In: Holland, H.D., Turekian, K.K. (Eds.), *Treatise on Geochemistry*. Elsevier-Pergamon, Oxford, pp. 289-308.
- McManus J. F., F.R., Gherardi J.-M., Keigwin L. D., Brown-Leger S., 2004. Collapse and rapid resumption of Atlantic meridional circulation linked to deglacial climate changes. *Nature* 428, 834 - 837.

- Meyers, P.A., 1997. Organic geochemical proxies of paleoceanographic, paleolimnologic, and paleoclimatic processes. *Organic Geochemistry* 27, 213-250.
- Miller, G.H., Alley, R.B., Brigham-Grette, J., Fitzpatrick, J.J., Polyak, L., Serreze, M.C., White, J.W.C., 2010. Arctic amplification: Can the past constrain the future? *Quaternary Science Reviews* 29, 1779-1790.
- Möller, P., Larsen, N.K., Kjær, K.H., Funder, S., Schomacker, A., Linge, H., Fabel, D., 2010. Early to middle Holocene valley glaciations on the northernmost Greenland. *Quaternary Science Reviews* 29, 3379-3398.
- Murton, J.B., Bateman, M.D., Dallimore, S.R., Teller, J.T., Yang, Z., 2010. Identification of Younger Dryas outburst flood path from Lake Agassiz to the Arctic Ocean. *Nature* 464, 740-743.
- Noffke, A., Hensen, C., Sommer, S., Scholz, F., Bohlen, L., Mosch, T., Graco, M., Wallmann, K., 2012. Benthic iron and phosphorus fluxes across the Peruvian oxygen minimum zone. *Limnology and Oceanography* 57, 851-867.
- Not, C., Hillaire-Marcel, C., 2012. Enhanced sea-ice export from the Arctic during the Younger Dryas. *Nature Communications* 3, 647.
- Parnell, J., Bowden, S., Andrews, J.T., Taylor, C., 2007. Biomarker determination as a provenance tool for detrital carbonate events (Heinrich events?): Fingerprinting Quaternary glacial sources into Baffin Bay. *Earth and Planetary Science Letters* 257, 71-82.
- Peltier, W.R., Vettoretti, G., Stastna, M., 2006. Atlantic meridional overturning and climate response to Arctic Ocean freshening. *Geophysical Research Letters* 33, L06713.
- Polyak, L., Alley, R.B., Andrews, J.T., Brigham-Grette, J., Cronin, T.M., Darby, D.A., Dyke, A.S., Fitzpatrick, J.J., Funder, S., Holland, M., Jennings, A.E., Miller, G.H., O'Regan, M., Savelle, J., Serreze, M., St. John, K., White, J.W.C., Wolff, E., 2010. History of sea ice in the Arctic. *Quaternary Science Reviews* 29, 1757-1778.
- Porcelli, D., Andersson, P.S., Baskaran, M., Frank, M., Björk, G., Semiletov, I., 2009. The distribution of neodymium isotopes in Arctic Ocean basins. *Geochimica et Cosmochimica Acta* 73, 2645-2659.
- Reichow, M.K., Pringle, M.S., Al'Mukhamedov, A.I., Allen, M.B., Andreichev, V.L., Buslov, M.M., Davies, C.E., Fedoseev, G.S., Fitton, J.G., Inger, S., Medvedev, A.Y., Mitchell, C., Puchkov, V.N., Safonova, I.Y., Scott, R.A., Saunders, A.D., 2009. The timing

and extent of the eruption of the Siberian Traps large igneous province: Implications for the end-Permian environmental crisis. *Earth and Planetary Science Letters* 277, 9-20.

Reimer, P.J., Baillie, M.G.L., Bard, E., Bayliss, A., Beck, J.W., Blackwell, P.G., Bronk Ramsey, C., Buck, C.E., Burr, G.S., Edwards, R.L., Friedrich, M., Grooted, P.M., Guilderson, T.P., Hajdas, I., Heaton, T.J., Hogg, A.G., Hughen, K.A., Kaiser, K.F., Kromer, B., McCormac, F.G., Manning, S.W., Reimer, R.W., Richards, D.A., Southon, J.R., Talamo, S., Turney, C.S.M., van der Plitch, J., Weyhenmeyer, C.E., 2009. INTCAL09 AND MARINE09 radiocarbon age calibration curves, 0-50,000 years cal BP. *Radiocarbon* 51, 1111 - 1150.

Rosenbaum, J., Sheppard, S.M.F., 1986. An isotopic study of siderites, dolomites and ankerites at high temperatures. *Geochimica et Cosmochimica Acta* 50, 1147-1150.

Rudels, B., Björk, G., Nilsson, J., Winsor, P., Lake, I., Nohr, C., 2005. The interaction between waters from the Arctic Ocean and the Nordic Seas north of Fram Strait and along the East Greenland Current: Results from the Arctic Ocean-02 Oden expedition. *Journal of Marine Systems* 55, 1-30.

Rudels, B., Jones, E.P., Schauer, U., Eriksson, P., 2004. Atlantic sources of the Arctic Ocean surface and halocline waters. *Polar Research* 23, 181-208.

Rudels, B., Meyer, R., Fahrbach, E., Ivanov, V.V., Østerhus, S., Quadfasel, D., Schauer, U., Tverberg, V., Woodgate, R.A., 2000. Water mass distribution in Fram Strait and over the Yermak Plateau in summer 1997. *Annales Geophysicae* 18, 687-705.

Rusakov, V.Y., Levitan, M.A., Roshchina, I.A., Spielhagen, R.F., Gebhardt, K., 2010. Chemical composition of late Pleistocene-Holocene pelagic sediments in Gakkel Ridge, Arctic Ocean. *Geochemistry International* 48, 999-1013.

Rysgaard, S., Thamdrup, B., Risgaard-Petersen, N., Fossing, H., Berg, P., Christensen, P.B., Dalsgaard, T., 1998. Seasonal carbon and nutrient mineralization in a high-Arctic coastal marine sediment, Young Sound, Northeast Greenland. *Marine Ecology Progress Series* 175, 261-276.

Sageman, B.B., Lyons, T.W., 2003. Geochemistry of Fine-grained Sediments and Sedimentary Rocks, In: Holland, H.D., Turekian, K.K. (Eds.), *Treatise on Geochemistry*. Elsevier-Pergamon, Oxford, pp. 115-158.

- Scholz, F., Hensen, C., Noffke, A., Rohde, A., Liebetrau, V., Wallmann, K., 2011. Early diagenesis of redox-sensitive trace metals in the Peru upwelling area - response to ENSO-related oxygen fluctuations in the water column. *Geochimica et Cosmochimica Acta* 75, 7257-7276.
- Serreze, M.C., Barry, R.G., 2005. *The Arctic Climate System*. Cambridge University Press, Cambridge.
- Shen, P., Huang, C., Ganguly, C., Gaboriault-Whitcomb, S., Rabideau, A.J., Van Benschoten, J.E., 2001. Comparison of soluble and immobilized acetate for removing Pb from contaminated soil. *Journal of Hazardous Materials* 87, 59-72.
- Stokes, C.R., Clark, C.D., 2001. Palaeo-ice streams. *Quaternary Science Reviews* 20, 1437-1457.
- Stokes, C.R., Clark, C.D., Storrar, R., 2009. Major changes in ice stream dynamics during deglaciation of the north-western margin of the Laurentide Ice Sheet. *Quaternary Science Reviews* 28, 721-738.
- Stokes, C.R., Tarasov, L., 2010. Ice streaming in the Laurentide Ice Sheet: A first comparison between data-calibrated numerical model output and geological evidence. *Geophysical Research Letters* 37.
- Svendsen, J.I., Alexanderson, H., Astakhov, V.I., Demidov, I., Dowdeswell, J.A., Funder, S., Gataullin, V., Henriksen, M., Hjort, C., Houmark-Nielsen, M., Hubberten, H.W., Ingólfsson, O., Jakobsson, M., Kjær, K.H., Larsen, E., Lokrantz, H., Lunkka, J.P., Lyså, A., Mangerud, J., Matiouchkov, A., Murray, A., Möller, P., Niessen, F., Nikolskaya, O., Polyak, L., Saarnisto, M., Siegert, C., Siegert, M.J., Spielhagen, R.F., Stein, R., 2004. Late Quaternary ice sheet history of northern Eurasia. *Quaternary Science Reviews* 23, 1229-1271.
- Svensson, A., Biscaye, P.E., Grousset, F.E., 2000. Characterization of late glacial continental dust in the Greenland Ice Core Project ice core. *Journal of Geophysical Research D: Atmospheres* 105, 4637-4656.
- Tachikawa, K., Athias, V., Jeandel, C., 2003. Neodymium budget in the modern ocean and paleo-oceanographic implications. *Journal of Geophysical Research C: Oceans* 108, 3254.
- Tachikawa, K., Jeandel, C., Roy-Barman, M., 1999. A new approach to the Nd residence time in the ocean: The role of atmospheric inputs. *Earth and Planetary Science Letters* 170, 433-446.

- Tanaka, T., Togashi, S., Kamioka, H., Amakawa, H., Kagami, H., Hamamoto, T., Yuhara, M., Orihashi, Y., Yoneda, S., Shimizu, H., Kunimaru, T., Takahashi, K., Yanagi, T., Nakano, T., Fujimaki, H., Shinjo, R., Asahara, Y., Tanimizu, M., Dragusanu, C., 2000. JNdI-1: A neodymium isotopic reference in consistency with LaJolla neodymium. *Chemical Geology* 168, 279-281.
- Tarasov, L., Peltier, W.R., 2005. Arctic freshwater forcing of the Younger Dryas cold reversal. *Nature* 435, 662-665.
- Tarasov, L., Peltier, W.R., 2006. A calibrated deglacial drainage chronology for the North American continent: evidence of an Arctic trigger for the Younger Dryas. *Quaternary Science Reviews* 25, 659-688.
- Taylor, S.R., McLennan, S.M., 1985. *The Continental Crust: its Composition and Evolution*. Blackwell Scientific Publications, Oxford.
- Teller, J.T., Boyd, M., Yang, Z., Kor, P.S.G., Fard, A.M., 2005. Alternative routing of Lake Agassiz overflow during the Younger Dryas: New dates, paleotopography, and a re-evaluation. *Quaternary Science Reviews* 24, 1890-1905.
- Thornalley, D.J.R., McCave, I.N., Elderfield, H., 2011. Tephra in deglacial ocean sediments south of Iceland: Stratigraphy, geochemistry and oceanic reservoir ages. *Journal of Quaternary Science* 26, 190-198.
- Tütken, T., Eisenhauer, A., Wiegand, B., Hansen, B.T., 2002. Glacial-interglacial cycles in Sr and Nd isotopic composition of Arctic marine sediments triggered by the Svalbard/Barents Sea ice sheet. *Marine Geology* 182, 351-372.
- Vovna, G.M., Mishkin, M.A., Sakhno, V.G., Zarubina, N.V., 2009. Early Archean sialic crust of the Siberian craton: Its composition and origin of magmatic protoliths. *Doklady Earth Sciences* 429, 1439-1442.
- Winter, B.L., Johnson, C.M., Clark, D.L., 1997. Strontium, neodymium, and lead isotope variations of authigenic and silicate sediment components from the Late Cenozoic Arctic Ocean: Implications for sediment provenance and the source of trace metals in seawater. *Geochimica et Cosmochimica Acta* 61, 4181-4200.
- Wooden, J.L., Czamanske, G.K., Fedorenko, V.A., Arndt, N.T., Chauvel, C., Bouse, R.M., King, B.S.W., Knight, R.J., Siems, D.F., 1993. Isotopic and trace-element constraints on

mantle and crustal contributions to Siberian continental flood basalts, Noril'sk area, Siberia.
Geochimica et Cosmochimica Acta 57, 3677-3704.

Zamelczyk, K., Rasmussen, T.L., Husum, K., Hafnidason, H., de Vernal, A., Ravna, E.K.,
Hald, M., Hillaire-Marcel, C., 2012. Paleoceanographic changes and calcium carbonate
dissolution in the central Fram Strait during the last 20 ka yr. *Quaternary Research* In press.

Table 1 : Nd- and Sr-isotopic composition of residues.

Interval depth. cm	Age. cal. ka	$^{143}\text{Nd}/^{144}\text{Nd}$	$\pm 2\sigma^a$	$\varepsilon_{\text{Nd}}^b$	$^{87}\text{Sr}/^{86}\text{Sr}^b$	$\pm 2\sigma^a$
0 - 1	0.2	0.511971	0.000024	-13	0.71874	0.000011
1 - 2	1.1	0.512025	0.000007	-12	0.71819	0.000010
2 - 3	2	0.512039	0.000009	-11.7	0.71787	0.000011
3 - 4	2.9	0.511995	0.000009	-12.5	0.71745	0.000011
4 - 5	3.8	0.512048	0.000008	-11.5	0.71806	0.000010
5 - 6	4.7	-	-	-	0.71782	0.000010
6 - 7	5.6	0.511994	0.000010	-12.6	0.71804	0.000009
7 - 8	6.5	0.512022	0.000007	-12	0.71793	0.000010
8 - 9	7.5	0.511994	0.000009	-12.6	0.71789	0.000009
9 - 10	8.3	0.511987	0.000007	-12.7	0.71806	0.000014
14 - 15	12	-	-	-	0.72029	0.000020
19 - 20	13	0.511961	0.000009	-13.2	0.7213	0.000016
21 - 22	13.9	0.512029	0.000008	-11.9	0.71978	0.000009
22 - 23	14.3	-	-	-	0.71933	0.000010
24 - 25	15.1	0.512044	0.000020	-11.5	0.71744	0.000011
26 - 27	16	0.512049	0.000007	-11.5	0.71747	0.000009
27 - 28	16.4	-	-	-	0.71653	0.000010
29 - 30	17.3	0.512078	0.000009	-10.9	0.71823	0.000010
34 - 35	19.4	0.512097	0.000006	-10.5	0.71707	0.000012
35 - 36	19.8	0.512106	0.000012	-10.4	0.71502	0.000008
36 - 37	20.2	0.512108	0.000009	-10.3	0.71603	0.000006
37 - 38	20.7	0.512174	0.000026	-10.1	0.71563	0.000020
39 - 40	21.5	-	-	-	0.71606	0.000008

^a Reflects the instrumental uncertainty.^b The overall procedure uncertainty is calculated as the higher 1 sigma standard deviation of duplicate analyses of different samples and is 0.3 ε unit for Nd-isotopes and 0.00035 for Sr-

isotopes. It takes into account: the leaching procedure, the chemical separation and purification and the analytical error.

Table 2 : Nd- and Sr- isotopic composition of second leaching step, thought to represent the authigenic phase.

Interval depth. cm	Age. cal. ka	$^{143}\text{Nd}/^{144}\text{Nd}$	$\pm 2\sigma^{\text{a}}$	$\varepsilon_{\text{Nd}}^{\text{b}}$	$^{87}\text{Sr}/^{86}\text{Sr}^{\text{b}}$	$\pm 2\sigma^{\text{a}}$
0 - 1	0.2	-	-	-	0.71044	0.000011
1 - 2	1.1	0.512151	0.000015	-9.5	0.71028	0.000019
2 - 3	2	0.512137	0.000022	-9.7	0.71019	0.000009
3 - 4	2.9	0.512174	0.000016	-9.1	0.71034	0.000008
4 - 5	3.8	0.512140	0.000018	-9.7	0.71062	0.000033
5 - 6	4.7	-	-	-	-	-
6 - 7	5.6	0.512125	0.000032	-10.0	0.71019	0.000010
7 - 8	6.5	0.512115	0.000018	-10.2	0.71076	0.000010
8 - 9	7.5	0.512119	0.000019	-10.1	0.71095	0.000013
9 - 10	8.3	-	-	-	0.71077	0.000009
14 - 15	12	0.512097	0.000008	-10.6	0.71100	0.000009
19 - 20	13	0.512116	0.000010	-10.2	0.71149	0.000023
21 - 22	13.9	0.512113	0.000016	-10.2	0.71364	0.000011
22 - 23	14.3	-	-	-	0.71220	0.000009
24 - 25	15.1	-	-	-	0.71073	0.000008
26 - 27	16	0.512132	0.000009	-9.9	0.71138	0.000012
27 - 28	16.4	-	-	-	0.71068	0.000011
29 - 30	17.3	0.512130	0.000017	-9.9	0.71059	0.000008
34 - 35	19.4	-	-	-	0.71209	0.000008
35 - 36	19.8	0.512203	0.000015	-8.6	0.71143	0.000008
36 - 37	20.2	0.512194	0.000016	-8.7	0.71081	0.000010
37 - 38	20.7	0.512197	0.000016	-8.6	0.71126	0.000015
39 - 40	21.5	-	-	-	0.71170	0.000010

^a Reflects the instrumental uncertainty.

^b The overall procedure uncertainty is calculated as the higher 1 sigma standard deviation of duplicate analyses of different samples and is 0.4 ϵ unit for Nd-isotopes and 0.00035 for Sr-isotopes. It takes into account: the leaching procedure, the chemical separation and purification and the analytical error. The possible detrital contribution is not considered in the leachates uncertainty.

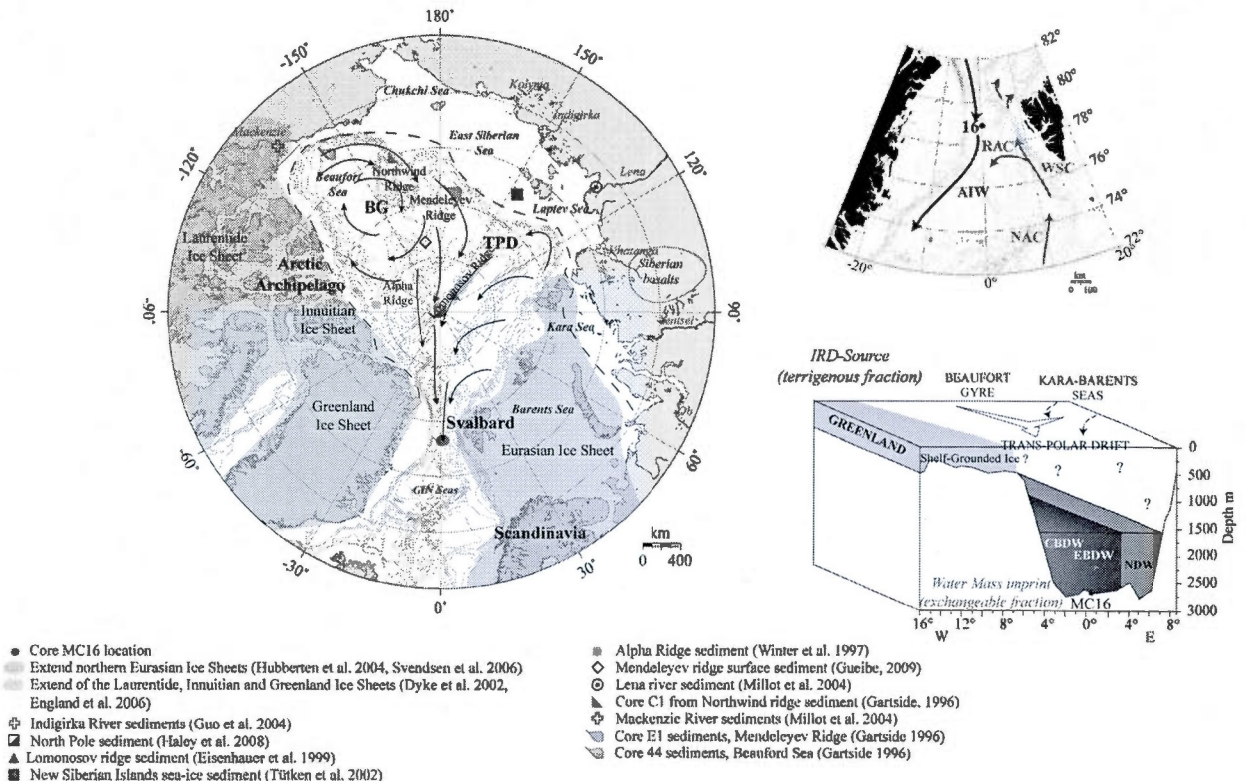


Figure 1 : Left: Map of the Arctic during LGM and early deglacial period showing core MC16 location (Red circle) and extent of ice-sheets. Italic Red: river locations; Bold-Italic blue: Arctic Seas; Bold Black: Land; Regular Black: Submarine ridges; Italic Grey: Arctic basins. Black arrows reflect the suggested sea-ice circulation patterns. The dashed line represents the assumed LGM sea-level.

Top Right : Bathymetric map of the Fram Strait along with major currents and MC16 core location. NAC : North Atlantic Current ; WSC :West Spitsbergen Current ; RAC : Return Atlantic Current ; AIW : Arctic Intermediate Waters

Bottom Right : Cross section of the Fram Strait showing deep water masses entering the Arctic (NDW : North-Atlantic Deep Water) and exiting the Arctic (CBDW : Canadian Basin Deep Water ; EBDW : Eurasian Basin Deep Water).

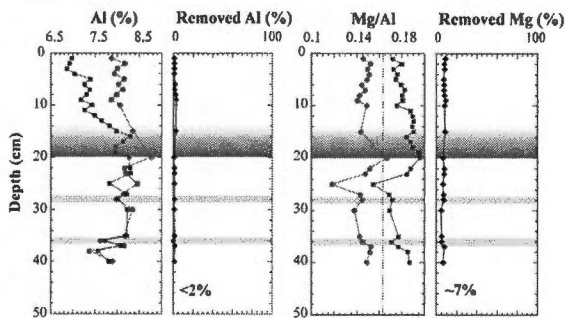
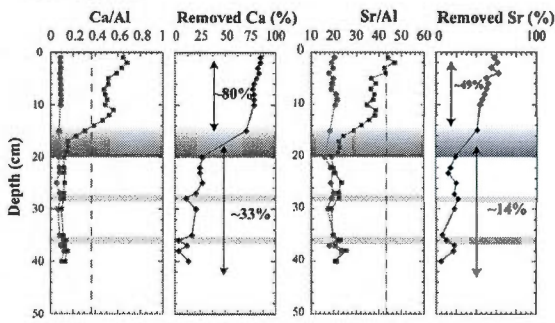
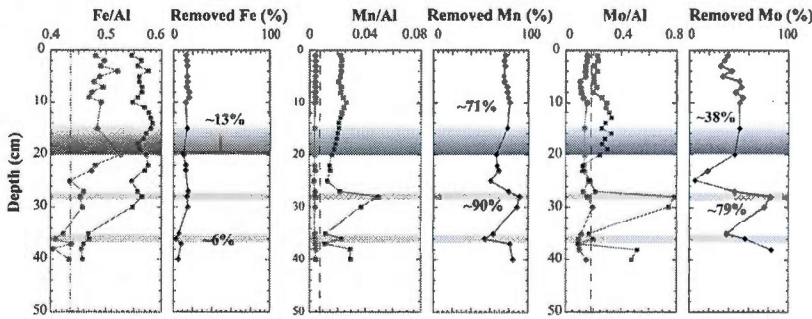
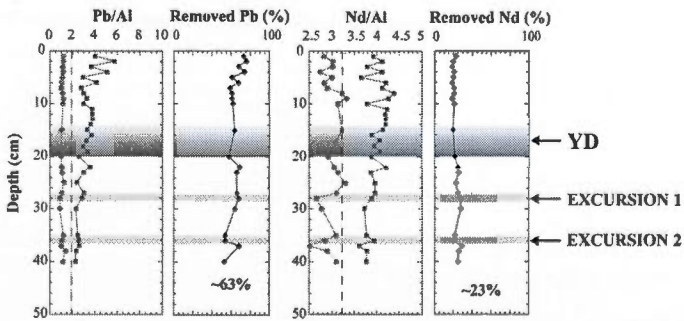
a. Detrital**b. Biogenic****c. Authigenic****d. Authigenic - Low mobility within the sediment**

Figure 2 : Profiles of Al contents and selected major and trace element contents normalized to Al in residues (red circles) and bulk (blue squares) fractions (<100 μ m). Examples of

representative elements are shown to illustrate the following behaviors:a. detrital; b. biogenic; c. authigenic and d. authigenic - low mobility elements within the sediment. Trace element (Mo, Sr, Pb and Nd) ratios are in ($\mu\text{g.g}/\%\text{wt Al}$). In panels a, c and d the profiles labelled "Removed ..%" represent the percentage of the element contained in the second leachate (designed to remove Fe-Mn oxides), normalized to the total content of that element in the residual and second leachate fractions. In panel b, "Removed ..%" refers to the wt% of Ca and Sr in the bulk fraction lost during the entire two-step leaching procedure (first leachate designed to remove carbonates; second designed to remove Fe-Mn oxides). Dashed lines represent average ratios of the upper continental crust (Taylor and McLennan, 1985). The Younger Dryas episode as well as two geochemical excursions identified on the basis of Pb and Sr isotopes are indicated.

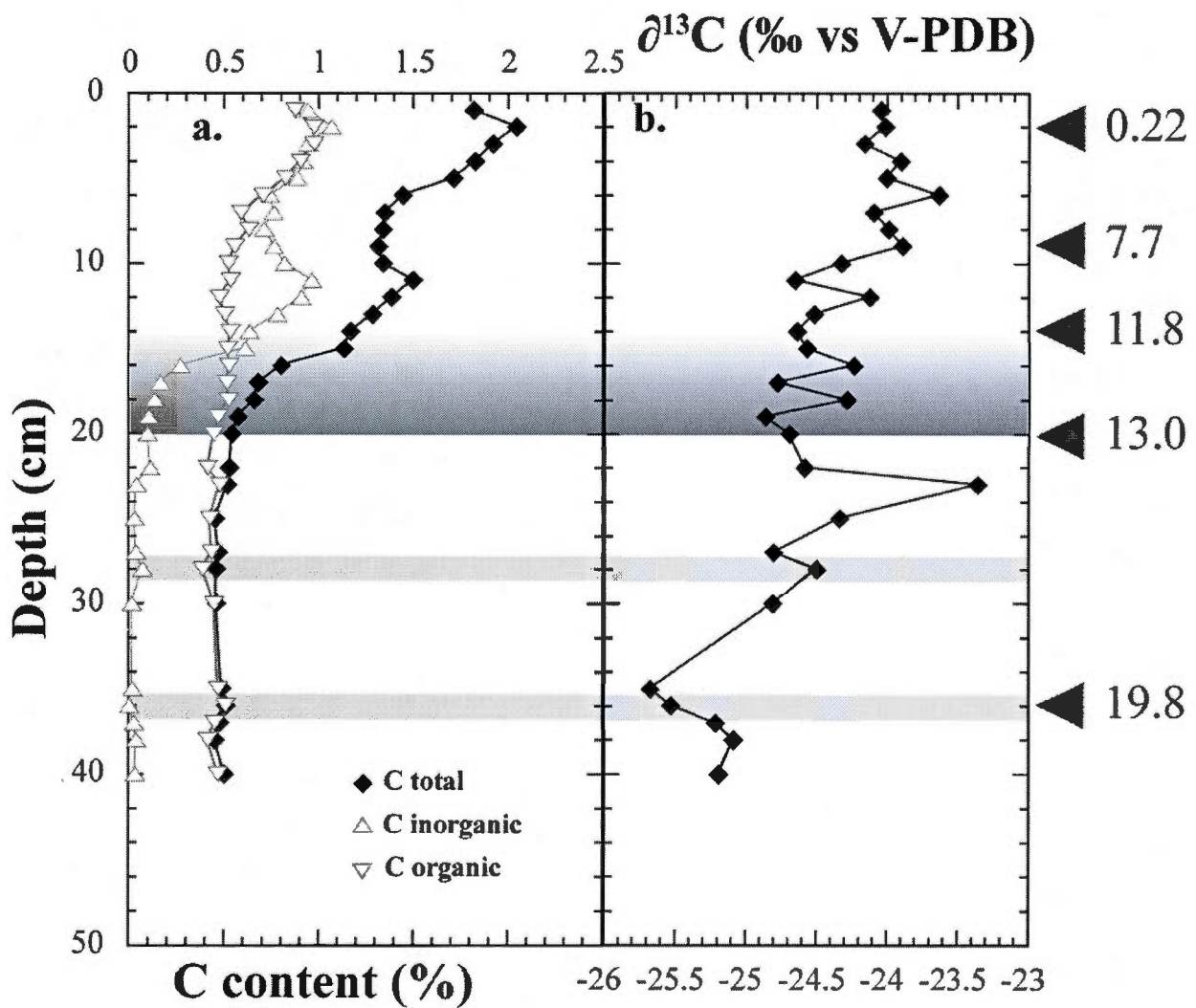


Figure 3 : a) Weight % carbon content in the bulk fraction. Total C (black diamonds); inorganic C (grey triangles); organic C (green triangles pointed downwards).

b) $\delta^{13}\text{C}$ of organic C from the bulk fraction expressed in ‰ vs V-PDB ($\pm 0.1\text{‰}$ uncertainty at 1σ).

Arrows represent age constraints from 3 AMS ages at 0.22, 7.7 and 19.8 ka. Geochemical correlations at 11.8 and 13 ka and an ash layer at 12.1 ka provided additional firm age constraints. Shaded bars indicate the YD and the two identified excursions (see caption Fig. 2).

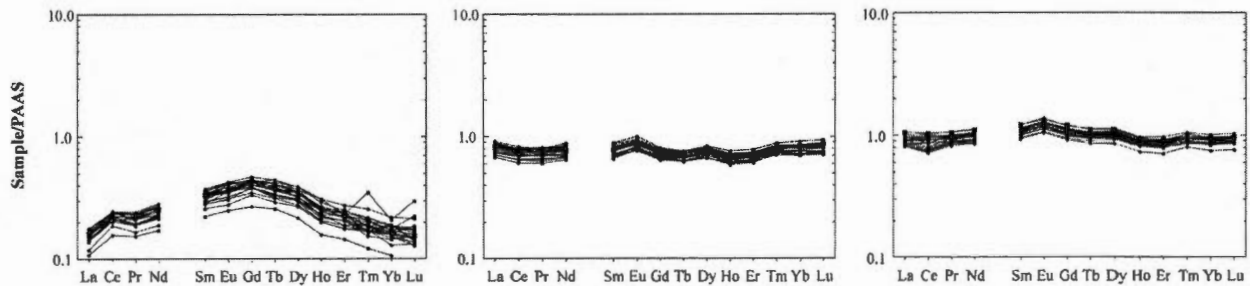


Figure 4 : REEs from a.) the leachates ; b.) the residues and c.) the bulk fraction. The REE concentrations are presented in $\mu\text{g.g}^{-1}$ and normalised to Post-Archean average Australian Shale values (Taylor and McLennan, 1985). Leachates show a typical MREE enrichment and a positive Ce anomaly, while both residues and the bulk fractions display relatively constant patterns.

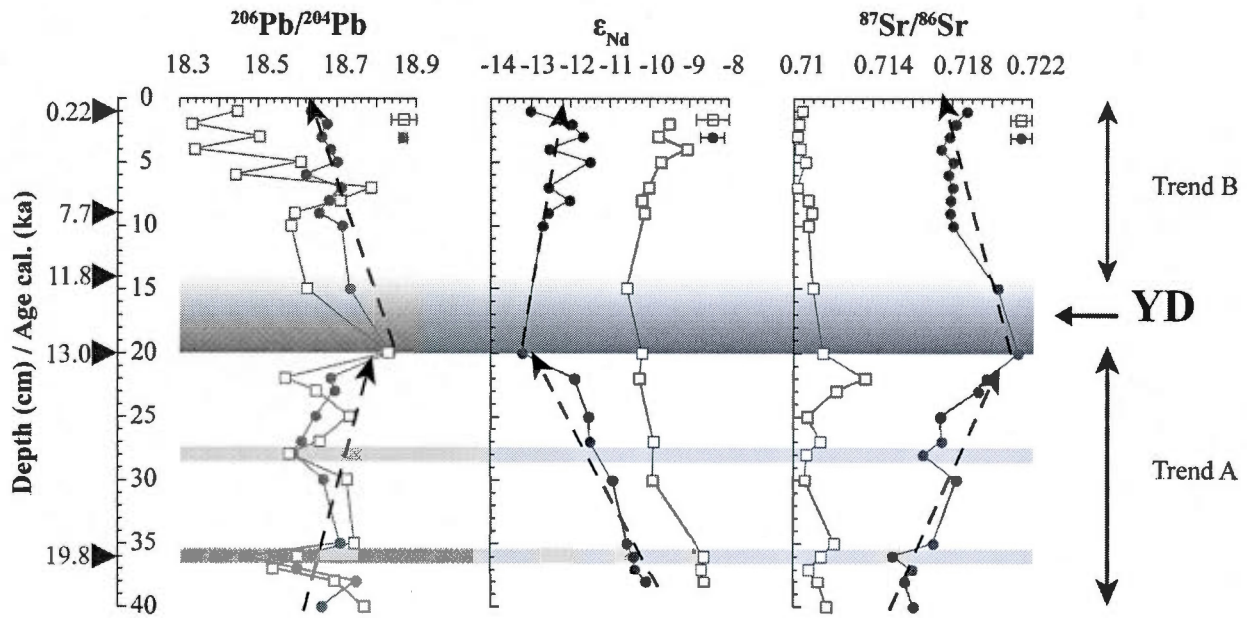


Figure 5 : Isotopic profile of $^{206}\text{Pb}/^{204}\text{Pb}$ ratios (left, red), ε_{Nd} (middle, blue), $^{87}\text{Sr}/^{86}\text{Sr}$ ratios (right, green) for residues (full circles) and leachates (open squares) from core MC16. The Sr isotopic results have been corrected to the accepted value for NIST-987 of 0.710248. Uncertainties for all values are represented as a scale bar in the top right corner of each plot. These uncertainties are 1 sigma standard deviations of duplicate analyses of several samples. The calculation takes into account the entire analytical procedure: leaching, chemical separation and purification, and the analytical measurement error. Arrows represent age constraints (see text and caption of figure 3). Shaded bars indicate the YD and the two identified excursions (see caption Fig. 2).

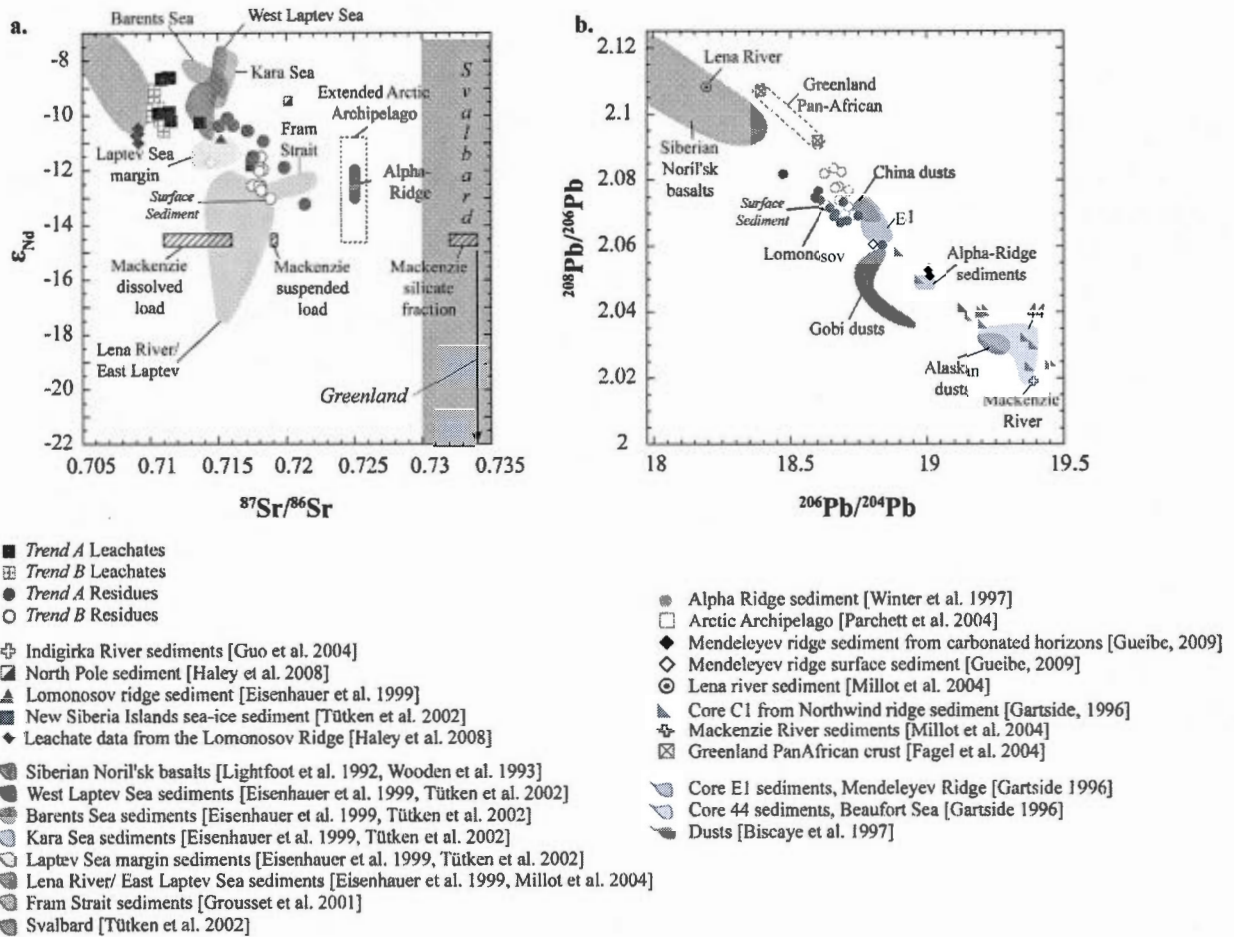
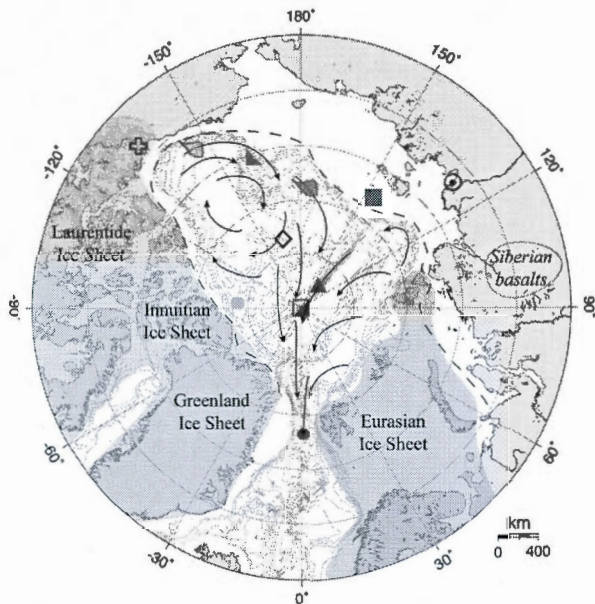
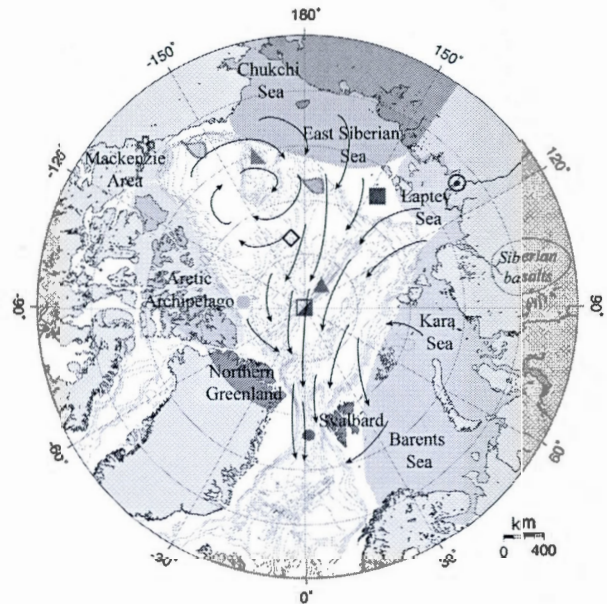


Figure 6 : a. ϵ_{Nd} vs $^{87}\text{Sr}/^{86}\text{Sr}$ diagram representing both residues and leachates from core MC16 and data from the literature. Trends A and B represent samples before and after the Younger Dryas respectively. b. $^{208}\text{Pb}/^{206}\text{Pb}$ vs. $^{206}\text{Pb}/^{204}\text{Pb}$ diagram for residues from core MC16 and data from Maccali et al. (2011).

Greenland and Svalbard: Greenland has a highly heterogenous isotopic composition. ϵ_{Nd} from the Greenland PanAfrican crust is between -15 and -25 (Gueibe 2009) and is represented by an arrow in the right bottom corner of panel a. Svalbard ϵ_{Nd} values also vary widely (from -8 to -25). However, granitoids from northern Svalbard have a ϵ_{Nd} value of -11.3 (Johansson et al. 2002).

Samples from the Arctic Archipelago, Alpha-Ridge, the Mackenzie and the Beaufort Sea contribute to the Canadian margins end-member.

a. LGM**b. Post Younger Dryas**

- Core MC16 location
- Extend northern Eurasian Ice Sheets (Hubberten et al. 2004, Svendsen et al. 2006)
- Extend of the Laurentide, Innuitian and Greenland Ice Sheets (Dyke et al. 2002, England et al. 2006)

Figure 7 : See Figure 1 legend.

a. Map of the Arctic during LGM and early deglacial (*Trend A*). Coloured zones represent a reconstruction of ice sheet extents during the LGM where the Eurasian Ice Sheet is in dark green and the Greenland-Innuitian-Laurentian Ice Sheet is in light blue. The dashed line represents the assumed LGM sea-level. The red circle represents core MC16. Other symbols show the locations of samples from the literature for which the data are shown in Fig. 6. Black arrows reflect the suggested sea-ice circulation pattern.

b. Map of the Arctic with proposed sea-ice conditions during *Trend B*, after the Younger Dryas. The red circle represents core MC16. Black arrows reflect the suggested sea-ice circulation pattern. Major detrital sediment sources identified from elemental and radiogenic isotope data are shown using the following colours : Greenland (Grey) ; Arctic Archipelago (Blue) ; Mackenzie area (orange) ; Chukchi and East Siberian Sea (Purple) ; East Laptev Sea (Light Green) ; West Laptev-Kara-Barents Sea (dark Green).

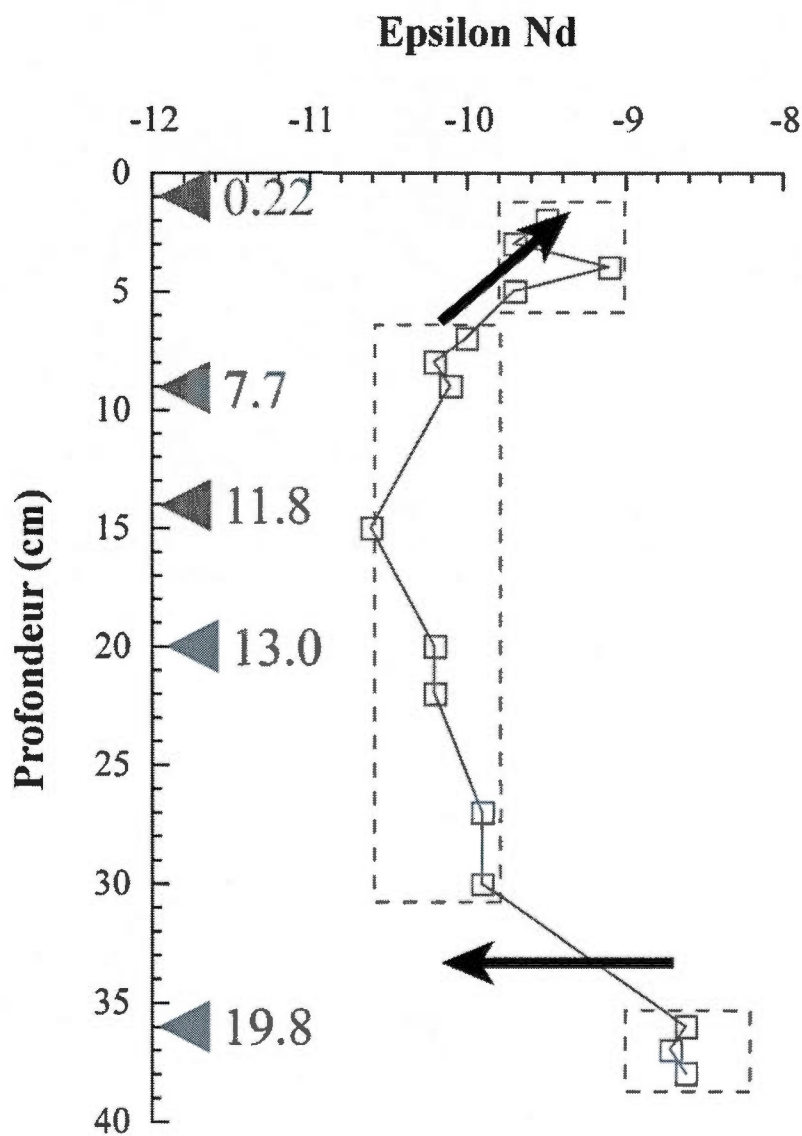


Figure 8 : Nd isotope compositions of leachates. Red arrows represent age constraints (see Figure 3). Black arrows represent change in ϵ_{Nd} values. Dashed blue rectangles represent the uncertainty envelopes.

7. AUXILIARY MATERIAL

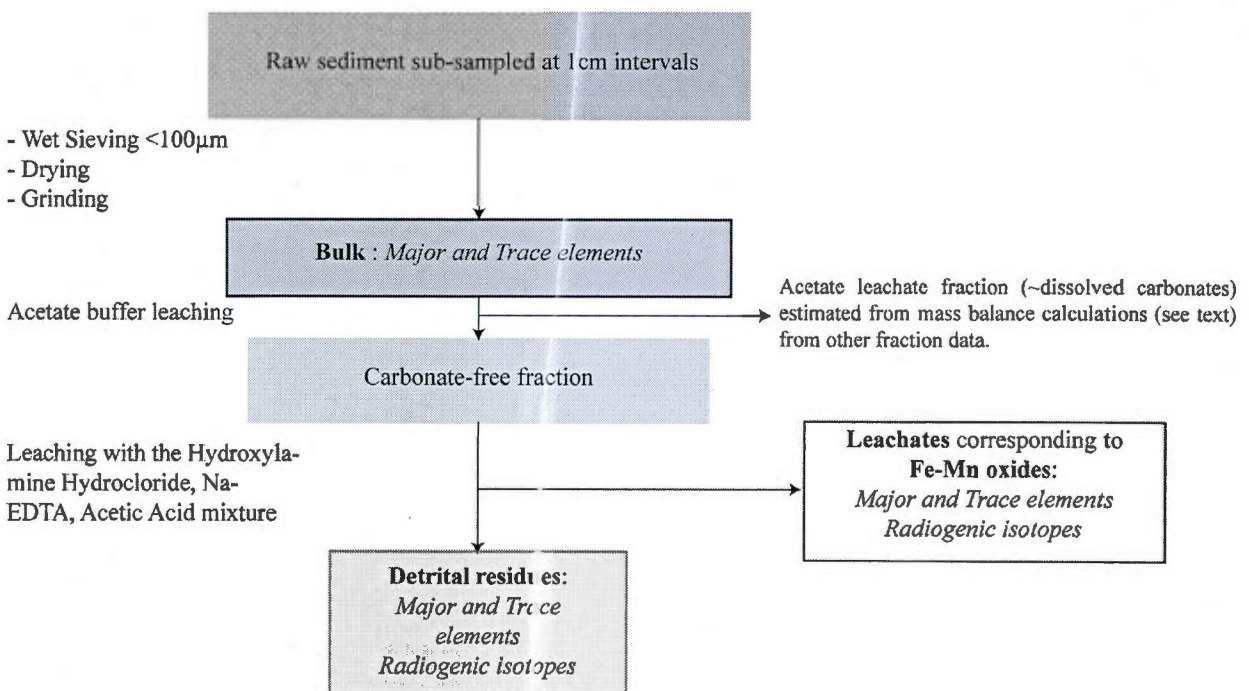


Figure 9: Analytical procedure followed for sample pre-treatment and analyses for major and trace elements and radiogenic isotopes. The second leaching step was designed to specifically extract Fe-Mn oxides. Leaching procedure adapted from Bayon et al. (2002) and Gutjahr et al. (2007).

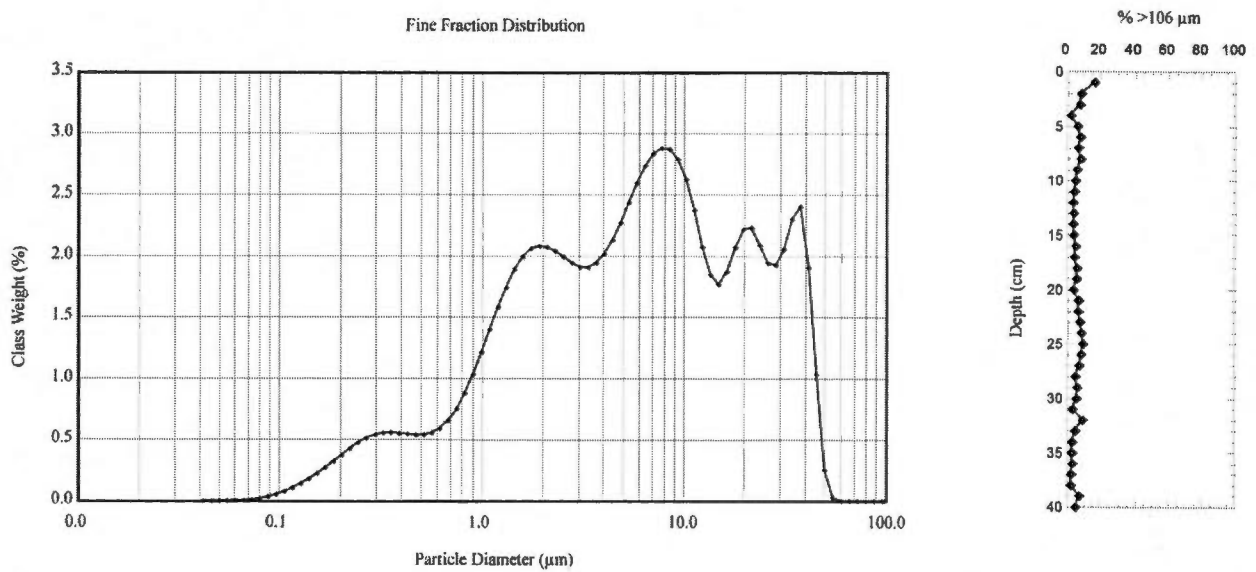


Figure 10: Average μ grain-size with a mode at 2 and 8 μm (Left). Coarse fraction distribution of core MC16 (right).

CHAPITRE III

CANADIAN RADIogenic ISOTOPE SIGNATURE OF YOUNGER DRYAS AGE ICE-RAFTED SEDIMENTS IN CORES FROM LOMONOSOV RIDGE AND FRAM STRAIT

Jenny Maccalli^{1,2}, Christelle Not^{1,3}, Claude Hillaire-Marcel¹ and André Poirier¹

¹Geotop, Université du Québec à Montréal, C.P. 8888, Montréal, QC, H3C 3P8, Canada

²CRPG, 15 Rue Notre-Dame-des-Pauvres, 54501 Vandoeuvre-lès-Nancy, France

³Department of Ocean Floor Geoscience, Atmosphere and Ocean Research Institute, University of Tokyo, Japan

Article à soumettre

ABSTRACT

Recent work on sediment-core from the central Lomonosov Ridge (TWC- & MC-18) yielded evidence for active Ice-Rafted Deposition (IRD) during the Younger Dryas (YD), following a sedimentary hiatus spanning broadly the Last Glacial Maximum (LGM) (Hanslik et al., 2010). The YD interval is also recorded in a core raised from below outflowing Arctic sea-ice and water masses in the Fram Strait area (MC-16), thus supporting the hypothesis of freshwater/sea-ice exports from the Arctic and playing a role in the YD-slowdown of the Atlantic Meridional Overturning Circulation (AMOC). We discuss here geochemical and radiogenic isotope data (Pb, Nd, Sr) of these YD-sediments in relation with potential sea-ice/sediment source areas in the Arctic Ocean. Three major regions with distinct isotopic characteristics have variably contributed to IRD along the Trans-Polar Drift route towards Fram Strait since the LGM : i) Arctic Canada ($^{206}\text{Pb}/^{204}\text{Pb} \geq 18.854$, epsilon-Nd ≤ -13.2 , $^{87}\text{Sr}/^{86}\text{Sr} \geq 0.721$), ii) Northern Russia- ($^{206}\text{Pb}/^{204}\text{Pb} \leq 18.45$, epsilon-Nd ≤ -10.3 and $^{87}\text{Sr}/^{86}\text{Sr} \leq 0.715$) and iii) Greenland- (YD; $^{206}\text{Pb}/^{204}\text{Pb} \leq 18.65$, epsilon-Nd ≤ -12.5 and $^{87}\text{Sr}/^{86}\text{Sr} \leq 0.718$). Whereas distinct mixing-trends are observed prior to and after the YD in the Fram Strait area, the YD itself is marked at both sites by a strong isotopic excursion towards the Canadian source with isotopic ratios of 18.84, -13.2 and 0.721 respectively for $^{206}\text{Pb}/^{204}\text{Pb}$, epsilon-Nd and $^{87}\text{Sr}/^{86}\text{Sr}$. Both sites also recorded a 5-fold higher IRD rates during the YD, in comparison with their respective mean Holocene rate. In MC-18, 5-fold higher ^{230}Th -excess also characterizes the YD unit which shows high carbonate contents, in its silt to sand fractions, with equal amounts of calcite and dolomite, also pointing to a major contribution of Canadian provenance. These features are interpreted as an indication for a strong freshwater pulse from northwestern Canada engendering a significant increase in the Arctic sea-ice exports through Fram Strait during the YD. Whereas marine ^{14}C -chronologies lack the precision required to identify unequivocally the actual trigger of the AMOC slowdown, during the YD, our findings strongly support the scenario of an Arctic trigger already put forth from model experiments by Tarasov and Peltier (2005) and field-based observations by Murton et al. (2010).

1. INTRODUCTION

Freshwater/sea-ice exports from the Arctic Ocean via Fram Strait represent a critical component of the ocean-climate system and act to modulate this system. Indeed, oceans store and transport a large amount of heat derived from solar insolation and hence play a central role in shaping the climate. The oceans reduce the thermal gradient between low and high latitudes by redistributing heat to the atmosphere. Release of heat to the atmosphere at high latitudes leads to the densification of the water-mass. The subsequent sinking of this cool and denser water-mass occurs in specific regions of the Atlantic Ocean such as in the Greenland-Iceland-Norwegian (GIN) Seas due to a less stable stratification of the water column (Hansen and Østerhus, 2000). Broecker et al. (1988) have suggested that massive inputs of freshwater in the GIN seas could cause a capping of the water column, preventing the sinking of deep-water and/or shifting the location of deepwater formation, thus altering the Atlantic Meridional Overturning Circulation (AMOC) as illustrated by McManus et al. (2004). This process has been observed during millennial scale events that punctuated the last deglaciation, as during the Younger Dryas (YD). The YD is a cold spell that occurred between 11.6 and 12.9 ka BP (Broecker et al., 1988; Carlson, 2010; Fanning and Weaver, 1997). A consensus has not yet been reached concerning an unequivocal cause for this event, however several hypotheses have been put forth in the past decade (Broecker, 2006; Broecker et al., 1988; Carlson, 2010; Firestone et al., 2007; Sima et al., 2004; Tarasov and Peltier, 2005). The drainage of the Laurentide Ice Sheet (LIS) is so far the most probable cause however the outlet routing system is still under debate (Carlson et al., 2007; de Vernal et al., 1996; Murton et al., 2010; Not and Hillaire-Marcel, 2012; Teller et al., 2005). Broecker et al. (1988) first hypothesized a major meltwater outflow through the St-Lawrence river system as a result of the eastern drainage of proglacial Lake Agassiz. This freshwater pulse would have capped the ocean surface preventing convective instabilities that drive deep-water formation. More recently, Tarasov and Peltier (2005, 2006) have introduced the concept of an “Arctic trigger” for the YD. They advanced the possibility of a northwestern routing via the Mackenzie river system to evacuate freshwater resulting from the melting of the Laurentide Ice Sheet and more specifically the Keewatin dome. Because of the intense stratification of the Arctic water column, the freshwater plume would have been advected with little or no modifications towards Fram Strait (which was the only exit pathway at the time as Nares

Strait was closed) and to the GIN Seas, rendering the region incapable of convective sinking and thus, slowing the AMOC and altering the climatic system. An increasing number of studies supports the hypothesis of a North routing of the meltwater and/or ice-calving pulse (Bradley and England, 2008; Maccalli et al., 2012a; Murton et al., 2010; Not and Hillaire-Marcel, 2012; Teller et al., 2005).

Radiogenic isotopes are widely used in paleoceanography notably for source identification (Abouchami et al., 1999; Eisenhauer et al., 1999; Fagel et al., 2002; Haley et al., 2008; Land Farmer et al., 2003; O'Nions et al., 1978; Tütken et al., 2002; Winter et al., 1997). In the Arctic Ocean, sediments that carry the signatures of their source regions are mostly transported via sea-ice. Thus, the isotopic and geochemical composition of sediments can be used to trace paleo sea-ice source area and circulation (Darby et al., 2002; Maccalli et al., 2012a, b; Winter et al., 1997). In a previous study (Maccalli et al., 2012a) we have demonstrated the suitability of radiogenic isotopes (e.g. Sr, Nd and Pb) for documenting source areas of terrigenous sediments. Here we present radiogenic isotope data from two cores (Fig. 1), one from the Lomonosov ridge (Core MC-18 ; Hanslik et al., 2010; Not and Hillaire-Marcel, 2012) and the second from central Fram Strait (Maccalli et al., 2012b) with a special interest to the sedimentary sequence corresponding to the YD event. A more complete dataset from both cores at depths corresponding to the YD event is presented here in order to more thoroughly document the implicated sediment sources.

2. REGIONAL SETTING

The Arctic Ocean is a semi-enclosed basin communicating with the world Ocean through Fram Strait, Bering Strait and the Canadian Arctic Archipelago (CAA ; Darby et al., 2006; Stein, 2008). The Arctic basin is divided by the Lomonosov Ridge into two sub-basins, the Amerasian basin and the Eurasian basin. The Arctic Ocean has a very specific sediment transport mechanism, involving sea-ice that forms over shallow margins where it incorporates suspended material. Currently, the sea-ice circulation pattern is dominated by the Beaufort Gyre (BG), which follows an anti-cyclonic movement over the Amerasian basin and the Trans-Polar Drift (TPD) circulating from Siberian margins towards Fram Strait (see Fig. 1 for circulation patterns). Under glacial conditions, speculative circulation pattern

inferred a BG type circulation however, with a relative intensity compare to present (Polyak et al., 2009; Polyak et al., 2007).

The core from the central Arctic (MC-18) is in an intra basin of the Lomonosov ridge and on the direct pathway of the merging BG and TPD, the two main circulation systems of the Arctic Ocean and is hence believed to receive contributions from both northern America and central Siberia (Fig. 1). Radiocarbon dates performed by Hanslik et al. (2010) along with ^{210}Pb data obtained by Not and Hillaire-Marcel (2012) have allowed the age model of core MC-18 to be established. One striking feature is the increased sedimentation rates of more than $\sim 10 \text{ cm.ka}^{-1}$ during the YD event as opposed to $\sim 1.7 \text{ cm.ka}^{-1}$ during the Holocene (Not and Hillaire-Marcel, 2012).

Fram Strait is one of the main sea-ice export pathways, and as noted above, was the only one during glacial periods (Bradley and England, 2008; Nørgaard-Pedersen et al., 2003; Tütken et al., 2002). Three AMS- ^{14}C measurements on planktonic assemblages along with tephrachronological and geochemical correlations allowed the establishment of an age model for core MC16, from Fram Strait (Maccalli et al., 2012b; Zamelczyk et al., 2012). Though poorly constrained, the age model retained for MC16 suggests a mean sedimentation rate of 2.3 cm.ka^{-1} for the LGM-early deglacial interval. The sedimentation rate increased to about 5 cm.ka^{-1} during the YD event itself. Finally during the Holocene, it decreased to a mean value of $\sim 1.1 \text{ cm.ka}^{-1}$. This suggests a ~ 5 fold higher sedimentation rates during the YD, compared to the Holocene, which is similar to the increase sedimentation rate estimated by Not and Hillaire-Marcel (2012), upstream on the IRD route, over the Lomonosov Ridge area.

Based on core MC-16, the late glacial-early deglacial interval seems to be controlled by ice-sheet dynamics: the merged Greenland, Innuitian and Laurentide ice-sheet over north America and the Eurasian ice-sheet over northern Europe were the two main providers of sedimentary supplies. During the Holocene sediments seem to originate from throughout the Arctic basin, reflecting more complex sea-ice circulation through both the BG and the TPD (Maccalli et al., 2012b). Data from core MC-18 show that the YD event marks a turning point in the sea-ice circulation patterns, from a dominant BG to an enhanced TPD after the YD event (Not and Hillaire-Marcel, 2012).

3. MATERIAL AND METHODS

Core MC-18, 47 cm long ($88^{\circ}26'N$; $146^{\circ}41'E$), from the central Arctic was collected during the HOTRAX expedition (Darby et al., 2005) in an intra basin from the Lomonosov Ridge at a water depth of 2654 m. Core MC16, 40 cm long ($78^{\circ}53.77'N$; $0^{\circ}16.92'E$) was collected during the 2006 WarmPast cruise on the R/V JanMayen (Husum, 2006) in central Fram Strait at a water depth of 2546m.

Fram Strait sediments were sieved at $100\text{ }\mu\text{m}$ and leached following the procedure adapted from Gutjahr et al. (2007) and described in Maccali et al. (2012b). This sequential leaching procedure has been designed to first remove the carbonate fraction with an acetate buffer solution and second to remove the Fe-Mn oxide fraction with a solution containing Hydroxylamine Hydrochloride - Na-EDTA-Acetic Acid buffered at pH 4. Residues obtained after the leaching procedure reflect the terrigenous component of the sediment and can directly be compared to sedimentary source areas.

Contrary to Fram Strait samples, Lomonosov sediments were not treated and were processed as non-sieved bulk fractions as they were initially thought to be discussed in a distinct study. However, our aim is not to compare directly results from the two cores but to discuss trends in both cores. Residues from Fram Strait core MC16 along with bulk samples from MC-18 from Lomonosov Ridge were digested with an acid mixture HF/HNO₃ on a hot plate at 130°C .

In order to collect Nd, samples were passed through two sets of column. A first column with TRU Spec[®] resin and diluted HNO₃ was used to separate REE and Sr-Rb. Nd was then isolated from other REE using LN Spec[®] resin with diluted HCl. Sr was purified through two elutions with Sr Spec[®] resin. Blanks for the Nd and Sr procedures were negligible (under 500 pg for Nd i.e. less than 0.04wt% and under 300ng for Sr i.e. less than 0.003wt%).

Sr-isotopes were measured with a ThermoScientific Triton Plus in static mode at GEOTOP, Montreal using Ta activator (Birck, 1986). $^{87}\text{Sr}/^{86}\text{Sr}$ ratios were normalized to $^{86}\text{Sr}/^{88}\text{Sr} = 0.1194$. Repeated analyses of standard NIST-987 yielded values of 0.710251 (± 0.000023 , 2σ reproducibility).

Nd-isotopes were analysed as Nd+ and loaded on Ta filaments and ionized with Re filaments using standard double filament mounting. Mass fractionation was corrected to

$^{146}\text{Nd}/^{144}\text{Nd} = 0.7219$. Replicate analyses of the standard JNDI-1 gave a mean value of $^{143}\text{Nd}/^{144}\text{Nd} = 0.512100 (\pm 0.000009, 2\sigma \text{ reproducibility})$ at GEOTOP.

The Nd isotopic composition will be expressed as :

$\varepsilon_{\text{Nd}} = \{(^{143}\text{Nd}/^{144}\text{Nd})_{\text{Sample}} / (^{143}\text{Nd}/^{144}\text{Nd})_{\text{CHUR}} - 1\} * 10^4$ where CHUR stands for Chondritic Uniform Reservoir and represents the present-day average earth value $(^{143}\text{Nd}/^{144}\text{Nd})_{\text{CHUR}} = 0.512638$ (Jacobsen and Wasserburg, 1980).

4. RESULTS

4.1 Core MC-18 from Lomonosov Ridge

$^{87}\text{Sr}/^{86}\text{Sr}$ ratios are homogenous though slightly decreasing in the upwards direction throughout the core except for the YD interval (Fig. 2). The deepest sample at the bottom of the core presents a $^{87}\text{Sr}/^{86}\text{Sr}$ value of 0.71625 while that at the surface displays a value of 0.71501. A strong excursion towards more radiogenic composition marks the YD interval, with $^{87}\text{Sr}/^{86}\text{Sr}$ values as high as 0.71858.

The Nd isotope profile displays a generally increasing trend with higher ε_{Nd} values of -10.5 towards the surface while the deepest samples present values < -11. Similar to Sr isotopes, the YD interval shows an excursion towards lower ε_{Nd} value (< -12; Fig. 2).

In a Nd vs Sr isotope diagram (Fig. 3), pre-YD glacial samples plot in an area with ε_{Nd} values between -11 and -11.6 and with $^{87}\text{Sr}/^{86}\text{Sr}$ values between 0.71591 and 0.71626. These samples correspond to Marine Isotopic Stage (MIS) 3 as a hiatus in sedimentation likely occurred during MIS 2 (Not and Hillaire-Marcel, 2012). Samples from the YD exhibit the most radiogenic and unradiogenic isotopic composition respectively for Sr and Nd isotopes. Samples from the end of the YD sequence and a sample from the onset of the Holocene sequence have intermediate values with a larger isotopic range; ε_{Nd} ratios are between -11.6 and -12.7 and $^{87}\text{Sr}/^{86}\text{Sr}$ ratios are between 0.71591 and 0.71719. Holocene samples seem to define a binary mixing trend (R^2 of 0.6) between two end-members, one with $\varepsilon_{\text{Nd}} > -10.5$ and $\varepsilon_{\text{Nd}} < -10.8$, and $^{87}\text{Sr}/^{86}\text{Sr} < 0.715$ and the other with $\varepsilon_{\text{Nd}} < -10.8$ and $^{87}\text{Sr}/^{86}\text{Sr} > 0.716$.

4.2 Core MC16 from Fram Strait

Sr isotopes present two trends before and after the YD event (Fig. 2). Prior to the YD, from the LGM to the early deglacial period, Sr isotopic composition is somewhat variable with a general increasing trend from $^{87}\text{Sr}/^{86}\text{Sr} \sim 0.716$ to ratios of ~ 0.719 . After the YD, i.e. during the Holocene, the profile displays homogenous $^{87}\text{Sr}/^{86}\text{Sr}$ ratios centered at about ~ 0.718 . During the YD itself, values rise to more radiogenic composition ($^{87}\text{Sr}/^{86}\text{Sr}$ ratios are > 0.721 with one exception at ~ 12.6 ka).

ϵ_{Nd} values decrease from -10.1 to -11.9 during the LGM-early deglacial interval. The YD interval displays the lowest value ranging from -12.7 to -13.2. During the Holocene, ϵ_{Nd} values are more variable and higher than those corresponding to the YD, except for the surface sample that shows a value of -13.0.

As discussed elsewhere (Maccali et al., 2012a, b) samples from MC16 defined two distinct temporal trends, prior and after the YD (Fig. 4). In the Nd vs Sr diagram, prior to the YD ϵ_{Nd} and $^{87}\text{Sr}/^{86}\text{Sr}$ values respectively decrease and increase with decreasing age. Samples from the YD sequence plot at the right bottom corner of the diagram with ϵ_{Nd} values ranging from -12.6 to -13.2 and with $^{87}\text{Sr}/^{86}\text{Sr}$ values between 0.7206 and 0.7217 except for the one sample at ~ 12.6 ka. After the YD event samples plot within an area define by ϵ_{Nd} values ranging from -11.5 to -12.7 and with $^{87}\text{Sr}/^{86}\text{Sr}$ values between 0.7175 and 0.7182.

5. DISCUSSION

In this section we discuss data from both core even though data are obtained from different phases. We feel that this is justified since we focus on trends rather than on absolute values (see supplement).

MC16 is on the pathway of sea-ice exiting from the Arctic through Fram Strait and sedimentary supplies are of circum Arctic origin. Because of the semi-enclosed character of the Arctic Ocean, potential source areas are limited to the surrounding land masses: Alaska, the Mackenzie delta area, the Canadian Arctic Archipelago, PanAfrican crust of northern Greenland, PanAfrican terrain of Svalbard, Barents Sea, Kara Sea, Laptev Sea, East Siberian Sea and Chukchi Sea. As Fram Strait is the main exit pathway, all of these areas should be considered as potential suppliers of sediment to core MC16.

On the other hand, considering known and/or reconstructed sea-ice circulation patterns, sources located downstream of core MC-18, such as northeastern Greenland, Svalbard, the Barents Sea and to some extent the Kara Sea, are less likely to contribute significantly to the sediments of this core.

Only limited radiogenic isotope data are available for most circum Arctic regions. These have been compiled from literature (Maccali et al., 2012a) and comprise various sample types including (Fig. 5): marine sediments (bulk and residues), basalts and marginal crustal rocks.

YD samples form distinct clusters in the Nd vs Sr diagram (Fig. 3, 4 and 5), with low ϵ_{Nd} and high $^{87}\text{Sr}/^{86}\text{Sr}$ signals reflecting the strongest Canadian influence corresponding to the Mackenzie river and/or Arctic Archipelago sources. In core MC16 however, a sample from the YD sequence has a distinct isotopic composition with significantly lower $^{87}\text{Sr}/^{86}\text{Sr}$ and might correspond to an isolated and short event, possibly some iceberg discharge. An analytical artifact cannot be completely excluded for this sample, even though this is unlikely, as we have treated all samples identically.

In core MC-18, the three pre-YD samples have similar isotopic compositions that might reflect contributions from ice-sheets over North America and over northern Europe (Fig. 3 and 5). During MIS 3 sea level was ~80 m lower, the Bering Strait was hence closed and most Siberian margins, where entrainment of sediment into sea-ice occurs currently, were emerged. As suggested by Maccali et al. (2012a, b) ice-sheets dynamics are one of the key factors controlling sedimentary supplies during glacial conditions. In core MC16, the binary mixing trend represented by pre-YD samples has been interpreted to reflect ice-sheet influences, with a gradual increase of the North America ice-sheet contribution over the Eurasian ice-sheet as this latter, which was not land-grounded, was decaying.

The Holocene interval in core MC16 shows little variability compared to the late glacial-early deglacial interval, suggesting contributions from throughout the circum-Arctic. In core MC-18, late Holocene samples suggest a mixture with gradual increase of ϵ_{Nd} and decrease of $^{87}\text{Sr}/^{86}\text{Sr}$. As for MC16 Holocene samples, no source regions can be excluded for the Holocene samples of core MC-18. However, Not and Hillaire-Marcel (2012) suggested a transport via the TPD from the Laptev Sea margin (Fig. 5) during the Holocene based on U

isotope data. In addition, our results suggest a contribution from the Bering Strait/Chukchi Sea area for late Holocene samples probably reflecting the opening of Bering Strait.

In core MC-18, the YD intervals seem to be followed by a transitional regime, with gradual increase of ε_{Nd} and decrease of $^{87}\text{Sr}/^{86}\text{Sr}$ (Fig. 3 and 4). This transition between the YD and the late Holocene might reflect the reorganization of the sea-ice circulation. Indeed, Not and Hillaire-Marcel (2012) and Bradley and England (2008) suggested that before the YD the ice-pack over the western basin would have been quite still with very little movement, as illustrated by the sedimentary hiatus in core MC-18, which probably corresponds to MIS 2. The freshwater drainage occurring during the YD would have destabilized the ice-pack which, along with incoming Pacific waters through Bering Strait, would have resulted in a more dynamic circulation. Isotopic data seem to confirm the hypothesis put forth by Not and Hillaire-Marcel (2012) that a change in sources occurred after the YD, with greater contributions from the Russian margins.

6. CONCLUSION

This study provides robust evidence of a strong isotopic Canadian signal in two cores from the Arctic, at a time corresponding to the YD event. Teller et al. (2005) and Murton et al. (2010) have published terrestrial data indicating a northward route for the drainage of lake Agassiz. Not and Hillaire-Marcel (2012) provided the first Arctic marine dataset illustrating enhanced scavenging and sedimentary supplies during the YD event. The drainage pulse from lake Agassiz would have not only affected the Arctic Ocean (i.e. core MC-18, Lomonosov Ridge) but would have also crossed the Arctic Ocean towards Fram Strait, upstream of the GIN Seas where deep-water formation occurs. Our data complete and confirm the evidence for a paleoceanographical event in the Arctic Ocean during the YD, they are also in agreement with the hypothesis first put forth by Tarasov and Peltier (2005) of an Arctic pathway for the drainage of the Laurentide ice-sheet during the YD, which later flowed towards the GIN Seas through Fram Strait (Peltier et al., 2006).

Our study also reveals that the YD event had a profound effect on the Arctic circulation and marked a turning point in the delivery of sediments to the Arctic Ocean. The drainage pulse, thought to occur during the YD, would have destabilized the ice-pack. A

transitional period that began after the YD would have probably reflected the equilibration of the sea-ice circulation with a likely strengthening of the TPD as earlier suggested by Bradley and England (2008).

7. REFERENCES

- Abouchami, W., Galer, S.J.G., Koschinsky, A., 1999. Pb and Nd isotopes in NE Atlantic Fe-Mn crusts: Proxies for trace metal paleosources and paleocean circulation. *Geochimica et Cosmochimica Acta* 63, 1489-1505.
- Bayon, G., German, C.R., Boella, R.M., Milton, J.A., Taylor, R.N., Nesbitt, R.W., 2002. An improved method for extracting marine sediment fractions and its application to Sr and Nd isotopic analysis. *Chemical Geology* 187, 179-199.
- Birck, J.L., 1986. Precision KRbSr isotopic analysis: Application to RbSr chronology. *Chemical Geology* 56, 73-83.
- Bradley, R.S., England, J.H., 2008. The Younger Dryas and the Sea of Ancient Ice. *Quaternary Research* 70, 1-10.
- Broecker, W.S., 2006. Was the Younger Dryas triggered by a flood? *Science* 312, 1146-1148.
- Broecker, W.S., Andree, M., Wolfli, W., Oeschger, H., Bonani, G., Kennett, J., Peteet, D., 1988. The chronology of the last deglaciation: implications to the cause of the Younger Dryas event. *Paleoceanography* 3, 1-19.
- Carlson, A.E., 2010. What caused the Younger Dryas cold event? *Geology* 38, 383-384.
- Carlson, A.E., Clark, P.U., Haley, B.A., Klinkhammer, G.P., Simmons, K., Brook, E.J., Meissner, K.J., 2007. Geochemical proxies of North American freshwater routing during the Younger Dryas cold event. *Proceedings of the National Academy of Sciences of the United States of America* 104, 6556-6561.
- Darby, D.A., Bischof, J.F., Spielhagen, R.F., Marshall, S.A., Herman, S.W., 2002. Arctic ice export events and their potential impact on global climate during the late Pleistocene. *Paleoceanography* 17, 1025.
- Darby, D.A., Jakobsson, M., Polyak, L., 2005. Icebreaker expedition collects key arctic seafloor and ice data. *Eos* 86.
- Darby, D.A., Polyak, L., Bauch, H.A., 2006. Past glacial and interglacial conditions in the Arctic Ocean and marginal seas - a review. *Progress in Oceanography* 71, 129-144.
- de Vernal, A., Hillaire-Marcel, C., Bilodeau, G., 1996. Reduced meltwater outflow from the Laurentide ice margin during the Younger Dryas. *Nature* 381, 774-777.

- Eisenhauer, A., Meyer, H., Rachold, V., Tütken, T., Wiegand, B., Hansen, B.T., Spielhagen, R.F., Lindemann, F., Kassens, H., 1999. Grain size separation and sediment mixing in Arctic Ocean sediments: Evidence from the strontium isotope systematic. *Chemical Geology* 158, 173-188.
- Fagel, N., Innocent, C., Gariepy, C., Hillaire-Marcel, C., 2002. Sources of Labrador Sea sediments since the last glacial maximum inferred from Nd-Pb isotopes. *Geochimica et Cosmochimica Acta* 66, 2569-2581.
- Fanning, A.F., Weaver, A.J., 1997. Temporal-geographical meltwater influences on the North Atlantic conveyor: Implications for the Younger Dryas. *Paleoceanography* 12, 307-320.
- Firestone, R.B., West, A., Kennett, J.P., Becker, L., Bunch, T.E., Revay, Z.S., Schultz, P.H., Belgia, T., Kennett, D.J., Erlandson, J.M., Dickenson, O.J., Goodyear, A.C., Harris, R.S., Howard, G.A., Kloosterman, J.B., Lechler, P., Mayewski, P.A., Montgomery, J., Poreda, R., Darrah, T., Que Hee, S.S., Smitha, A.R., Stich, A., Topping, W., Wittke, J.H., Wolbach, W.S., 2007. Evidence for an extraterrestrial impact 12,900 years ago that contributed to the megafaunal extinctions and the Younger Dryas cooling. *Proceedings of the National Academy of Sciences of the United States of America* 104, 16016-16021.
- Gutjahr, M., Frank, M., Stirling, C.H., Keigwin, L.D., Halliday, A.N., 2008. Tracing the Nd isotope evolution of North Atlantic Deep and Intermediate Waters in the western North Atlantic since the Last Glacial Maximum from Blake Ridge sediments. *Earth and Planetary Science Letters* 266, 61-77.
- Gutjahr, M., Frank, M., Stirling, C.H., Klemm, V., van de Flierdt, T., Halliday, A.N., 2007. Reliable extraction of a deepwater trace metal isotope signal from Fe-Mn oxyhydroxide coatings of marine sediments. *Chemical Geology* 242, 351-370.
- Haley, B.A., Frank, M., Spielhagen, R.F., Fietzke, J., 2008. Radiogenic isotope record of Arctic Ocean circulation and weathering inputs of the past 15 million years. *Paleoceanography* 23.
- Hansen, B., Østerhus, S., 2000. North Atlantic-Nordic Seas exchanges. *Progress in Oceanography* 45, 109-208.
- Hanslik, D., Jakobsson, M., Backman, J., Björck, S., Sellén, E., O'Regan, M., Fornaciari, E., Skog, G., 2010. Quaternary Arctic Ocean sea ice variations and radiocarbon reservoir age corrections. *Quaternary Science Reviews* 29, 3430-3441.

- Husum, K., 2006. Cruise Report JM06-WP: Marine geological cruise to West Spitsbergen Margin and Fram Strait. University of Tromsø.
- Jacobsen, S.B., Wasserburg, G.J., 1980. Sm-Nd isotopic evolution of chondrites. *Earth and Planetary Science Letters* 50, 139-155.
- Land Farmer, G., Barber, D., Andrews, J., 2003. Provenance of Late Quaternary ice-proximal sediments in the North Atlantic: Nd, Sr and Pb isotopic evidence. *Earth and Planetary Science Letters* 209, 227-243.
- Maccalli, J., Hillaire-Marcel, C., Carignan, J., Reisberg, L.C., 2012a. Geochemical signatures of sediment to document Arctic sea-ice and water-mass exports through Fram Strait since the Last Glacial Maximum. Submitted to *Quaternary Science Reviews*.
- Maccalli, J., Hillaire-Marcel, C., Carignan, J., Reisberg, L.C., 2012b. Pb-isotopes and geochemical monitoring of Arctic sedimentary supplies and water-mass export through Fram Strait since the Last Glacial Maximum. *Paleoceanography* 27, PA1201.
- McManus, J.F., Francois, R., Gherardi, J.M., Kelgwin, L., Brown-Leger, S., 2004. Collapse and rapid resumption of Atlantic meridional circulation linked to deglacial climate changes. *Nature* 428, 834-837.
- Murton, J.B., Bateman, M.D., Dallimore, S.R., Teller, J.T., Yang, Z., 2010. Identification of Younger Dryas outburst flood path from Lake Agassiz to the Arctic Ocean. *Nature* 464, 740-743.
- Nørgaard-Pedersen, N., Spielhagen, R.F., Erlenkeuser, H., Grootes, P.M., Heinemeier, J., Knies, J., 2003. Arctic Ocean during the Last Glacial Maximum: Atlantic and polar domains of surface water mass distribution and ice cover. *Paleoceanography* 18, 8-1.
- Not, C., Hillaire-Marcel, C., 2012. Enhanced sea-ice export from the Arctic during the Younger Dryas. *Nature Communications* 3, 647.
- O'Nions, R.K., Carter, S.R., Cohen, R.S., Evensen, N.M., Hamilton, P.J., 1978. Pb, Nd and Sr isotopes in oceanic ferromanganese deposits and ocean floor basalts. *Nature* 273, 435-438.
- Peltier, W.R., Vettoretti, G., Stastna, M., 2006. Atlantic meridional overturning and climate response to Arctic Ocean freshening. *Geophysical Research Letters* 33, L06713.
- Polyak, L., Bischof, J., Ortiz, J.D., Darby, D.A., Channell, J.E.T., Xuan, C., Kaufman, D.S., Løvlie, R., Schneider, D.A., Eberl, D.D., Adler, R.E., Council, E.A., 2009. Late Quaternary

stratigraphy and sedimentation patterns in the western Arctic Ocean. *Global and Planetary Change* 68, 5-17.

Polyak, L., Darby, D.A., Bischof, J.F., Jakobsson, M., 2007. Stratigraphic constraints on late Pleistocene glacial erosion and deglaciation of the Chukchi margin, Arctic Ocean. *Quaternary Research* 67, 234-245.

Porcelli, D., Andersson, P.S., Baskaran, M., Frank, M., Björk, G., Semiletov, I., 2009. The distribution of neodymium isotopes in Arctic Ocean basins. *Geochimica et Cosmochimica Acta* 73, 2645-2659.

Sima, A., Paul, A., Schulz, M., 2004. The Younger Dryas - An intrinsic feature of late Pleistocene climate change at millennial timescales. *Earth and Planetary Science Letters* 222, 741-750.

Stein, R., 2008. Chapter Two Modern Physiography, Hydrology, Climate, and Sediment Input, In: Ruediger, S. (Ed.), *Developments in Marine Geology*. Elsevier, pp. 35-84.

Tarasov, L., Peltier, W.R., 2005. Arctic freshwater forcing of the Younger Dryas cold reversal. *Nature* 435, 662-665.

Tarasov, L., Peltier, W.R., 2006. A calibrated deglacial drainage chronology for the North American continent: evidence of an Arctic trigger for the Younger Dryas. *Quaternary Science Reviews* 25, 659-688.

Teller, J.T., Boyd, M., Yang, Z., Kor, P.S.G., Fard, A.M., 2005. Alternative routing of Lake Agassiz overflow during the Younger Dryas: New dates, paleotopography, and a re-evaluation. *Quaternary Science Reviews* 24, 1890-1905.

Tütken, T., Eisenhauer, A., Wiegand, B., Hansen, B.T., 2002. Glacial-interglacial cycles in Sr and Nd isotopic composition of Arctic marine sediments triggered by the Svalbard/Barents Sea ice sheet. *Marine Geology* 182, 351-372.

Winter, B.L., Johnson, C.M., Clark, D.L., 1997. Strontium, neodymium, and lead isotope variations of authigenic and silicate sediment components from the Late Cenozoic Arctic Ocean: Implications for sediment provenance and the source of trace metals in seawater. *Geochimica et Cosmochimica Acta* 61, 4181-4200.

Zamelczyk, K., Rasmussen, T.L., Husum, K., Haflidason, H., de Vernal, A., Ravna, E.K., Hald, M., Hillaire-Marcel, C., 2012. Paleoceanographic changes and calcium carbonate dissolution in the central Fram Strait during the last 20 ka yr. *Quaternary Research* In press.

Table 1 : Isotopic composition of bulk samples from the Lomonosov Ridge (core MC-18). * indicates samples from the YD interval.

Depth (cm)	$^{87}\text{Sr}/^{86}\text{Sr}$	\pm	$^{143}\text{Nd}/^{144}\text{Nd}$	\pm	ϵ_{Nd}
1.5	0.715009	0.000009	0.512099	0.000010	-10.5
6	0.715588	0.000007	0.512098	0.000028	-10.5
10.5	0.715622	0.000009	0.512089	0.000018	-10.7
15.5	0.715917	0.000008	0.512084	0.000019	-10.8
20.5	0.716190	0.000008	0.512044	0.000011	-11.6
23*	0.715912	0.000008	0.512033	0.000011	-11.8
24*	0.716066	0.000015	0.512032	0.000005	-11.8
25*	0.717192	0.000020	0.511988	0.000040	-12.7
25.5*	0.718580	0.000011	0.512009	0.000006	-12.3
25.5*	0.718448	0.000015	0.511999	0.000015	-12.5
26*	0.718499	0.000019	0.511993	0.000010	-12.6
26.5*	0.718253	0.000014	0.511997	0.000009	-12.5
30.5	0.715905	0.000008	0.512076	0.000016	-11.0
35	0.716258	0.000008	0.512046	0.000012	-11.6
39.5	0.716252	0.000009	0.512067	0.000020	-11.1

Table 2 : Isotopic composition of residue samples from Fram Strait (core MC16). * indicates samples from the YD interval and were performed for this study other data were taken from Maccalli et al. [2011a].

Depth (cm)	$^{87}\text{Sr}/^{86}\text{Sr}$	\pm	$^{143}\text{Nd}/^{144}\text{Nd}$	\pm	ε_{Nd}
1	0.718791	0.000012	0.511971	0.000024	-13.0
2	0.718241	0.000010	0.512025	0.000007	-12.0
3	0.717913	0.000011	0.512039	0.000009	-11.7
4	0.717499	0.000011	0.511995	0.000009	-12.5
5	0.718111	0.000010	0.512048	0.000008	-11.5
6	0.717869	0.000010	-	-	-
7	0.718088	0.000009	0.511994	0.000010	-12.6
8	0.717972	0.000010	0.512022	0.000007	-12.0
9	0.717936	0.000009	0.511994	0.000009	-12.6
10	0.718111	0.000014	0.511987	0.000007	-12.7
13	0.719600	0.000011	0.511977	0.000009	-12.9
15*	0.720335	0.000020	-	-	-
16*	0.721250	0.000023	0.511978	0.000011	-12.9
17*	0.720620	0.000014	0.511980	0.000019	-12.8
18*	0.721190	0.000014	0.511965	0.000002	-13.1
19*	0.718320	0.000020	0.511985	0.000009	-12.7
20*	0.721346	0.000016	0.511961	0.000009	-13.2
20*	0.721020	0.000015	0.511986	0.000003	-12.7
21*	0.721700	0.000013	0.511978	0.000011	-12.9
22	0.719828	0.000009	0.512029	0.000008	-11.9
23	0.719380	0.000010	-	-	-
25	0.717490	0.000020	0.512044	0.000020	-11.6
27	0.717514	0.000009	0.512049	0.000007	-11.5
28	0.716572	0.000021	-	-	-
30	0.718272	0.000012	0.512078	0.000009	-10.9

35	0.717117	0.000012	0.512097	0.000006	-10.5
36	0.715069	0.000008	0.512106	0.000012	-10.4
37	0.716073	0.000018	0.512108	0.000009	-10.3
38	0.715681	0.000013	0.512174	0.000026	-9.1
40	0.716108	0.000008	-	-	-

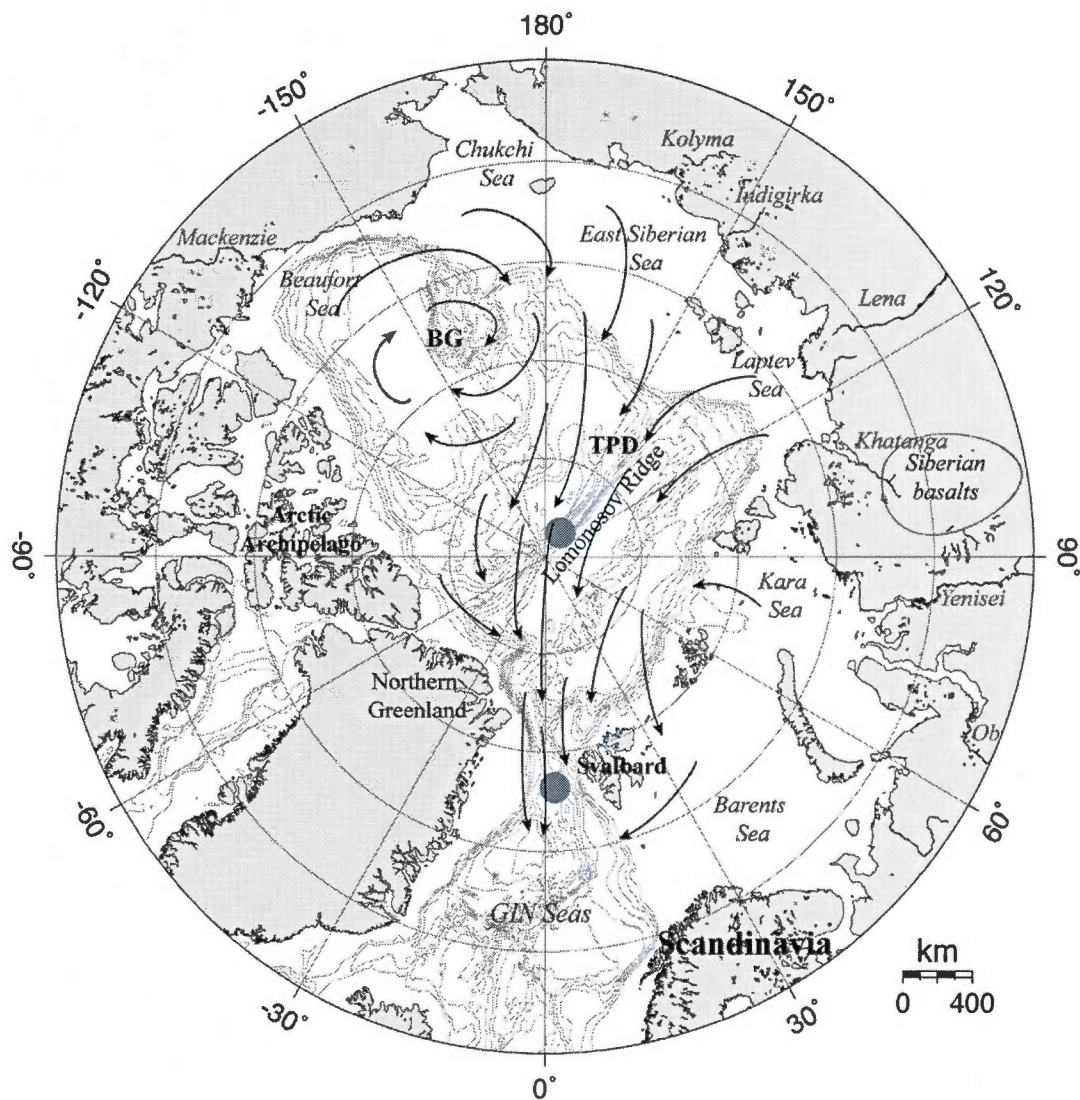


Figure 1: Bathymetric map of the Arctic (<https://sfb574.geomar.de/gmt-maps>). Cores locations are indicated with red circles. Black arrows represent surface currents. Main rivers are written in red.

BG: Beaufort Gyre; TPD: Trans-Polar Drift

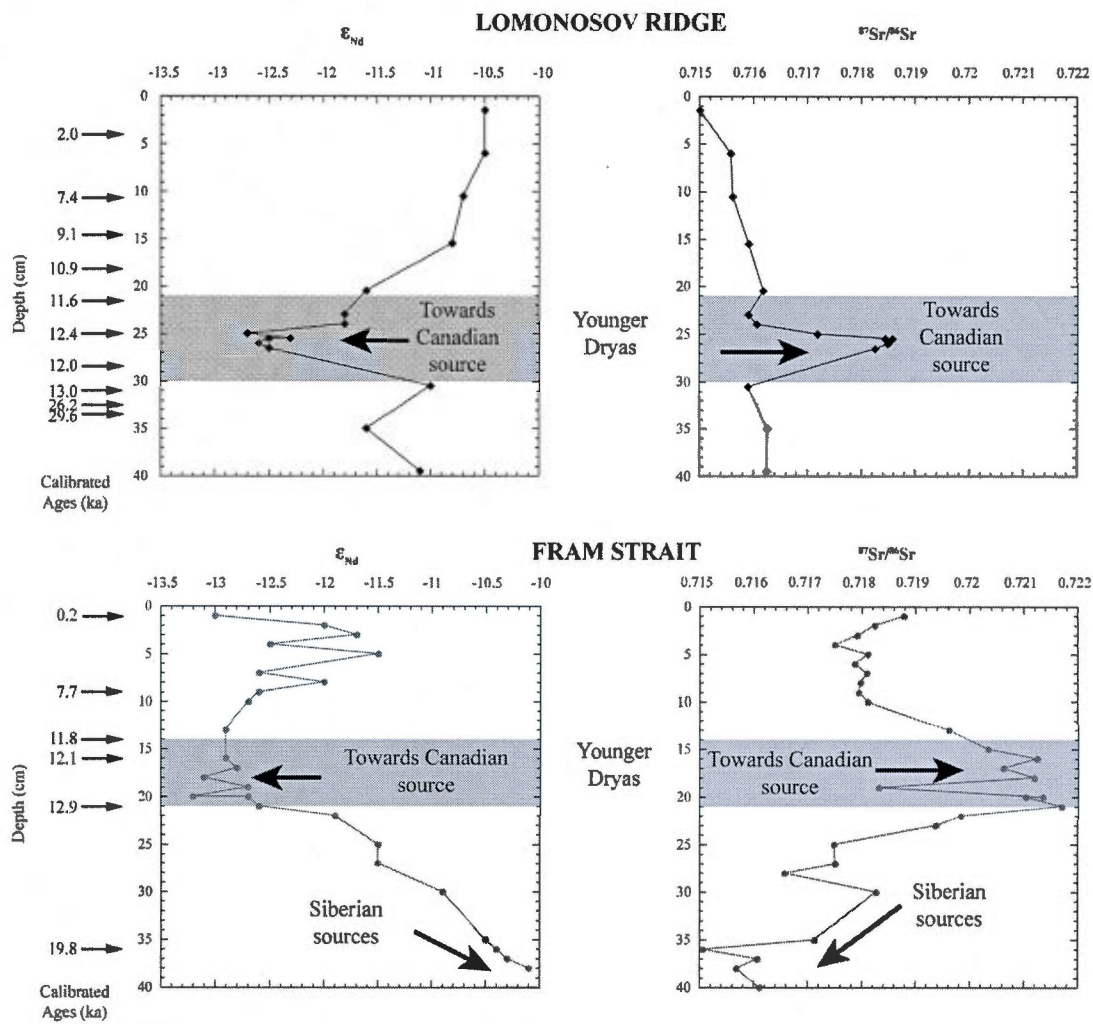


Figure 2: Nd- (left) and Sr- (right) isotopic composition of bulk samples from the Lomonosov Ridge (Top) and of residues from Fram Strait (Bottom). The blue zone corresponds to the YD interval.

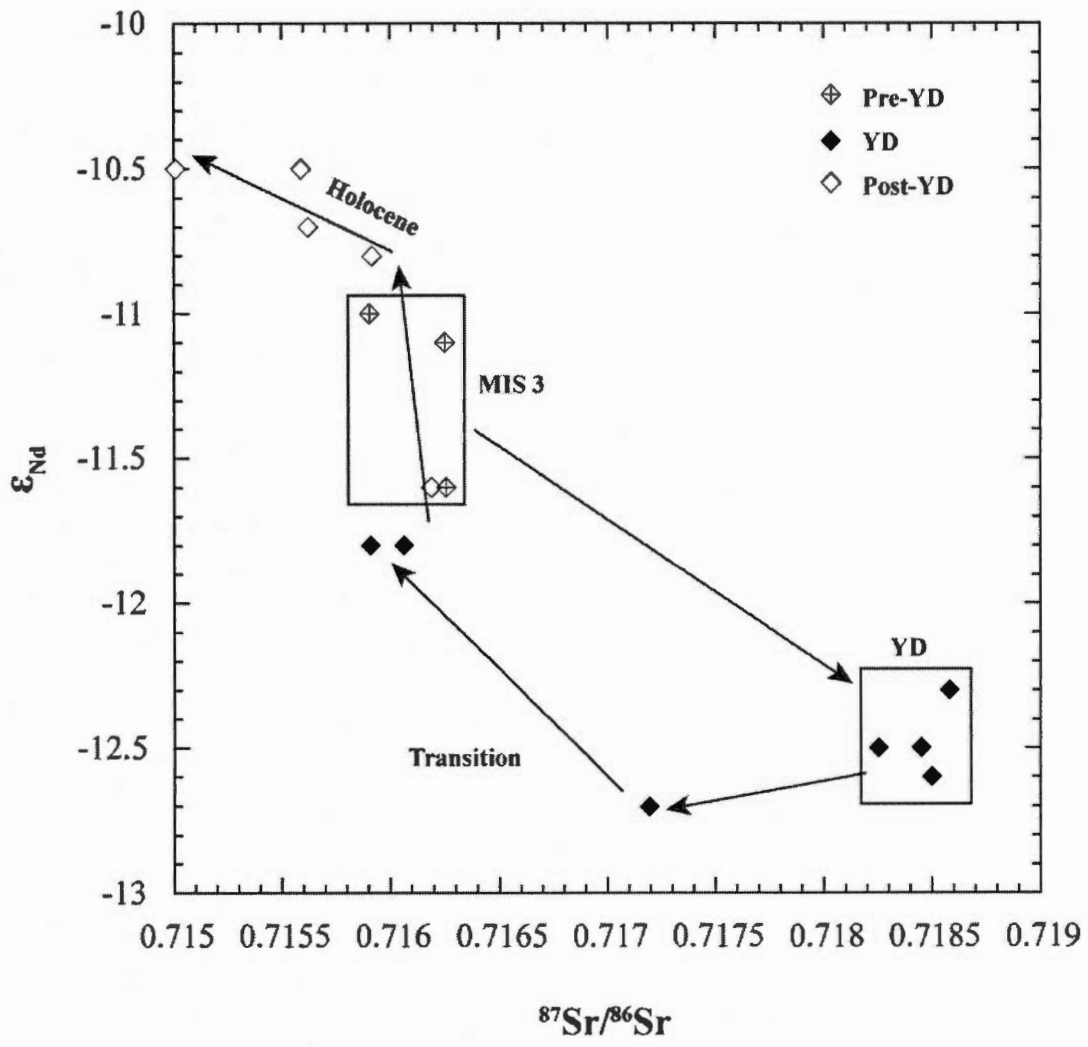


Figure 3: Nd- vs Sr-isotopes from core MC-18 (i.e. Lomonosov Ridge). Full black diamonds represent samples from the YD interval.

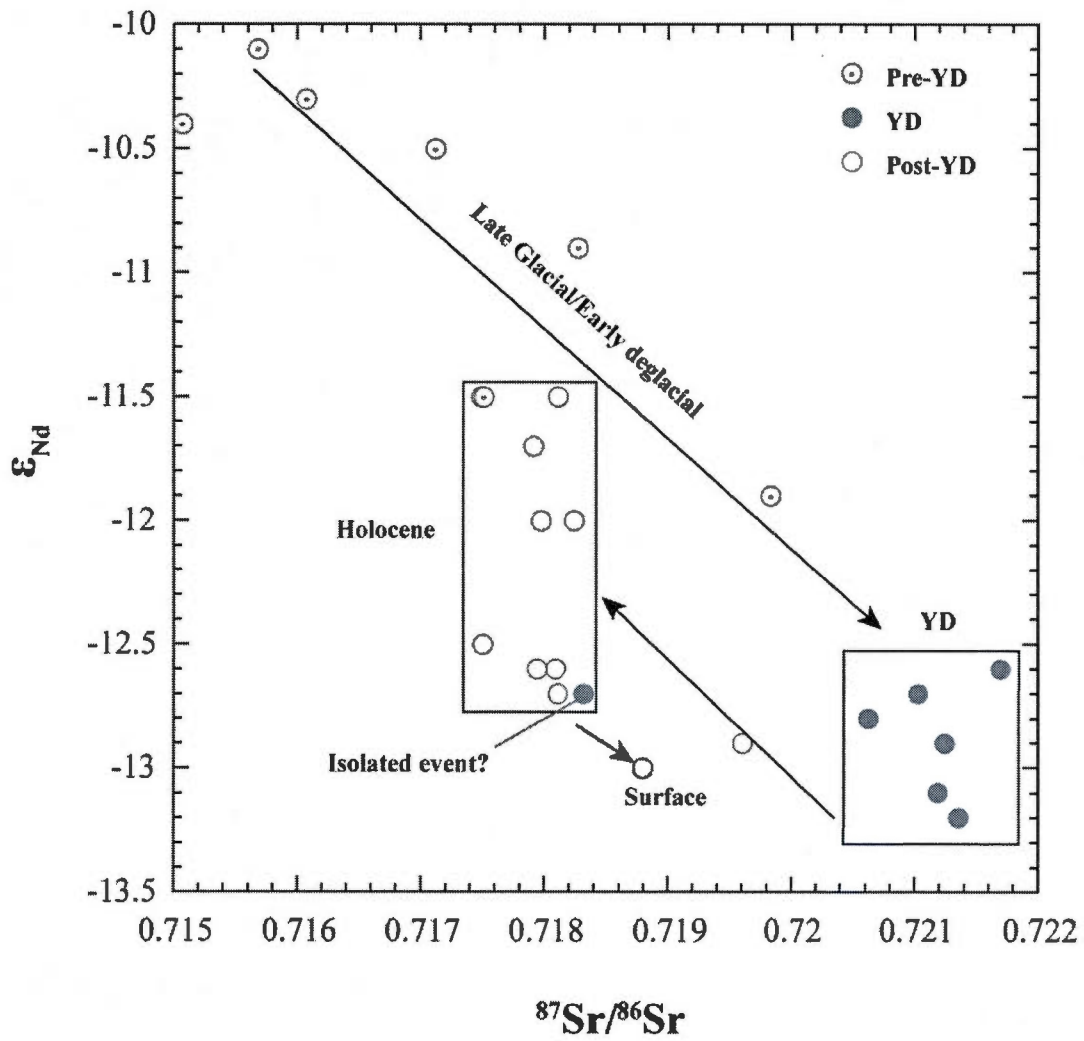


Figure 4: Nd- vs Sr-isotopes from core MC16 (i.e. Fram Strait). Full red circle represent samples from the YD interval.

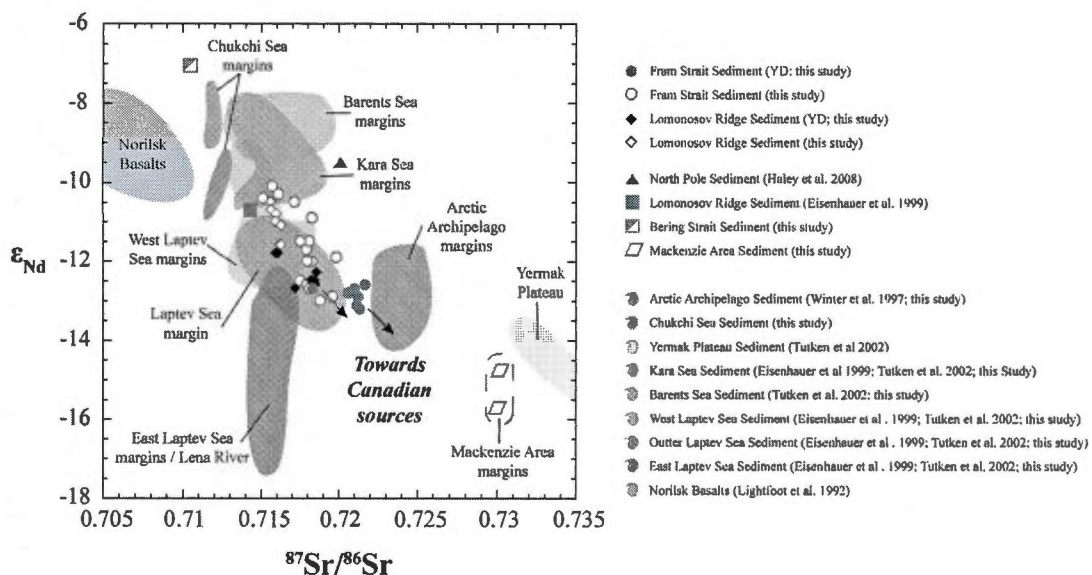


Figure 5: Nd- vs Sr-isotope data from core MC-18 (black diamonds) and core MC16 (red circles) along with potential source data from the literature.

YD samples are indicated with full symbols.

8. AUXILIARY MATERIAL

Residues vs bulk fraction

Both core MC-18 and MC16 exhibit isotopic excursion at time corresponding to the YD event. However, absolute values for both Nd and Sr isotopes are significantly different for each core. An issue must be considered here: the chemical treatment undergone. Indeed, samples from each core were treated differently. Whereas samples from core MC-18 were processed as the bulk, samples from core MC16 were sieved and leached to remove not only carbonates but also Fe-Mn oxyhydroxides. Previous studies (Bayon et al., 2002; Gutjahr et al., 2008; Gutjahr et al., 2007; and references therein), including our previous work on core MC16 (Maccali et al., 2012a, b), have illustrated the difference in isotopic composition of each considered fraction. We have estimated what the residual (i.e. purely terrigenous) isotopic composition would be in core MC-18. To do so, we used mass budget calculations from core MC16 (Maccali et al., 2012a).

In core MC16, an average of ~20 wt% of Nd was removed, likely to correspond to the Fe-Mn fraction. In addition, an average of ~50 wt% of Sr has been removed from level with high inorganic carbon content i.e ~1%. Samples from MC-18 corresponding to the YD interval displays inorganic carbon content half those of samples from core MC16, i.e. ~0.5%.

In addition, we have used sea-water and leachate data to estimate what the isotopic composition of the authigenic phase might be in core MC-18. Deep-water isotopic composition from a station nearby MC-18 (Porcelli et al., 2009) along with leachate data from a bulk sedimentary sequence at the North Pole (Haley et al., 2008) exhibit similar ε_{Nd} values of ~ -10.6.

Considering the extreme scenario with an authigenic component of ~20 wt% of Nd with ε_{Nd} of -10.6 in the whole core, and with a biogenic component for the YD interval of ~25 wt% (half that of level with high inorganic content from core MC16) having Sr isotopic composition of seawater ($^{87}\text{Sr}/^{86}\text{Sr} \sim 0.7091$), we have estimated the isotopic composition of the terrigenous fraction. As shown in figure 5, these calculations do not alter trends. In addition, corrected values of core MC-18 from the YD interval have isotopic composition similar to those of samples from core MC16 (Fig. 5).

Uncertainties are difficult to estimate but must be quite large. However, the lower $^{87}\text{Sr}/^{86}\text{Sr}$ ratios of YD samples from core MC-18 is likely buffered by the high carbonate content of these samples, and these calculations make us confident to compare trends from both cores.

Table 3: Estimated isotopic composition of residue samples from the Lomonosov Ridge (core MC-18) considering extreme conditions with ~25 wt% of carbonates (with $^{87}\text{Sr}/^{86}\text{Sr}$ of 0.7091) and ~20 wt% of Nd (with ε_{Nd} of -10.6) from Fe-Mn oxides.

Depth (cm)	$^{87}\text{Sr}/^{86}\text{Sr}$	ε_{Nd}
1.5	-	-10.5
6	-	-10.5
10.5	-	-10.7
15.5	-	-10.9
20.5	-	-11.8
23	0.717614	-12.1
24	0.717807	-12.1
25	0.719215	-13.2
25.5	0.720950	-12.7
25.5	0.720785	-12.9
26	0.720849	-13.1
26.5	0.720541	-13.0
30.5	-	-11.0
35	-	-11.8
39.5	-	-11.3

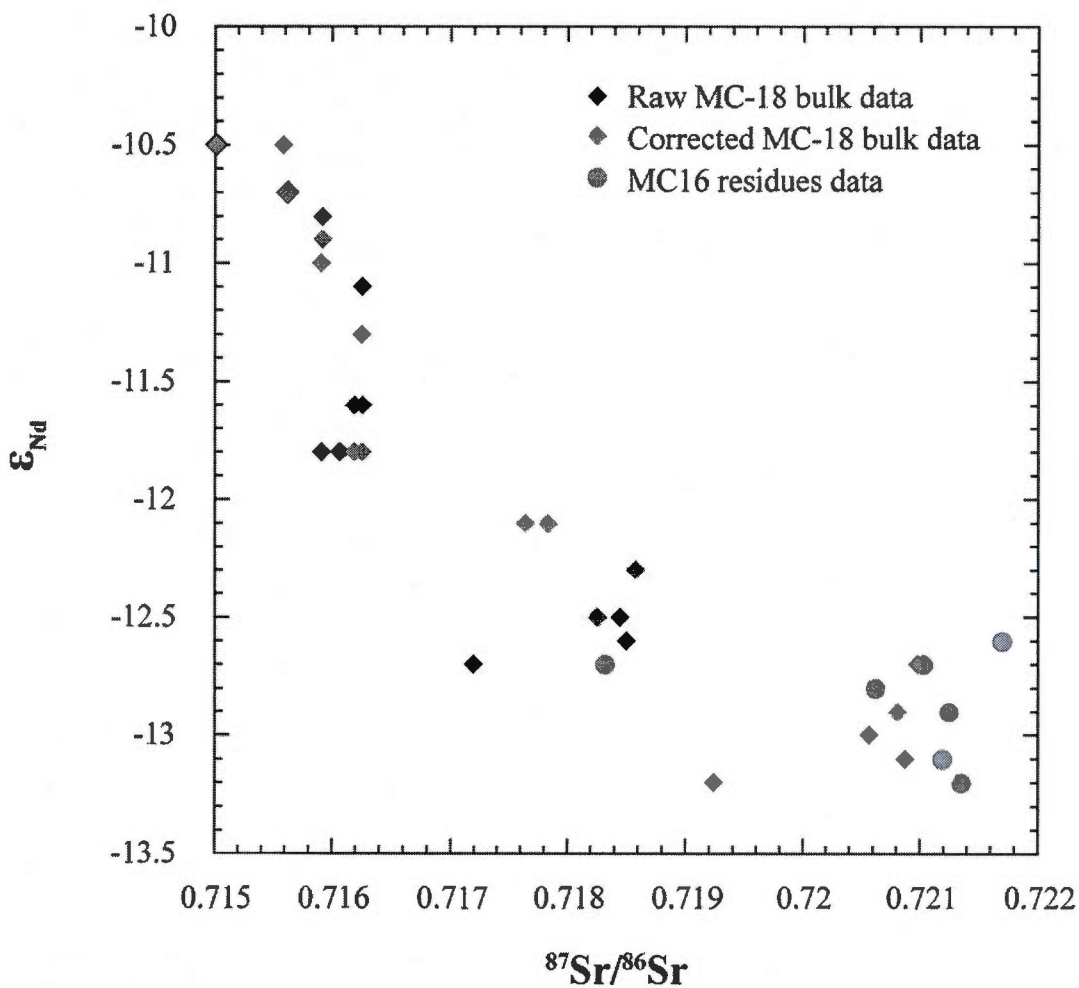


Figure 6 : Nd- vs Sr-isotopes diagram. Black diamonds represent the raw, uncorrected data from core MC-18. Light blue diamonds represent the corrected data from core MC-18, as described in the text. Light red circle represent data from the YD sequence of core MC16.

CONCLUSION

Les résultats présentés dans cette thèse ont permis de reconstituer les changements de signature isotopique de la masse d'eau profonde et de la glace de mer, dans le détroit de Fram, depuis le dernier maximum glaciaire. Le détroit de Fram est le seul exutoire d'eau douce et de glace de mer de l'océan Arctique vers l'Atlantique Nord, en période glaciaire, et l'un des deux exutoires majeurs en période interglaciaire. L'étude révèle donc une dynamique courantologique du bassin arctique dans son ensemble depuis le dernier maximum glaciaire, avec une attention particulière pour le Dryas Récent, i.e., l'un des événements brefs les plus importants de la déglaciation.

L'étude a d'abord permis de définir l'information paléocéanographique portée par certains traceurs géochimiques et les isotopes du Pb, Nd et Sr dans des sédiments marins, en combinant l'analyse de lessivats et de résidus. Ce travail a notamment démontré que la teneur en Pb commun dans les lessivats est corrélée à l'activité du ^{210}Pb et peut donc être employée pour estimer l'épaisseur de la couche de mélange dans la colonne sédimentaire. Certains ratios géochimiques (e.g. Th/Zr, Th/Pb) ainsi que les isotopes du Pb ont permis de mettre en évidence une distribution spatiale des apports sédimentaires dans le détroit de Fram, suivant un axe Est-Ouest. La partie ouest du détroit reflète une influence arctique alors que la partie est, est influencée par les mers nordiques et le Svalbard, à l'extrême est.

La composition géochimique des sédiments du détroit de Fram a permis de regrouper certains éléments en fonction de leur comportement chimique dans le sédiment (terrigène, biogénique ou authigène). Les éléments associés à la fraction terrigène sont peu ou pas lessivés (lessivage spécifique des oxydes mixtes de Fe-Mn) et sont donc conservés dans la fraction résiduelle (e.g. Fe, Al, Si, Ti). La fraction biogénique est liée au carbone (e.g. Sr et Ba) et, le carbone inorganique est supposé être principalement contenu dans les carbonates calcitiques (e.g. micro-fossiles et calcite détritique). La zone d'étude est à la limite des glaces et la matière organique ayant probablement été délivrée de manière discontinue (e.g. *bloom* printanier) a engendré des migrations du front oxydo-réducteur dans la colonne sédimentaire. Une telle migration du front redox a entraîné la redistribution de certains éléments sensibles

aux conditions oxydo-réductrices, tels que le Mn et le Mo, comme le démontre la présence d'un pic de Mn à ~16.4 ka. Le Fe présente une mobilité moins importante que celle du Mn et nous suggérons que les hydroxydes de Fe sont les principaux hôtes du Pb et du Nd. Ces éléments ne devraient donc pas avoir subi de redistribution majeure dans la colonne sédimentaire.

La composition isotopique de la fraction résiduelle des échantillons présente deux tendances temporelles A et B, illustrant respectivement le début de la déglaciation (pré-Dryas Récent) et l'Holocène (post-Dryas Récent). Les échantillons de la tendance A sont caractérisés par du matériel sédimentaire en provenance des marges continentales canadiennes et russes. La région du delta de la Mackenzie et de l'Archipel canadien sont les sources les plus plausibles dans le bassin ouest, alors que les régions des mers de Barents-Kara et Laptev ouest auraient fourni le matériel russe dans le détroit de Fram. Les calottes de glaces, Laurentienne et Innuitienne en Amérique du Nord, et Eurasienne au nord de la Russie, auraient donc fortement influencé la dynamique sédimentaire en fournissant le matériel détritique via la glace de mer et/ou les icebergs lors de la dernière déglaciation.

Les échantillons de la tendance B, post-Dryas Récent, suggèrent l'influence du bassin ouest de l'Arctique ainsi que des marges groenlandaises. Les contributions du bassin ouest de l'Arctique comprennent la région de la Mackenzie, l'archipel canadien mais également les mers de Chukchi et Est Sibérienne. Les contributions des régions des mers de Barents-Kara et Laptev ouest semblent avoir été largement interrompues alors que les marges nord groenlandaises auraient été plus actives.

Les données de lessivats permettent de documenter l'évolution des masses d'eaux et indiquent une surimposition de signaux arctiques aux masses d'eaux nordiques qui entrent dans l'océan Arctique via le détroit de Fram. Les isotopes de Nd illustrent l'influence majeure des marges russes, probablement liée aux échanges de surface (*boundary exchanges processes*) avec le matériel particulaire. Avant le Dryas Récent, la signature des masses d'eaux est influencée par les marges de Russie occidentale, en raison d'un flux particulaire élevé le long de la calotte Eurasienne. Après le Dryas Récent, les isotopes de Nd suggèrent l'influence croissante des mers Est Sibérienne et de Chukchi en raison de l'ouverture du détroit de Bering. Les marges groenlandaises ne semblent pas contribuer au signal dissous,

soit par absence de flux particulaire, soit parce que les masses d'eaux transitent trop loin des marges groenlandaises.

Enfin, nous avons fourni des résultats isotopiques indiquant du matériel sédimentaire portant une signature canadienne durant le Dryas Récent, dans deux carottes arctiques. Nos données indiquent non seulement un exutoire de ce drainage par le nord, vers l'océan Arctique, mais également un transport jusqu'au détroit de Fram, et probablement vers les mers nordiques, lieu de formation des eaux profondes. Ces travaux confirment donc la présence d'un événement paléocéanographique dans l'océan Arctique durant le Dryas Récent, et corroborent ainsi l'hypothèse avancée par Tarasov et Peltier (2005) et Peltier et al. (2006) d'un drainage par le nord via l'océan Arctique qui aurait eu un impact significatif sur l'AMOC. Cette recherche met en évidence des événements paléocéanographiques ayant eu des effets marqués sur la circulation arctique. Nos travaux pointent en effet vers un changement permanent de la dynamique de la glace de mer suite au Dryas Récent avec une probable mise en place progressive de la dérive trans-polaire.

Une meilleure résolution ainsi qu'une chronologie mieux définie seraient indispensables pour des reconstructions paléocéanographiques plus précises. En effet, la cause de la quasi-cessation de l'AMOC pendant le Dryas Récent ne peut être déterminée ici. Le drainage par l'océan Arctique du lac Agassiz, au vu des données présentées, correspond à l'intervalle du Dryas Récent, mais ne peut être défini ni comme cause ou conséquence. Nous nous heurtons ici à un point crucial de la paléocéanographie en général, et de la paléocéanographie arctique en particulier. Les faibles vitesses de sédimentation des bassins arctiques, et plus particulièrement dans le bassin ouest, limitent considérablement la résolution. À ceci s'ajoute une couche de mélange qui, bien que moindre en raison d'une activité biologique restreinte, pourra toutefois limiter d'autant plus la résolution temporelle accessible sur des carottes marines. Il faut également considérer l'âge réservoir employé, en effet, celui-ci diffère dans l'espace et dans le temps en raison du couvert de glace et de la stratification de la colonne d'eau qui limitent les échanges avec l'atmosphère. D'autres méthodes de datation pourraient toutefois être une alternative intéressante, comme le paléomagnétisme.

Afin de travailler à plus haute résolution, il serait intéressant d'étudier des carottes ayant une vitesse de sédimentation suffisamment élevée, comme cela peut être le cas sur les marges continentales. Cette approche présente l'avantage de pouvoir non seulement réduire le nombre de sources potentielles mais également d'avoir un signal plus « originel ». En effet, l'analyse de la fraction lessivable aux marges pourrait sans nul doute permettre mettre en évidence de brefs événements paléogéographiques. L'inconvénient serait cependant de ne pas avoir accès à la dynamique d'ensemble du bassin arctique.

L'extraction et l'analyse du signal dissous par lessivage soulèvent la question de la représentativité de ce signal. En effet, outre les possibles redistributions d'éléments en fonction des migrations du front oxydo-réducteurs, les contaminations par la phase détritique sont à prendre en considération. En effet, la contamination détritique de sédiments riches en matériel volcanique semble au-delà de toute correction raisonnable. Une étude récente a démontré que la composition isotopique (Nd) de foraminifères planctoniques, issus d'échantillons de surface, présente une meilleure corrélation avec la composition de l'eau de mer que celle obtenue par lessivage. L'analyse de microfossiles présente donc l'avantage de s'affranchir de contaminations détritiques. Toutefois, cette approche est limitée aux échantillons présentant une forte abondance en microfossile en raison de la faible teneur en Nd dans les matrices carbonatées.

En conclusion, la caractérisation géochimique des sédiments arctiques apporte des informations permettant de mettre en évidence la nature et les sources de ce matériel sédimentaire. L'approche multi-isotopiques s'est révélée un outil puissant afin de déterminer les sources potentielles terrigènes qui par la suite, ont permis une reconstruction de la circulation de la glace de mer depuis le dernier maximum glaciaire. Une détermination plus fine de la composition isotopique des sources potentielles serait toutefois une étape intéressante pour toutes caractérisations isotopiques futures.